平成２７年度博士学位論文

Studies on Molecular Mechanisms of Geranylgeranoic Acid-induced Cell Death in Human Hepatoma Cells

ヒト肝癌細胞におけるゲラニルゲラノイン酸による細胞死誘導の分子メカニズムに関する研究

D3212002

岩尾千絵子

2016 年 3 月
長崎県立大学大学院
人間健康科学研究科　栄養科学専攻

専攻分野　細胞生化学

指導教員　四童子好廣　　印

Contents

List of abbreviations

ACSL3; acyl-CoA synthetase long-chain family member 3

ATF6α; activating transcription factor 6α

ATRA; all-*trans* retinoic acid

Atg8; autophagy-related gene-8

BBC3; BCL2-binding component 3

BECN1; beclin 1

BH-3; bcl-2 homology domain 3

BiP; binding immunoglobulin protein

BMH; bis(maleimido) hexane

BN-PAGE; blue native-gradient PAGE

BSA; bovine serum albumin

cDNA; complementary DNA

COX; cytochrome *c* oxidase complex

DIC; differential interference contrast

DDIT3; DNA-damage-inducible transcript 3

$\Delta\Psi m$; mitochondrial inner membrane potential

D-MEM; Dulbecco's modified Eagle's medium

DRAM; damage-regulated autophagy modulator

eIF2α; eukaryotic initiation factor 2 alpha

ER; endoplasmic reticulum

FA; farnesoic acid

FBS; fetal bovine serum

F1,6-DP ; D-fructose 1,6-bisphosphate

F2,6-DP; D-fructose 2,6-bisphosphatase

F6-P; D-fructose 6-phosphate

GFP; green fluorescent protein

GGA; geranylgeranoic acid

GGOH; geranylgeraniol

GRP78; glucose-regulated protein 78

G6-P; glucose 6-phosphate

HGNC; HUGO Nomenclature Committee

HRP; horseradish peroxidase

HSPs; heat-shock proteins

IRE1α; inositol requiring 1α

KEGG: Kyoto Encyclopedia of Genes and Genomes

LC3; microtubule-associated protein 1 light chain 3

MCP; multi-channel plate

MD; mega dalton

MPCs; multiple protein complexes

m/z; mass-to-charge ratio

NADH; β-nicotinamide adenine dinucleotide, reduced

NetCDF; network common data file

ODC; ornithine decarboxylase

OPLS-DA; orthogonal partial least squares-discriminant analysis

PAGE; polyacrylamide gel electrophoresis

PARC; p53-associated, parkin-like cytoplasmic protein

PBS(-); phosphate buffered saline, Ca-free

PBS-T; PBS(-) containing 0.1% polyoxyethylene sorbitan monolaurate

PCA; principal component analysis

PDIA4; protein disulfide isomerase family A, member 4

PEP; phosphoenolpyruvic acid

PERK; protein kinase RNA (PKR)-like ER kinase

PKR; protein kinase RNA

PUMA; p53 upregulated modulator of apoptosis

PVDF; Polyvinylidene difluoride

Q-Tof/MS; quadrupole time-of-flight type mass spectrometry

RIPA; radioimmuno precipitation assay

RNase; endoribonuclease

ROS; reactive oxygen species

RT-qPCR; reverse-transcription real-time polymerase chain reaction

SAGE; serial analysis of gene expression

SCD1; stearoyl-CoA desaturase 1

SCO2; Synthesis of cytochrome *c* oxidase 2

SDS; sodium dodecylsulfate

SSAT; spermidine/spermine-N^1-acetyltransferase

TE; 10 mM Tris-HCl, pH 7.4 and 1 mM EDTA buffer

TIGAR; TP53-induced glycolysis and apoptosis regulator

TP53; Tumor protein 53

UPLC; ultra-performance liquid chromatography

UPR; unfolded protein response

VIP; variable importance in the projection

XBP1: X-box binding protein 1

WT; wild type

9CRA; 9-*cis* retinoic acid

Chapter I

General Introduction

Chieko Iwao

Molecular and Cellular Biology, Graduate School of Human Health Science,
University of Nagasaki, Nagasaki, Japan

I-1. Geranylgeranoic acid

Geranylgeranoic acid (GGA, **Fig. I-1**) is a natural diterpenoid found in several medicinal herbs including turmeric [1]. GGA and its derivatives have been repeatedly reported to induce cell death in human hepatoma cells [2, 3]. In placebo-controlled randomized clinical trials, 4,5-didehydroGGA both safely and effectively prevented tumor recurrence in postoperative hepatoma-free patients [4-6]. While 4,5-didehydroGGA has been utilized for clinical trials, it has so far not been identified in natural resources.

GGA and 4,5-didehydroGGA were initially screened as acyclic retinoids to bind to cellular retinoic acid-binding protein [7]. Furthermore, both compounds were later shown to possess ligand activities for retinoid receptors (retinoic acid receptor and retinoid X-activated receptor) [2].

In human hepatoma-derived HuH-7 cells, GGA-induced cell death has been demonstrated by the chromatin condensation, large-scale DNA fragmentations, nucleosomal-scale ladder formation and dissipation of mitochondrial inner membrane potential ($\Delta\Psi m$) [8, 9]. It has been also reported that some caspase inhibitors delayed GGA-induced cell death and, furthermore, α-tocopherol prevented HuH-7 cells from dissipation of $\Delta\Psi m$ as well as programmed cell death in the presence of GGA. Importantly, GGA induces a dramatic loss of $\Delta\Psi m$ in 1 h and in a dose dependent manner in HuH-7 cells, but not in the primary hepatocytes [9].

In this thesis study, I have tried to investigate the mechanisms by which GGA induces cell death in hepatoma cells with a focus on the tumor suppressor gene *TP53*, endoplasmic reticulum (ER) stress response and autophagy.

I-2. Tumor protein p53 and energy metabolism

First I examined p53 because it has been well established that HuH-7 cells harbor the mutant *TP53* gene [10]. *TP53* is the first tumor suppressor gene linked to apoptosis [11], inhibits tumor growth through activation of both cell cycle arrest and apoptosis, and is thought to be central to tumor-suppressor activity [12-14]. It seems likely that activation of p53-dependent cell death can

contribute to inhibition of cancer development at several stages during tumorigenesis [11]. The p53 pathway is crucial for effective tumor suppression in humans [15]. However, the frequencies of reported *TP53* mutations vary considerably between cancer types, ranging from ~15% (for example, in bone cancers) to 50% (for example, in colorectal and head and neck cancers) (**Fig. I-2**).

The transcription factor p53 responds to diverse stresses (including DNA damage, overexpressed oncogenes and various metabolic limitations) to regulate many target genes (**Fig. I-3**) that induce cell-cycle arrest (e.g. *p21*), apoptosis (e.g. *PUMA*) or respiration (e.g. *SCO2*) [16, 17].

The *PUMA* (p53 upregulated modulator of apoptosis or official name is BBC3, BCL2-binding component 3) gene is identified as a downstream target of the tumor suppressor p53 and a potent inducer of apoptosis in diverse tissues and cell types [18]. PUMA is one of BH-3 (bcl-2 homology domain 3) only proteins, which can induce mitochondrial outer membrane permeability transition and consequent mitochondria-dependent cell death through complex formation with anti-apoptotic Bcl-2 (or Bcl-xl) protein. Therefore, expression of PUMA will cause hyper-production of reactive oxygen species (ROS) from mitochondria and then induce mitophagy in order to recycle the damaged mitochondria.

Among p53 target genes, another cell-death-related gene, the *TIGAR* (TP53-induced glycolysis and apoptosis regulator) gene is regulated as a part of the p53 tumor suppressor pathway and encodes a protein with sequence similarity to the bisphosphatase domain of the glycolytic enzyme, fructose 2,6-bisphosphatase (F2,6-DP) that degrades F2,6-DP to fructose 6-phosphate (F6-P) (**Fig. I-4**). The protein functions by blocking glycolysis and instead the resultant accumulated glucose 6-phosphate (G 6-P) directs the pathway into the pentose phosphate shunt, which provides antioxidant electron donor NADPH. Therefore, expression of the TIGAR protein also protects cells from DNA-damaging ROS and thereby from DNA damage-induced apoptosis [19].

As another p53-targeted gene, *SCO2* (Synthesis of cytochrome *c* oxidase 2) is identified [19, 20]. Upon discovering that $p53^{+/+}$ mice consumed significantly more oxygen and produced more ATP by

aerobic respiration than their $p53^{-/-}$ counterparts, the authors conducted a SAGE (serial analysis of gene expression) database search for potential p53-target gene products that could potentially modulate the process of aerobic respiration. And the protein is required for the proper assembly of the cytochrome *c* oxidase complex (COX) that is directly responsible for the reduction of oxygen during aerobic respiration.

I-3. Warburg effect

In general, cells that lack functional p53 represent a metabolic shift from respiration to glycolysis for the production of energy and lower oxygen consumption by mitochondrial respiration – thereby contributing to the Warburg effect [21].

The metabolic change known as the Warburg effect is a major feature of virtually all of clinical cancers [21]. In other words, unlike most normal cells, cancer cells acquire a mode of dependency on glycolysis for energy production (**Fig. I-5**). Although for many years considered to be a by-product or just accompanying phenomenon of the oncogenic process, this shift to high rate of glycolysis is suggested to be required for malignant progression [22]. Several different tumor-associated changes – in addition to loss of p53 function – participate in the shift to aerobic glycolysis in cancer cells [16, 23].

I-4. GGA-induced incomplete autophagic response

Second Okamoto et al recently identified that HuH-7 cells undergo an incomplete autophagic response following GGA treatment [24], which may also contribute to GGA-induced cell death. While GGA causes the initial phase of autophagy, the late stage of autophagy such as maturation of autolysosomes or late stage of autophagy fail to proceed, leading to cell death in HuH-7 cells [24].

Most intracellular short-lived proteins are selectively degraded by ubiquitin-proteasome pathway [25], while most long-lived proteins are degraded in lysosomes [26]. The mechanism to deliver cytoplasmic components to the lysosomes is called autophagy in general. Three types of autophagy have been proposed: macroautophagy, microautophagy and chaperone-mediated

autophagy [27]. Among them, macroautophagy is believed to be responsible for the majority of the intracellular protein degradation, particularly of the starvation-induced proteolysis [26]. In macroautophagy (simply referred to as autophagy hereafter), cytoplasmic constituents including organelles such as mitochondrion and peroxisome, are first enwrapped by a membrane sac called "isolation membrane". Closure of isolation membrane results in formation of double membrane structure called "autophagosomes". Autophagosomes, then, either through fusion with endosomes to become amphisomes or not, eventually, become autolysosomes, which are generated by the fusion of the outer membrane of the autophagosomes (or amphisomes) and lysosomes. Lysosomal hydrolases degrade the cytoplasm-derived contents of the autophagosome, together with its inner membrane [28].

LC3 (microtubule-associated protein 1 light chain 3) is specific to autophagy marker. LC3 was originally discovered as one of three light chains complexed with microtubule-associated proteins 1A and 1B. Unlike LC1 and LC2, LC3 are transcribed and translated as single proteins and conserved in fungi, plants and animals. In humans, three genes encode highly homologous LC3 proteins such as LC3α, β, and γ. Although LC3γ is an ortholog of the yeast autophagosome protein Atg8 and all 3 proteins have been demonstrated to be involved in autophagosome biogenesis, LC3β has been used exclusively as a hallmark of autophagosome formation in mammalian cells. Hence, in this manuscript, I use a word of LC3 in place of LC3β. LC3 is homolog of autophagy-related gene-8 (Atg8) essential for autophagy in yeast, and is associated to the autophagosome membranes after processing. Two forms of LC3, called LC3-I and -II, were produced post-translationally in various cells. LC3-I (apparent molecular size of approximately 18 kDa) is cytosolic and nonlipidated, whereas LC3-II (approximately 16 kDa) is membrane bound and lipidated with phosphatidyl ethanolamine [29].

In recent years, it has become clear that autophagy plays an important role in a variety of physiological responses as follows: starvation, development, differentiation, tumorigenesis, immunity and neurodegeneration [30]. Autophagy, particularly that responsive to starvation, is

generally considered a nonselective degradation of cellular constituents [30]. This large-scale degradation enables cells to survive during starvation by recycling of the degradation products for resources of energy production and macromolecule synthesis. In addition to the starvation-induced adaptive autophagy, growing lines of evidence point to the importance of basal autophagy that operates constitutively at low rates even under a nutrient-rich environment and plays a vital role in the maintenance of cellular homeostasis [27-34]. Indeed, studies using mouse genetics have indicated that autophagy-deficient mice exhibit remarkable accumulation of ubiquitinated protein aggregates followed by hepatocytic and neuronal cell death irrespective of nutrient stresses [31, 32, 34].

I-5. Lipid-induced unfolded protein responses

Third, I investigated what kind of cellular events GGA initially induces occurred during incomplete autophagic response. One of the possible mechanisms by which GGA could induce autophagy is the ER stress-mediated unfolded protein response (UPR) as an upstream signal of lipotoxicity with fatty acids [35].

In general, the conventional UPR is an adaptive stress response that responds to the accumulation of misfolded proteins in ER lumen (ER stress) and adjusts the protein-folding capacity to the needs of the cell [36, 37]. The UPR is sensed by the binding immunoglobulin protein (BiP)/glucose-regulated protein 78 (GRP78). The accumulation of unfolded proteins sequesters BiP/GRP78, so it dissociates from three ER-transmembrane transducers leading to their activation. These transducers are inositol requiring 1α (IRE1α), protein kinase RNA (PKR)-like ER kinase (PERK), and activating transcription factor 6α (ATF6α) (**Fig. I-6**).

PERK phosphorylates eukaryotic initiation factor 2 alpha (eIF2α) resulting in global mRNA translation attenuation, and concurrently selectively increases the translation of several mRNAs, including the transcription factor *ATF4*, and its downstream target *CHOP*. IRE1α has kinase and endoribonuclease (RNase) activities. IRE1α autophosphorylation activates the RNase activity to

splice X-box binding protein 1 (*XBP1)* mRNA and then to produce the active transcription factor XBP1s. Activation of IRE1α kinase also recruits and activates the stress kinase JNK. ATF6α transits to the Golgi compartment where it is cleaved by intramembrane proteolysis to generate a soluble active transcription factor, which is then conveyed into the nucleus. These UPR pathways act in concert to increase ER content, expand the ER protein folding capacity, degrade misfolded proteins, and reduce the load of new proteins entering the ER. Faced with persistent ER stress, adaptation starts to fail and apoptosis occurs, possibly mediated through calcium perturbations, ROS, and the proapoptotic transcription factor DNA-damage-inducible transcript 3 (DDIT3 or previously named CHOP) [38].

UPR is also activated by an aberrant lipid accumulation or a perturbation of cellular lipid accumulation, especially it is called "lipid-induced UPR". In cultured cells, the UPR is activated by the accumulation of free cholesterol in the ER [39], exogenously supplied saturated fatty acids [40, 41] and perturbation of cellular fatty acid composition [42]. Activation of the UPR has been observed in the liver of dietary and genetically obese mice [43, 44] and in the tissue of obese human [45].

And recently one novel study discovers that lipid-induced UPR activates IRE1α and PERK, but does not activate ATF6α [46]. In brief, activation of the UPR by membrane lipid saturation occurs by a mechanism different from the conventional unfolded protein stress-sensing mechanism. The mechanism of the lipid-induced UPR is unclear, but it has been reported that palmitic acid treatment or knockdown of stearoyl-CoA desaturase 1 (SCD1) promotes an increase of saturated fatty acids in membrane phospholipids and activates the UPR in HeLa cells [42].

I-6. Protein chemistry approach with Blue native-gradient PAGE and cross-linking SDS-PAGE

Finally, in this thesis I applied a couple of protein chemistry methods, "Blue Native-gradient PAGE (BN-PAGE)" and "Cross-linking SDS-PAGE" to examine intracellular molecular assembly

of p53.

Multiple protein complexes (MPCs) play a crucial role in cell signaling, since most protein can be found in functional or regulatory complexes with other proteins [48]. Thus, the study of protein-protein interaction networks required the detailed characterization of MPCs to gain an integrative understanding of protein function and regulation. For identification and analysis, MPCs must be separated under native conditions. BN-PAGE is a technique that allows separation of MPCs in a native conformation with higher resolution [49]. Therefore it is useful to determine MPC size, composition, and relative abundance. By this method, proteins are separated according to their hydrodynamic size and shape in a polyacrylamide matrix. Moreover in cross-linking SDS-PAGE, cross-linking reagents provide the means for capturing MPCs by covalently binding them. So it also can be captured in its native conditions, one can get greater and more shape resolution of protein-protein interactions.

I-7. The aim of this thesis

We have been facing with super aging society, so that achievement of the prevention of life-style and aging related diseases such as cancer and obesity should be a way to solve the emerging social problem with health.

With regard to a national strategy against cancer, over the last 2 decades development of targeting drug therapies has become an important field of research. The aim with these emerging therapies is to specifically target one or several tumor suppressor genes including *p53*, *BRCA1*, *Rb* and so on, thus inhibiting tumor growth and inducing cell death. However, many drugs have only a transient effect and recurrence is often inevitable for certain types of cancer such as hepatoma. But as progressed in the understanding of carcinogenesis, new potential targets are enhancing the scope for the development of novel treatment specifically targeted to eliminate cancer cells.

This thesis provides a basic research for prevention of human hepatoma with GGA.

As mentioned above, GGA induces cell death thorough an incomplete autophagic response in

HuH-7 cells [24], which harbor the mutant *TP53* gene [10]. However it has not yet been revealed how GGA-induces cell death at the molecular mechanism. So in this thesis, I have tried to clarify how GGA induces cell death by focusing on p53.

In chapter II, I investigated in HuH-7 cells whether or not GGA upregulates p53-target genes including *SCO2* and *TIGAR*, both of which are related to energy metabolism. Prior to the scrutinized investigation, I started to globally compare cellular metabolites in between control and GGA-treated cells. From the results of chapter II, GGA may shift an energetic state from glycolysis to respiration dependency by reactivating the mutant p53 to upregulate TIGAR and SCO2 proteins in HuH-7 cells. Hence, in chapter III, I examined in detail how GGA affected the mutant p53 in HuH-7 cells. As a result, it was found that cytoplasmic p53 protein accumulated as huge complexes with PARC and other proteins on the endoplasmic reticulum (ER) in the cytoplasm. Moreover, it was discovered that GGA released the p53 protein from these huge complexes, and induced nuclear translocation of the cytoplasmic p53 protein.

In chapter IV, I finally surveyed how GGA affected the state of ER, where the p53 containing huge complexes were harbored. Then, it was discovered that UPR was immediately induced in ER after addition of GGA, and was also initiating signal linked to autophagic cell death. And it was found GGA induced lipid-induced UPR and more the UPR was linked to GGA-induced autophagy and cell death.

Through my doctoral thesis, I have now sincere hope that intensive basic research on natural cancer preventive compounds, such as GGA will pave a concrete road to protect super-aging society from cancer disease.

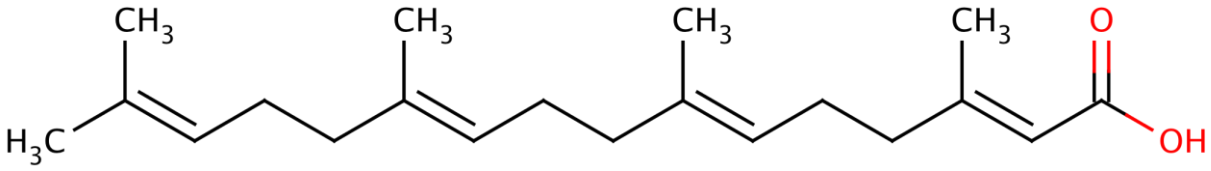

Fig. I-1. Chemical structure of geranylgeranoic acid.

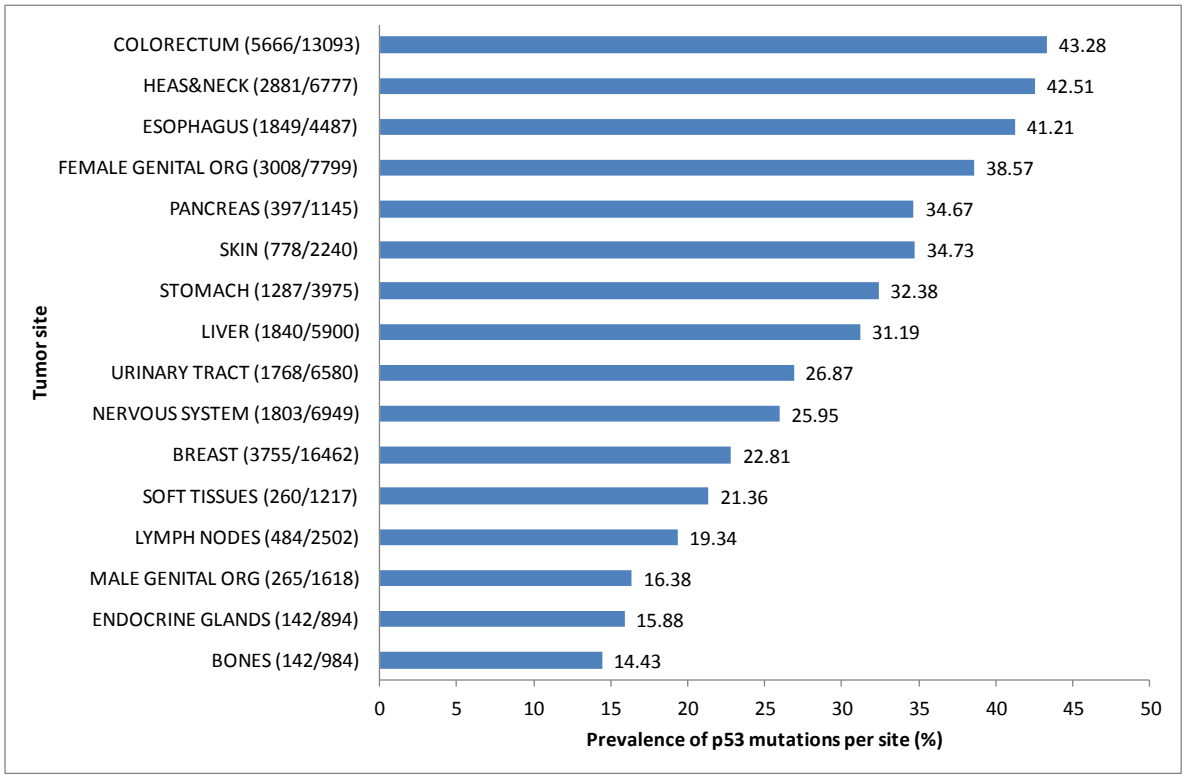

Fig. I-2. Frequency of *TP53* mutations in human tumors.
adopted from IARC p53 database, R17 release, November 2013, WHO, IARC

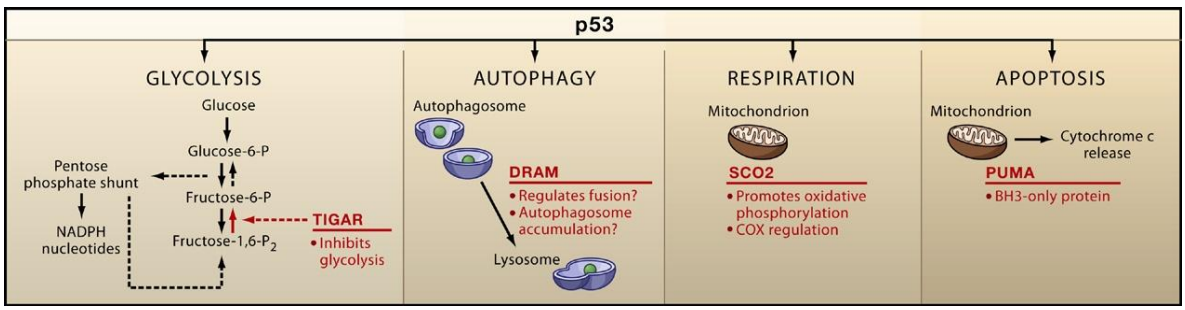

Fig. I-3. Diverse function of p53 through multiple target genes.
adopted from Green DR and Chipuk JE: *Cell*, 126: 30-32 (2006)

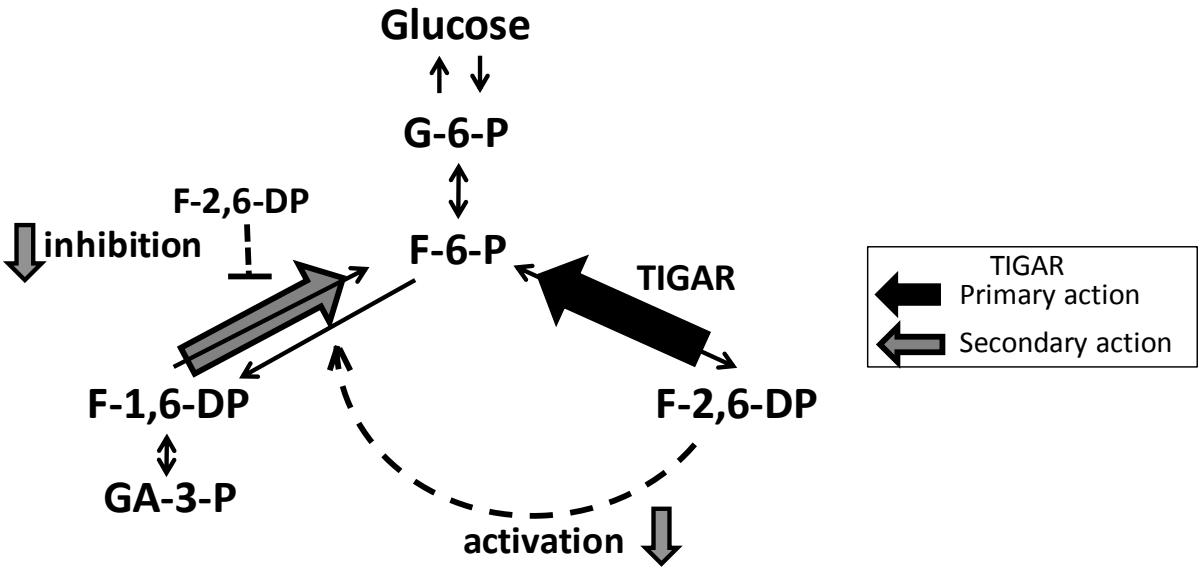

Fig. I-4. Regulation of glycolysis pathway by TIGAR.

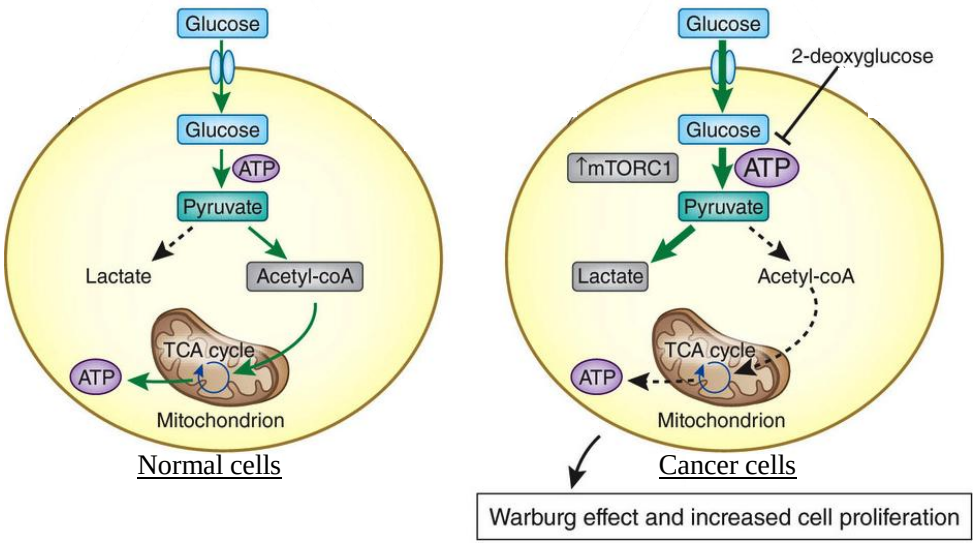

Fig. I-5. Warburg effect in malignant cells.

modified from Priolo C and Henske EP, *Nature Medicine* 19: 407–409 (2013)

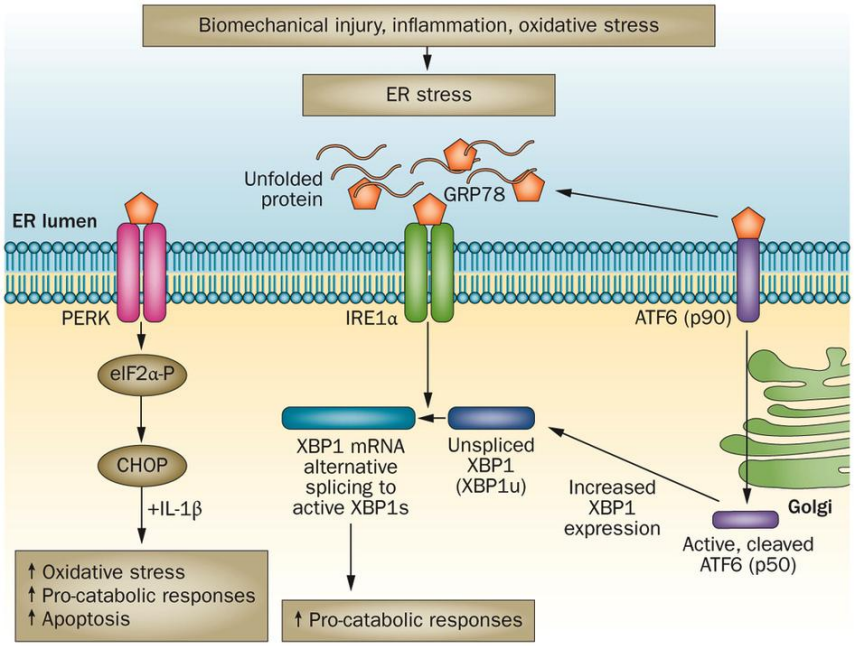

Fig. I-6. Canonical unfolded protein responses.

Liu-Bryan R and Terkeltaub R. *Nature Reviews Rheumatology* 11: 35–44 (2015)

Chapter II

Upregulation of energy metabolism-related, p53-target TIGAR and SCO2 in HuH-7 cells by GGA treatment

Chieko Iwao
Yoshihiro Shidoji

Upregulation of energy metabolism-related, p53-target TIGAR and SCO2 in HuH-7 cells with p53 mutation by geranylgeranoic acid treatment

Biomedical Research (2015) ***36****(6): 371-381*

Molecular and Cellular Biology, Graduate School of Human Health Science,
University of Nagasaki, Nagasaki, Japan

II-1. Abstract

Metabolic alternation in cancer cells is one of the most common characteristics that distinguish malignant cells from normal cells. Many studies have explained the Warburg hypothesis that cancer cells obtain more energy from aerobic glycolysis than mitochondrial respiration. Here, ~~we~~it is shown that a branched-chain C-20 polyunsaturated fatty acid, geranylgeranoic acid (GGA), induces upregulation of the cellular protein levels of *TP53-induced glycolysis and apoptosis regulator* (TIGAR) and *synthesis of cytochrome c oxidase 2* (SCO2) in human hepatoma-derived HuH-7 cells harboring the mutant *TP53* gene, suggesting that GGA may shift an energetic state of the tumor cells from aerobic glycolysis to mitochondrial respiration. In addition, UPLC/TOF/MS-based metabolomics analysis supported the GGA-induced energetic shift, as it revealed that GGA induced a time-dependent increase in the cellular contents of fructose 6-phosphate and decrease of fructose 1,6-diphosphate. Furthermore, metabolomics analysis revealed that GGA rapidly induced spermine accumulation with slight decrease spermidine. Taken together, the present study strongly suggests that GGA may shift HuH-7 cells from aerobic glycolysis to mitochondrial respiration through the immediate upregulation of TIGAR and SCO2 protein levels.

II-2. Introduction

In HuH-7 cells, GGA induces cell death has so far been illustrated by at least 3 lines of evidence; 1) the chromatin condensation, 2) large-scale DNA fragmentations and nucleosomal-scale ladder formation, and 3) dissipation of mitochondrial inner membrane potential ($\Delta\Psi m$) [2, 3]. And recently, it is reported that GGA induces an incomplete autophagic response in HuH-7 cells, which may be linked to GGA-induced cell death [24].

In most cancer cells, the tumor suppressor *TP53* gene is modified through mutations or changes in its expression. It has also been well established that human hepatoma-derived HuH-7 cells possess the mutant *TP53* gene with a missense mutation of Y220C (tyrosine at a residue of 220 is converted to cysteine) in the DNA-binding domain of p53 [50]. As mentioned in chapter I, p53 is involved both in TIGAR-mediated suppression of glycolysis and in SCO2-mediated enhancement of aerobic respiration, so that cells that lack functional p53 represent a metabolic shift from aerobic respiration to glycolysis for the production of cellular energy and lower oxygen consumption by mitochondrial respiration – thereby contributing to the Warburg effect [21]. In chapter II, I am going to demonstrate that it is very important for cancer chemoprevention to induce metabolic shift from glycolysis to aerobic respiration in tumor cells.

Furthermore, it has been proposed for several times that activation of p53-dependent cell death can contribute to inhibition of cancer development at several stages during tumorigenesis [51], and the p53 pathway is expected to be absolutely crucial for effective tumor suppression in humans [52]. This may be true also in tumor cells with p53 mutation.

Hence, in chapter II, in order to clarify a molecular mechanism of GGA-induced cell death in the mutant *TP53* gene-harboring cells, I focused my attention on p53-target, energy metabolism-related genes, *SCO2* and *TIGAR* in HuH-7 cells after GGA treatment. As a result, it was found a rapid increase in the cellular levels of SCO2 and TIGAR by western blotting without upregulation of their

transcript levels. Furthermore, metabolomics analysis revealed GGA-induced upregulation of cellular F6-P and NADH levels and downregulation of F1,6-DP.

II-3. Materials and Methods

II-3-1. Materials

GGA and farnesoic acid (FA) were generous gifts from Kuraray (Okayama, Japan). Geranylgeraniol (GGOH), D-fructose 6-phosphate (F6-P) dipotassium salt, D-fructose 1,6-bisphosphate (F1,6-DP) trisodium salt hydrate, phosphoenolpyruvic acid (PEP) monopotassium salt, and β-nicotinamide adenine dinucleotide, reduced (NADH) disodium salt hydrate were all purchased from Sigma Aldrich, St. Louis, MO, USA.

II-3-2. Cell culture

Human hepatoma-derived HuH-7 cells were obtained from RIKEN BioResource Center, Tsukuba, Japan, and cultured in high-glucose Dulbecco's modified Eagle's medium (D-MEM; Wako Pure Chemical Industries, Osaka, Japan) supplemented with 5% fetal bovine serum (FBS; Hyclone Laboratories, ThermoFisher Scientific, Waltham, MA, USA).

II-3-3. GGA, GGOH or FA treatment

3.0×10^4 cells were inoculated in 3-cm dishes (ThermoFisher Scientific, Nunc, Roskilde, Denmark) and cultured with D-MEM containing 5% FBS for 2 days, thereafter the medium was replaced with FBS-free D-MEM a day before GGA, ethanol, GGOH or FA addition. The ethanolic solution of GGA, GGOH or FA (2.5 - 50 mM) was added at a final concentration of 2.5 - 50 μM. Ethanol was added as a negative control at its final concentration of 0.1% (v/v).

II-3-4. Immunoblotting

Following treatment with GGA, GGOH or FA, HuH-7 cells were lysed with cell lysis buffer (Tris-based buffered saline containing 1% Nonidet P40, 0.5% sodium deoxycholate and 0.1% SDS) containing complete mini protease inhibitor cocktail (Roche Diagnostics, Basel, Switzerland) and proteins were quantified by Bradford assay (Bio-Rad, Hercules, CA, USA). Equal amounts (2.5 or 5 μg) of protein per sample were separated by SDS-PAGE. The semi-dry blotted polyvinylidene

fluoride membranes (Bio-Rad) were probed with anti-TIGAR polyclonal antibody (#37910, Abcam, Cambridge, MA, USA), anti-SCO2 polyclonal antibody (#54654, Anaspec, San Jose, CA, USA), anti-COX2 monoclonal antibody (#65239, Santa Cruz, CA, USA), anti-Porin polyclonal antibody (#548, Calbiochem, Merck, Tokyo, Japan) or anti-β-actin polyclonal antibody (#4967, Cell Signaling Technology, Boston, MA, USA). Horseradish peroxidase (HRP)-labeled secondary antibody (GE Healthcare, Tokyo, Japan) was detected with Immobilon Western Chemiluminescent HRP substrate (Merck Millipore Japan, Tokyo, Japan) using an ImageQuant LAS 4000 (GE Healthcare).

II-3-5. Isolation of total cellular RNA

After drug treatment, total RNA was isolated from cells by using QuickGene RNA cultured Cell kit S (Fujifilm, Tokyo, Japan). Cells in 3-cm dishes were washed with 2 mL of phosphate-buffered saline (PBS(-)), scraped off with lysis buffer of the kit S, and transferred into each 1.5-mL tubes. Then, the cells were homogenized by 1-mL syringe with a 21-G needle. Total cellular RNA was purified with nucleic acid isolation system, QuickGene-800 (Fujifilm). Total RNA was quantified by absorbance at 260 nm with NanoDrop® spectrophotometer ND-1000 (NanoDrop Technologies, Wilmington, DE, USA), and 260:280 nm ratio was used as index of purity. The integrity of RNA preparations was further confirmed by electrophoresis in a denaturing agarose gel containing 1% formaldehyde and 1 × MOPS [3-(N-morpholinopropanesulfonic) acid] running buffer to detect 2 major rRNAs of 28S and 18S. After confirmation of the integrity, a preparation of total RNA was kept frozen at -20ºC until use for reverse transcription polymerase chain reaction (RT-PCR).

II-3-6. Reverse transcription for cDNA synthesis

The aliquot corresponding to 300 ng of total cellular RNA of each sample, water (PCR-grade) and random hexamer primer included in Transcriptor® first strand cDNA synthesis kit (Roche, Diagnostics, Mannheim, Germany) were incubated at 65ºC for 10 min. To the mixture 5 × Transcriptor® RT reaction buffer, Protector® RNase inhibitor, deoxynucleotide mix and

Transcriptor® reverse transcriptase were added and incubated at 25ºC for 10 min, at 55ºC for 30 min, at 85ºC for 5 min and at 4ºC for over 5 min.

II-3-7. Quantitative PCR with cDNA

Nucleotide sequences of the primers including the *SCO2*, *TIGAR* and *28S rRNA* cDNAs are listed in **Table II-1**. Real-time PCR was performed with 9 μL reaction mixture containing 1 μL of primer solution (0.5 μM, the stock solution was diluted by 1:10), 5 μL of 2 × DyNAmo™ Capillary SYBR® Green qPCR master mix (Finnzymes, Espoo, Finland) and 1 μL of cDNA containing solution in a PCR-capillary (Roche). The mixture was incubated in a LightCycler1.5 (Roche) under condition described in **Table II-2.**

Table II-1. The nucleotide sequences of each primers used for real time RT-PCR.

Genes	Primer	Sequence (5' – 3')
SCO2	F	CCCAAGACTGTTGGGTCTG
	R	GCCGTAGTAATCCGTGAAGAG
TIGAR	F	CCAACGGTTCAGTGTATTTGTATG
	R	AGAACTAGCAGAGGAGAGAAGTAA
28S rRNA	F	TTAGTGACGCGCATGAATGG
	R	TGTGGTTTCGCTGGATAGTAGGT

F: forward primer, R: reverse primer

Table II-2. The conditions of thermal cycler for real-time RT-PCR of *SCO2*, *TIGAR* and *28s rRNA*.

	SCO2	
	Temperature	Slope
Denature	95ºC, 600 s	20ºC / s
PCR (40 cycles)	95ºC, 10 s 56ºC, 20 s 72ºC, 20 s	20ºC / s
Melting	95ºC, 0 s 57ºC, 15 s 98ºC, 0 s	20ºC / s 0.1ºC / s
Cooling	40ºC, 30 s	20ºC / s

	TIGAR	
	Temperature	Slope
Denature	95ºC, 600 s	20ºC / s
PCR (45 cycles)	95ºC, 10 s 56ºC, 20 s 72ºC, 15 s	20ºC / s
Melting	95ºC, 0 s 57ºC, 15 s 98ºC, 0 s	20ºC / s 0.1ºC / s
Cooling	40ºC, 10 s	20ºC / s

	28s rRNA	
	Temperature	Slope
Denature	95ºC, 600 s	20ºC / s
PCR (40 cycles)	95ºC, 15 s 60ºC, 30 s	20ºC / s
Melting	95ºC, 0 s 65ºC, 15 s 95ºC, 0 s	20ºC / s 0.1ºC / s
Cooling	40ºC, 30 s	20ºC / s

II-3-8. Extraction of metabolites

Cells were inoculated in 9-cm dishes at 2.5 × 10^6 cells/dish. After 0, 2, 4, 8 or 24-h incubation with 10 μM GGA, the cells were quenched by replacement of the conditioned medium with 12 mL of ice-cold 0.9% (w/v) NaCl for 5 min, washed twice with 6 mL of PBS(-) and scraped off twice with 0.6 mL of PBS(-) on ice. The scraped cells were transferred into 2-mL tube by pipetting and centrifuged at 200 × *g* for 6 min at 0ºC. Cell pellets were re-suspended in 1 mL of ice-cold 50% (v/v) aqueous acetonitrile (LC-MS Chromatosolv®, Fluka, Sigma-Aldrich), and the cell suspensions were agitated for 30 s by vortexing twice. The suspensions were centrifuged at 19300 × *g* for 8 min

(at 0ºC), and precipitates were used for DNA measurement with SYBR Green, and the supernatants were transferred to new 1.5-mL tubes, frozen at -80ºC, and dried on the following day using a vacuum evaporator centrifuge, VEC-100 (Iwaki, Tokyo, Japan) equipped with a vapor trap of dry-ice/ethanol. The dried extracts were re-suspended in water and incubated on ice with frequent periods (30 s × 5) with bath-type sonication. After centrifuging the cell extracts at 19300 × *g* for 8 min at 0ºC, the supernatants were transferred to new 2-mL tubes and stored frozen at -80ºC until analysis.

Samples were thawed out on ice and their aliquots were transferred to 0.3-mL screw-capped vial with pre-slit septum (Nihon Waters, Tokyo, Japan) filtered through a 0.2-μm pore-size membrane (Millipore Japan, Tokyo, Japan), and analyzed by ultra-performance liquid chromatography (UPLC) and quadrupole time-of-flight type mass spectrometric apparatus (Xevo™ Q-Tof/MS, Nihon Waters) described below.

II-3-9. UPLC

Reversed-phase chromatographic separation was performed on a 2.1 × 100 mm ACQUITY™ UPLC® BEH C18, 1.7 μm column connected with the VanGuard pre-column (Waters). The column temperature was kept constant at 40ºC. The mobile phase consisted of water containing 0.1% formic acid (Wako, HPLC grade) as solvent A and acetonitrile (LC-MS Chromatosolv®, Sigma-Aldrich) containing 0.1% formic acid as solvent B. The gradient duration was 20 min at a flow rate of 0.3 mL/min. From the start to 0.5 min, a volume proportion of acetonitrile in eluent was kept at 1% (A:B = 99:1, v/v) and linearly increased to 95% (A:B = 5:95) in 10 min at a constant flow rate. Then, acetonitrile (%B) was kept at 95% for 4 min. After that acetonitrile (%B) was reduced to 1% in 4 min and kept at that concentration for 5 min. A 10-μL aliquot of each sample was injected automatically onto the column. The same sample was injected three times each for either negative or positive ion recordings.

II-3-10. Q-Tof/MS

In-line mass spectrometry was performed on a Waters Xevo™ Q-Tof mass spectrometry apparatus (Waters MS Technologies, Manchester, UK), which was calibrated with sodium formate and lock-sprayed with Leu-encephalin (Nihon Waters) each time operating in either positive or negative ion modes. The nebulization gas was set to 800 L/h at a temperature of 450ºC, and the cone gas was set to 50 L/h. Source temperature was set to 120ºC. The capillary voltage and cone voltage were set to 3000 V and 30 V, respectively. The voltage of the MCP (multi-channel plate) detector was set to 2150 V. The data acquisition rate was set to 0.2 sec. Data were recorded between m/z 80 to 1000 in centroid mode.

II-3-11. UPLC/Q-Tof Mass spectrometric measurement of F6-P, F1,6-DP, PEP and NADH

The authentic m/z and retention times were obtained with 10 μM each standard solution on Waters UPLC/Q-Tof/MS apparatus as shown in **Table II-3**. As described below, the obtained data from UPLC/Q-Tof/MS for each metabolite were transformed by calculating the validated metabolite contents on a 10^6 cellular basis.

Table II-3. UPLC/Q-Tof/MS measurement of F6-P, F1.6-DP, PEP and NADH.

	m/z [+]	retention time
F6-P	283.0164	0.83
F1,6-DP	363.0023	0.83
PEP	168.9978	0.91
NADH	664.1193	1.34

II-3-12. Data collection, processing and multivariate statistical analysis

Raw chromatogram data of UPLC/Q-Tof/MS were initially converted to NetCDF (network common data file) formatted by Databridge in software of MarkerLynx® (Waters). The peak width

at 50% height was set to 3 s. Other parameters were all in default settings. Detected and matched peaks with retention time and m/z, and their corresponding intensities were electronically exported to an excel table. Prior to multivariate data analysis, the raw data of each sample was normalized to total mass-signal area to correct for the MS response shift from the first injection to the last injection.

To reproduce the difference in metabolites from between GGA-treated and ethanol-treated control HuH-7 cells, multivariate statistical analysis was performed using MarkerLynx® XS software (Waters). Principal component analysis (PCA) and orthogonal partial least squares-discriminant analysis (OPLS-DA) models were constructed. Cross validation was used to calculate the number of significant components. Potential biomarkers for GGA-treated cells were selected according to variable importance in the projection (VIP) value of more than 1 (1>) in the S-plot.

Statistical analysis was carried out using PASW Statistics 18 (SPSS Japan, Tokyo, Japan). Differences were considered statistically significant if P value was <0.05.

II-3-13. DNA measurement

The cell precipitates, mentioned above, were suspended by 10 mM Tris-HCl, pH 7.4 and 1 mM EDTA buffer (TE) 1 mL, centrifuged at 19300 × g for 8 min at 0ºC, and then the supernatants (100 μL) were diluted with TE (400 μL). 100 μL each of the mixture was put into each well of a 96-well plate. After adding SYBR® Green solution to each well and applying the 96-well plate containing samples to a plate-shaker, DNA measurements were performed with 2030 ARVO™ X4 Multilabel Reader (PerkinElmer, Waltham, MA, USA) in duplicate in order to calculate each validated metabolite contents on cellular basis.

II-4. Results

II-4-1. SCO2 protein was upregulated by GGA treatment.

The *SCO2* gene is one of the p53-target genes and its gene product is involved in respiratory function. First of all, I investigated time-dependent changes in the cellular levels of SCO2 protein after GGA treatment (**Fig. II-1A**). Treatment with 10 μM GGA led to detection of SCO2 protein at as early as 2 h and the protein became most evident at 8 h and decreased at 24 h following the treatment. Next I examined concentration dependence of GGA-induced upregulation of SCO2 protein. The cellular level of SCO2 protein was induced by 6-h incubation with GGA at as low as 2.5 μM and at concentrations of 10 - 50 μM the cellular SCO2 levels increased dramatically, although the cellular level of porin, a mitochondria-resident protein, did not show such a change (**Fig. II-1B**).

As described above, the *SCO2* gene is one of the p53-target genes, which means p53 is able to transactivate the *SCO2* gene. Hence, I measured the cellular levels of the *SCO2* gene transcript to dissect a mechanism of GGA-induced upregulation of SCO2 protein. However, cellular mRNA level of the *SCO2* gene was not essentially induced by addition of GGA (**Fig. II-1C**).

II-4-2. Specificity for GGA in SCO2 protein upregulation.

To examine chemical structure specificity for GGA to induce upregulation of the cellular SCO2 protein level in HuH-7 cells, I tested a couple of GGA-analogous compounds, GGOH and FA (chemical structures are shown in **Fig. II-1D**, lower part) at the same concentration of 10 μM for 16 h. As described above, GGA was repeatedly shown to induce upregulation of the cellular SCO2 protein level, whereas FA showed no activity and GGOH showed only slight activity for the upregulation (**Fig. II-1D**).

II-4-3. Specificity for SCO2 protein in GGA-induced upregulation.

SCO2 is a copper-binding protein involved in formation of the CuA center of the mitochondria-genome encoded cytochrome c oxidase II (COX2 or MT-CO2) subunit as a metallochaperone with SCO1 [53]. So, it was also interested to examine GGA-induced changes in the cellular level of COX2. As shown in **Fig. II-2A**, COX2 protein level was upregulated at as early as 2 h after GGA treatment and the upregulated levels were maintained until 24 h.

Cellular levels of TIGAR, another p53-target energy-metabolism related gene, were further assessed after GGA treatment. **Fig. II-2B** clearly showed GGA-induced immediate upregulation of TIGAR protein level, but no induction was observed in its transcript level (**Fig. II-2C**), as in the case of SCO2 induction with GGA.

II-4-4. Upregulation of cellular F6-P level after GGA treatment.

Next, UPLC/Q-Tof/MS analyses were performed to know how GGA-induced simultaneous upregulation of TIGAR, SCO2 and COX2 proteins, which mimic activation of p53, affects the cellular contents of glycolysis-related metabolites. As shown in **Fig. II-3**, it was indeed found a time-dependent significant increase in the cellular contents of F6-P and a time-dependent decrease in the cellular F1,6-DP contents in GGA-treated cells. The cellular contents of PEP fluctuated after GGA treatment. GGA-treated cells showed a time-dependent increase in the cellular content of NADH (**Fig. II-3**).

II-4-5. Metabolomics changes in GGA-treated cells.

Then, global metabolites were compared in between control and GGA-treated cells. Although total positive ion chromatograms of the cellular metabolites were apparently similar between 24-h GGA-treated cell extracts and 0-h control cell extracts (**Fig. II-4**), the OPLS-DA score plot clearly distinguished the GGA-treated group from control group in triplicate (**Fig. II-5A**). The S-plot analysis was performed to find potential biomarkers for GGA effects. As shown in **Fig. II-5B**, S-plots apparently provide a visual representation of biomarker candidates for both groups.

Especially, spots marked with red square mean important variables contributed for two-group discrimination. In the first quadrant (upper right), spots in a red square were selected as potent markers for GGA-treated cells. On the other hand, the third quadrant (lower left) included several spots in a red square as potent markers lost or decreased in GGA-treated cells. These markers selected by red squares show high score of reliability/responsiveness in the S-plot. Although all of these selected spots have been dropped into database survey connected to Internet (KEGG: Kyoto Encyclopedia of Genes and Genomes <http://www.genome.jp/kegg/>, HMDB: Human Metabolome Database <http://www.hmdb.ca/>, and ChemSpider <http://www.chemspider.com/>) in order to identify each metabolite, which is still in the middle of work identification of these biomarkers.

Among the potent biomarkers suggested in the present study, a spot of 203.2221, indicated by a pink arrow in **Fig. II-5B**, was identified as spermine and a spot of spermine was detected as a potent biomarker also in 2 other pair-wise comparisons between 0-h vs 4-h and between 0-h vs 8-h metabolites (pink arrows indicate a spot of spermine in **Fig. II-6**). Therefore, when the signal intensity of the spermine peak area was plotted along to the time after treatment with GGA, GGA was found to rapidly induce spermine (**Fig. II-7A**). Then, a spot of spermidine, a direct precursor polyamine intermediate of spermine, was searched by its protonated monoisotopic mass (m/z = 146.1657). As shown in **Fig. II-7B**, although GGA upregulated the cellular content of spermine, the cellular content of spermidine rather decreased after GGA treatment.

II-5. Discussion

In chapter II, it has been found that GGA immediately upregulates the cellular protein levels of the *SCO2* and *TIGAR* genes, both of which are p53-target genes in HuH-7 cells. Furthermore, GGA-induced metabolic shift from glycolysis to aerobic respiration found in chapter II is very important for cancer chemoprevention.

Interestingly, GGA-induced upregulation of the *SCO2* and *TIGAR* genes was found at their protein level but not at their mRNA level by GGA treatment. I failed to detect any significant upregulation of these mRNA levels. Therefore, the upregulatory effects of GGA on p53-targeted genes of *SCO2* and *TIGAR* should be post-transcriptional.

Prior to further investigation of a molecular mechanism how GGA induces upregulation of the *SCO2* and *TIGAR* genes at their protein level, it was decided to survey metabolic alterations associated with GGA-induced upregulation of TIGAR and SCO2 protein. At first, pair-wise comparison of several metabolites in metabolome was performed and then it was further validated by quantitative measurement on UPLC/Q-Tof/MS analysis by using each authentic standard compounds. As a result, it was found GGA-induced time-dependent increase of the cellular F6-P level and inversely decrease of the cellular F1,6-DP level, which is consistent with GGA-induced upregulation of TIGAR protein. In other words, these metabolic changes strongly suggest that GGA-induced TIGAR protein was expectedly active to decrease the cellular content of F1,6-DP through its bisphosphatase activity and consequently increase the cellular content of F6-P, indicating that GGA really works as suppressive to glycolysis through upregulation of TIGAR protein level. As described in General Introduction section, TIGAR protein is known to inhibit glycolysis by catalyzing the hydrolysis of both F2,6-DP and F1,6-DP to F6-P [17, 19].

Furthermore, a pair-wise comparison of metabolomes and the following validation by UPLC/Q-Tof/MS analysis revealed another important finding of GGA-induced upregulation of the cellular NADH level (**Fig. II-3**). In the present study, I did not analyze the subcellular distribution of NADH so that I am not aware how NADH was increased after GGA treatment, but one can

easily speculate that GGA might enhance aerobic respiration, because GGA rapidly and efficiently upregulated both of the nuclear *SCO2* and the mitochondrial *COX2* gene products as shown in the present study. Mitochondrial electron transfer chain itself is NADH-consuming system, but it is highly linked to citrate cycle, which is an efficient NADH-producing system. Hence, I speculated that GGA might shift cellular energy metabolism from glycolysis to citrate cycle-aerobic respiration system. In this regard, it is reported important findings that GGA rapidly induces hyperproduction of mitochondrial superoxide and consequent dissipation of $\Delta\Psi m$ [24]. These previous observations, apparently contradictory to the enhanced aerobic respiration, might have better describe GGA-induced accumulation of the cellular NADH as well as GGA-induced cell death in HuH-7 cells.

It is worth noting that metabolomics analysis is very powerful to identify a potential biomarker without any prediction. In chapter II, global comparison of the cellular metabolites in HuH-7 cells after GGA treatment unexpectedly revealed that GGA rapidly and time-dependently upregulated the cellular content of spermine with significant decrease of spermidine. In general, polyamines such as spermine, spermidine and ornithine affect a plethora of cellular processes including transcription, translation, gene expression, autophagy and stress resistance and the regulation of polyamine levels is highly critical for the cell [54]. Although spermidine has an essential and unique role as the precursor for hypusine, which is an unusual amino acid and is found in post-translationally modified elongation factor eIF5A, no unique role for spermine has so far been identified unequivocally [55].

Recently, chemically induced oxidative stress such as tert-butylhydroxyquinone or hydrogen peroxide treatment in HuH-7 cells was reported to increase spermine level in 18 h by activating the transcription of ornithine decarboxylase (ODC) and spermidine/spermine-N^1-acetyltransferase (SSAT) [56]. As mentioned above, GGA also induces superoxide hyperproduction in HuH-7 cells [24], hence, one can easily speculate that GGA may increase the spermine content via gene activation of these polyamine synthetic enzymes. However, the oxidative stress-upregulated

expression of the *ODC* and *SSAT* genes brought to increase also spermidine level [56]. Therefore, GGA-induced specific upregulation of spermine (spermidine was inversely downregulated after GGA treatment) may have a different mechanism from oxidative stress-induced upregulation of polyamines.

In summary, first GGA induced upregulation of the *TIGAR* gene, which might inhibit the glycolysis in HuH-7 cells with p53 mutation. Second GGA also increased the *SCO2* gene expression, which might enhance aerobic respiration. So I speculated GGA might repair the Warburg effect by inhibiting glycolysis and also enhancing oxygen respiration or shifting back to normal mode of energy metabolism in the p53-mutated cells. Third UPLC/Q-Tof/MS-based metabolomics analyses partially support this concept and have provided a working hypothesis that GGA may perturb polyamine metabolism.

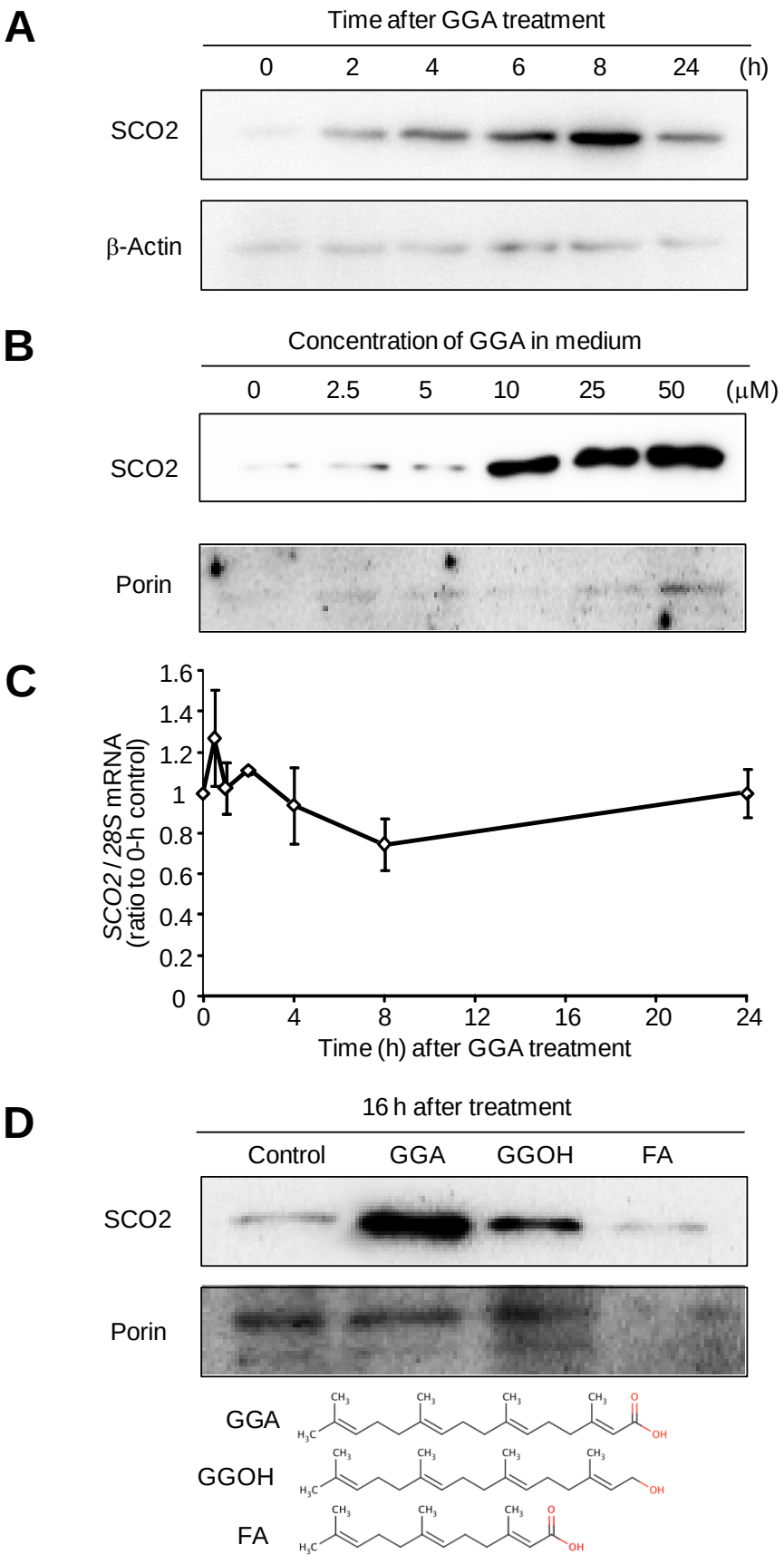
A
Time after GGA treatment
0
2
4
6
8
24
(h)
SCO2
β-Actin
B
Concentration of GGA in medium
0
2.5
5
10
25
50
(μM)
SCO2
Porin
C
SCO2 / 28S mRNA (ratio to 0-h control)
1.6
1.4
1.2
1
0.8
0.6
0.4
0.2
0
0
4
8
12
16
20
24
Time (h) after GGA treatment
D
16 h after treatment
Control
GGA
GGOH
FA
SCO2
Porin
GGA
GGOH
FA

Fig. II-1. Upregulation of the cellular levels of SCO2 protein in HuH-7 cells by GGA treatment.

(A) HuH-7 cells were treated with or without 10 μM GGA for 2, 4, 6, 8 and 24 h. Whole-cell lysates were prepared and SCO2 protein levels were analyzed by western blotting. β-Actin was used as a loading control. (B) HuH-7 cells were treated with or without GGA (2.5-50 μM) for 6 h. Whole-cell lysates were prepared and SCO2 levels were analyzed by western blotting. Porin was used as a loading control. (C) Time course of changes in the cellular mRNA levels of *SCO2* gene relative to *28S rRNA* level after GGA treatment. (D) HuH-7cells were treated with or without 20 μM of GGA, GGOH or FA for 16 h, and SCO2 levels were analyzed by western blotting. Porin was used as a loading control.

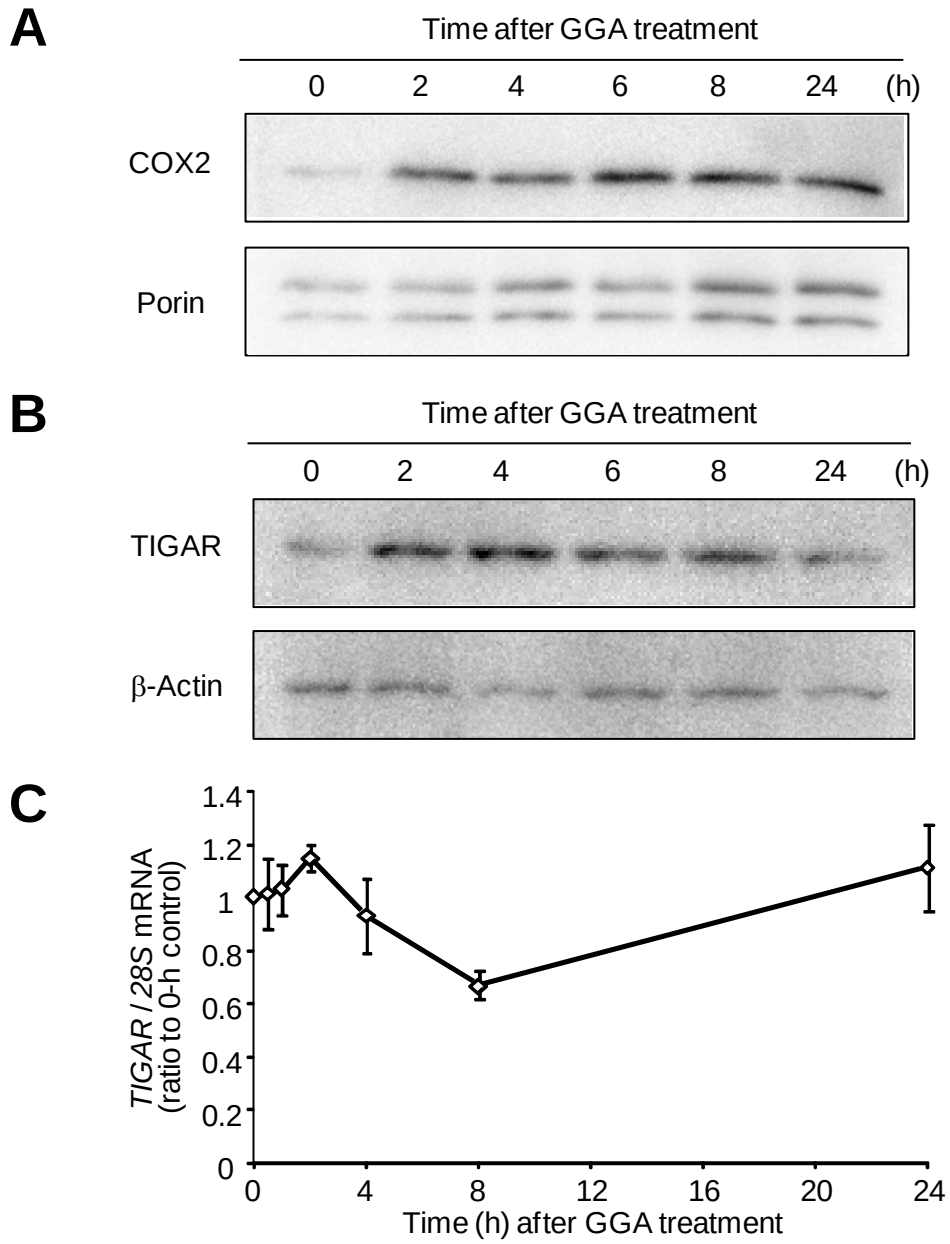

Fig. II-2. GGA-induced upregulation of the cellular COXII and TIGAR protein levels. HuH-7 cells were treated with or without 10 μM GGA for 2, 4, 6, 8 and 24 h. Whole-cell lysates were prepared, and then COX2 (A) and TIGAR (B) levels were analyzed by western blotting. Either porin or β-actin was used as a loading control. (C) Time course of changes in the cellular mRNA level of *TIGAR* gene relative to *28S rRNA* level after GGA treatment.

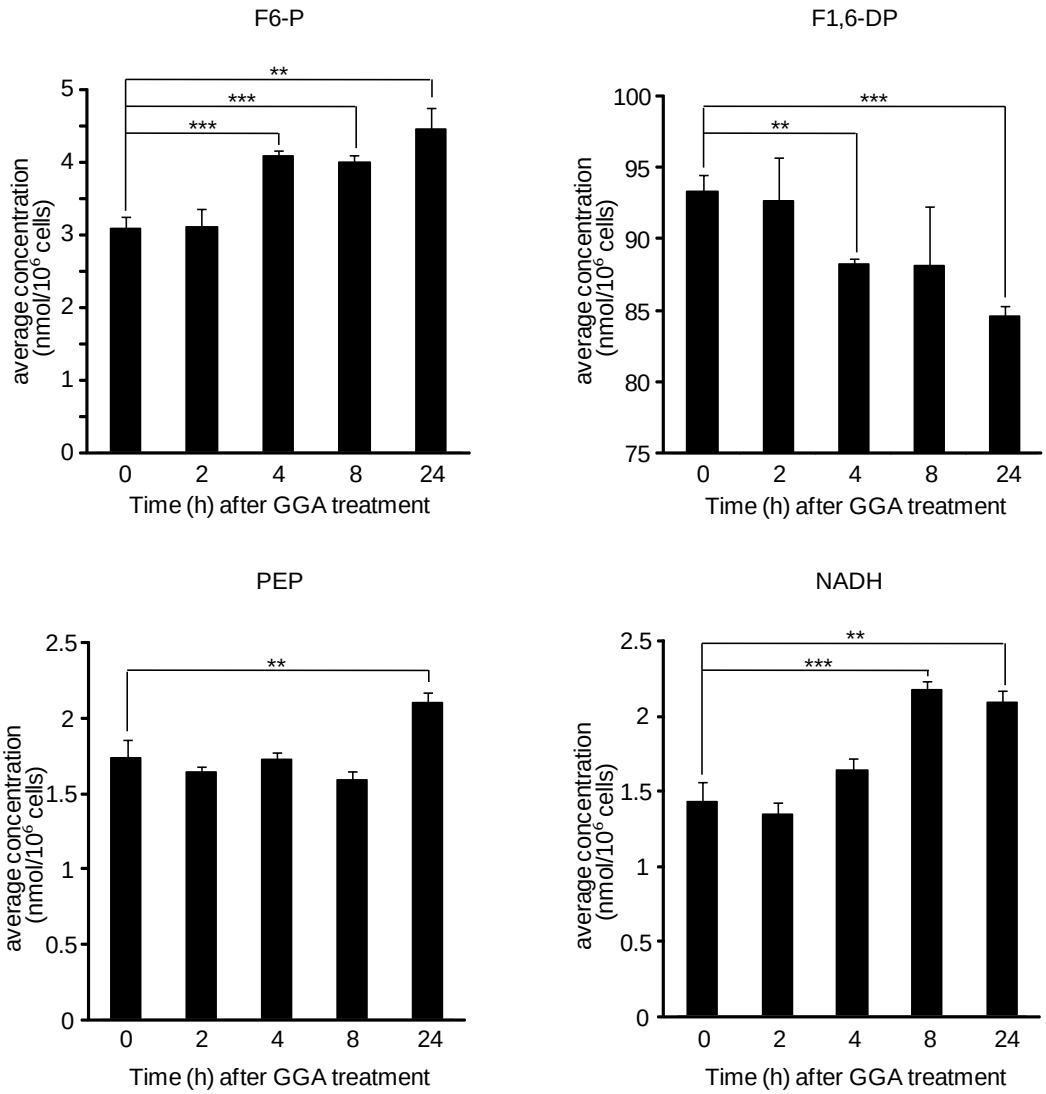

Fig. II-3. Metabolic alterations of glycolysis intermediates after GGA treatment.

HuH-7 cells were treated with or without 10 μM GGA for 2, 4, 8 and 24 h. Pair-wise comparison of each metabolites shown in Fig. II-3 in metabolomics was performed and then the cellular concentrations of each metabolites were further validated by quantitative measurement on UPLC/Q-Tof/MS analysis by using each authentic standard compounds. Columns show average concentrations (nmol/10^6 cells) ±SD (n=3) per cellular basis. All the P values were evaluated by t-test. *, P<0.05, **, P<0.01, ***, P<0.005.

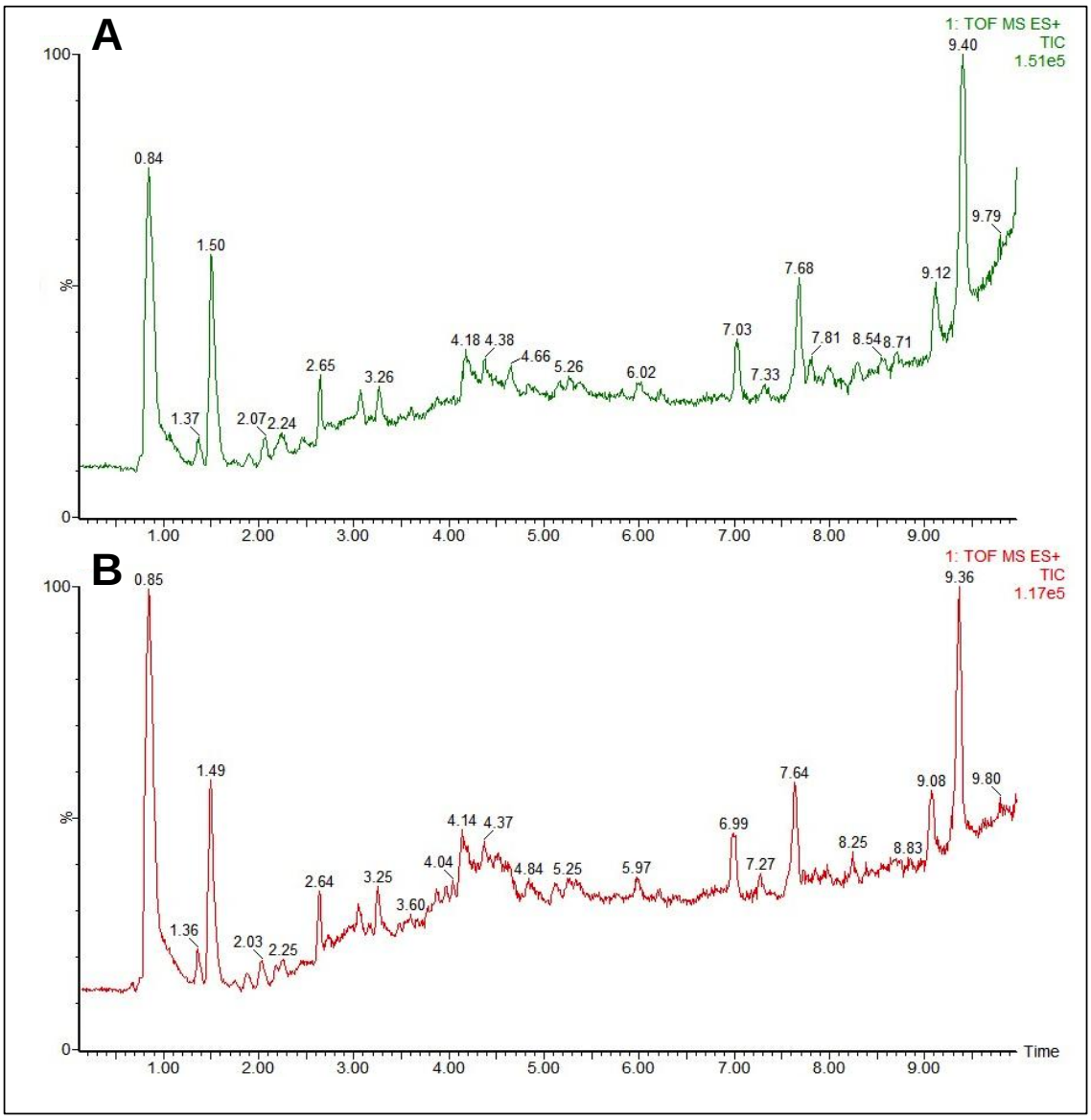

Fig. II-4. Total positive ion chromatograms of the cellular metabolites were apparently similar between 24-h GGA-treated cell extracts and 0-h control cell extracts.

Representative UPLC/Q-Tof/MS total positive ion chromatograms of 24-h GGA-treated HuH-7 cell extracts (A) and 0-h control cell extracts (B).

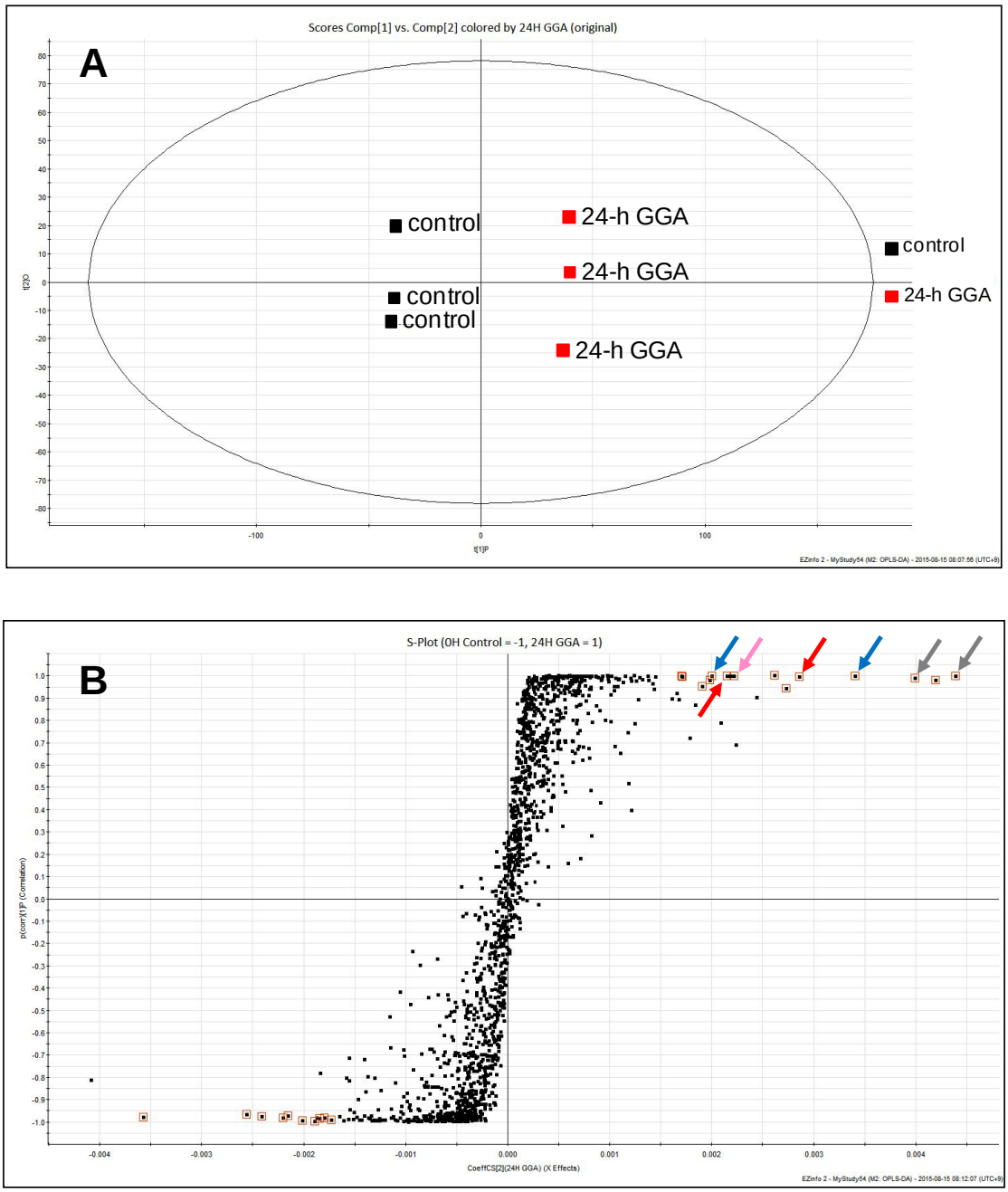

Fig. II-5. OPLS-DA multivariate analyses of the data from ESI positive ion mode of UPLC/Q-Tof/MS.

(A) Score plot. Black square shows 0-h control and red square shows 24-h GGA treated cells. (B) S-plot. Potential biomarkers for GGA-treated cells were selected according to variable importance in the projection (VIP) value of more than 1 (1>) in the S-plot and are marked by red squares. A pink arrow indicates a spot of spermine; blue arrows indicate the potential biomarkers upregulated and identified at 2, 4, 8 and 24 h; red arrows at 4, 8 and 24 h; gray arrows at 8 and 24 h after GGA treatment.

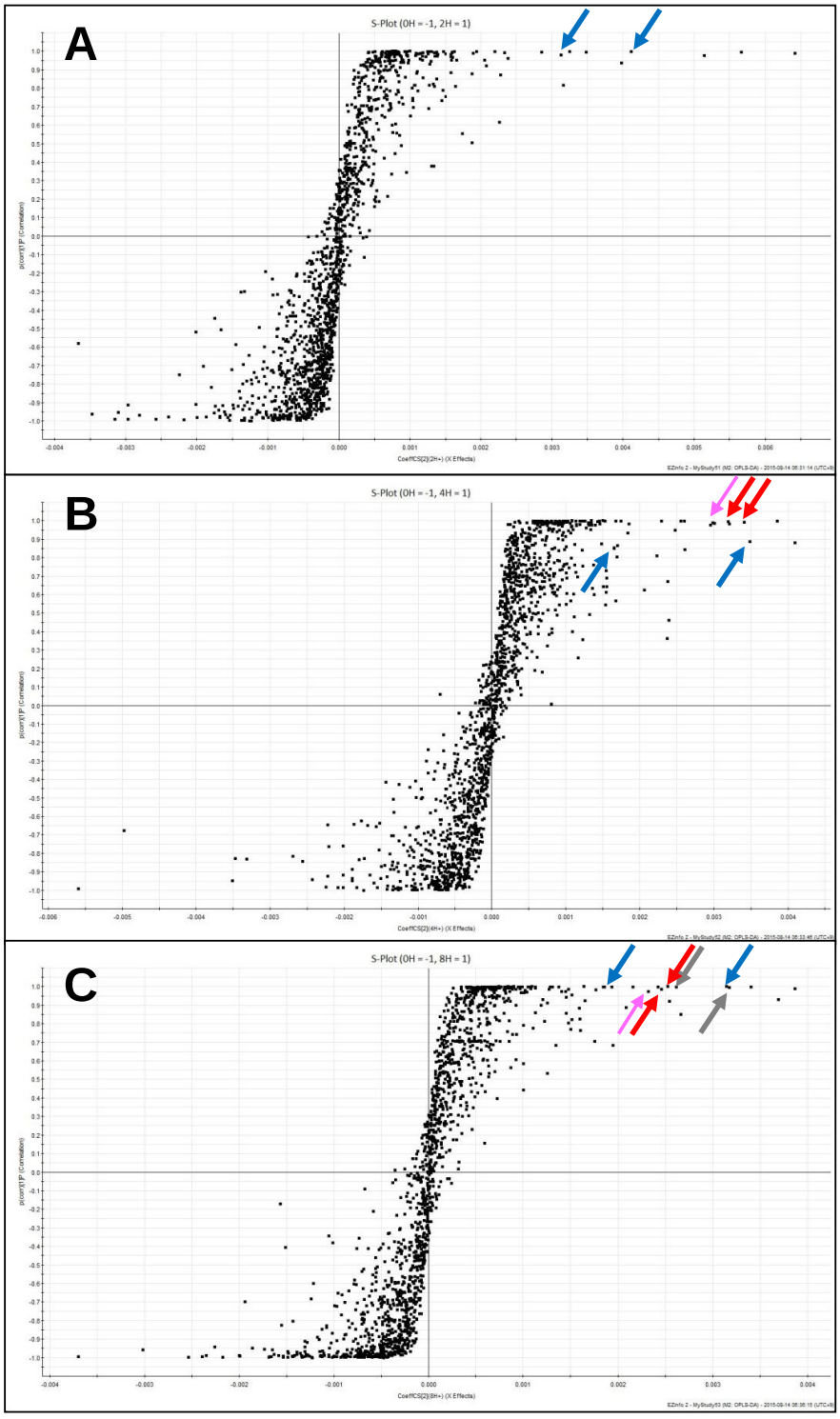

Fig. II-6. OPLS-DA S-plots.

0-h control vs 2-h GGA treated (A), 0-h control vs 4-h GGA treated (B), 0-h control vs 8-h GGA treated (C). A pink arrows indicates a spot of spermine; blue arrows indicate the potential biomarkers upregulated and identified at 2, 4, 8 and 24 h; red arrows at 4, 8 and 24 h; gray arrows at 8 and 24 h after GGA treatment.

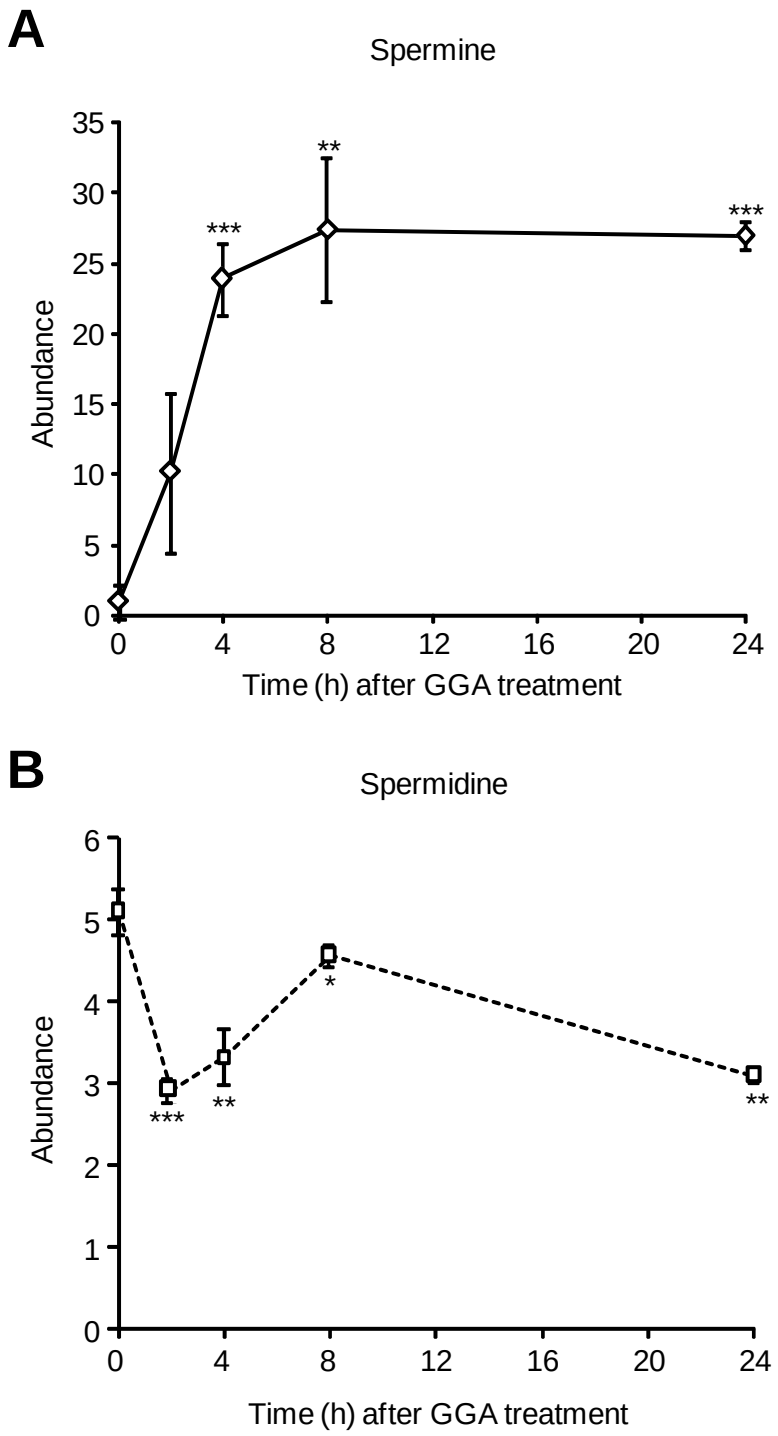

Fig. II-7. Rapid upregulation of the cellular spermine level after GGA treatment in HuH-7 cells.

From pair-wise comparison of 24-h GGA-treated metabolomes shown in Fig. II-5 and 2, 4 and 8-h metabolomes shown in Fig. II-6 against 0-h control metabolome was performed with the protonated monoisotopic mass of 203.2236 for spermine (A) and 146.1657 for spermidine (B) and then the signal intensity of each peak area was plotted against time after GGA treatment. *, $P<0.05$, **, $P<0.01$, ***, $P<0.005$.

Chapter III

Induction of nuclear translocation of mutant cytoplasmic p53 by GGA in HuH-7 cells

Chieko Iwao
Yoshihiro Shidoji

Induction of nuclear translocation of mutant cytoplasmic p53 by geranylgeranoic acid in a human hepatoma cell line.

Scientific Reports (2014) ***4****: 4419 / DOI: 10.1038/srep04419*

Molecular and Cellular Biology, Graduate School of Human Health Science,
University of Nagasaki, Nagasaki, Japan

III-1. Abstract

Mutant p53 proteins in human hepatoma cell lines such as HuH-7 (Y220C) and PLC/PRF/5 (R249S) accumulate in the cytoplasm, and lose their transcriptional function. Geranylgeranoic acid (GGA) is a naturally occurring acyclic diterpenoid that induces cell death in both cell lines, but not in HepG2 cells harboring wild-type p53. Here, it is demonstrated that micromolar concentrations of GGA induce a rapid nuclear translocation of cytoplasmic p53 in both p53-mutant cell lines and p53 knockdown attenuates GGA-induced cell death in HuH-7 cells. Cell-free experiments demonstrate that GGA is able to release 670-kD p53-containing complexes from putative huge macromolecular aggregates in post-mitochondrial fractions as revealed on blue-native gradient PAGE. Among several p53-target genes tested, GGA upregulates *PUMA* gene expression, and ivermectin, an inhibitor for importin α/β, blocks GGA-induced nuclear translocation of cytoplasmic p53 and suppresses GGA-induced upregulation of *PUMA* mRNA levels in HuH-7 cells. Taken together, these data suggest that GGA treatment stimulates a nuclear translocation of mutant p53 through its dissociation from cytoplasmic aggregates, which may be essential for GGA-induced cell death.

III-2. Introduction

The structure, function, and clinical significance of the p53 tumor suppressor protein in oncology have been previously described in extensive detail [57, 58]. The p53 transcription factor responds to diverse stresses (including DNA damage, overexpressed oncogenes, and various metabolic limitations) to regulate many target genes that induce cell-cycle arrest (e.g., *p21* or *CDKN1A* as provided by the HUGO Nomenclature Committee [HGNC]), cell death (e.g., *PUMA*, or *BBC3*, BCL2 binding component 3, as indicated by HGNC), respiration (e.g., *SCO2*), and inhibition of glycolysis (e.g., *TIGAR*) [16]. All of these p53 targets have been linked to p53-mediated prevention of tumorigenesis.

Among these targets, the *PUMA* gene is particularly interesting in terms of cancer prevention, as the gene was identified as a p53-dependent potent inducer of mitochondria-mediated cell death in diverse tissues and cell types [59]. PUMA is one of the BH-3-only proteins, which induce the mitochondrial outer membrane permeability transition. Therefore, overexpression of PUMA causes hyperproduction of ROS from mitochondria, resulting in mitochondria-mediated cell death. Although PUMA is well established as an essential component of p53-mediated apoptosis [59], PUMA also contributes to induction of autophagy during p53-dependent cell death [60].

Almost half of clinical cancers have been reported to harbor mutations in the *TP53* gene [58]. In clinical cancers, most mutation hotspots reside in the core or DNA-binding domain of p53. Mutations in the core domain give rise to either loss of function or gain of function in p53 transcriptional activity. In terms of cellular fate of the *TP53* mutations, mutations in the core domain can be subdivided into two groups with distinct functional consequences: p53 enhanced degradation or p53 cytoplasmic accumulation [61, 62].

Several p53-interacting proteins have been reported to be involved in its cytoplasmic sequestration, blocking it from degradation as well as restricting its access to the nuclear compartment, where p53 plays a role in transcription. Among the p53-interacting proteins, the 250-kDa CUL9 (previously named PARC, p53-associated, parkin-like cytoplasmic protein, by

HGNC), a member of the cullin family and a potential E3 ubiquitin ligase [63], is one of the major players that sequester p53 in cytoplasm. The CUL9 N-terminus binds the C-terminus of p53 and forms an approximately 1-MDa multi-protein complex that then blocks transport of cytosolic p53 into the nucleus, thus retaining p53 in cytoplasm [64].

p53 has attracted much attention over recent years in the autophagy field, as p53 exhibits dual distinct roles in autophagy [65]. p53 transactivates the autophagy-related gene *DRAM* (damage-regulated autophagy modulator) [66], which is required for p53's ability to induce autophagy [67]. Cytoplasmic p53 has been shown to repress autophagy via poorly characterized mechanisms [68].

Shidoji and his colleague previously examined the molecular mechanism underlying second primary hepatoma-preventive action of the polyprenoic acid, and showed that GGA induces cell death of human hepatoma-derived HuH-7 and PLC/PRF/5 cells, both of which have p53 protein mutated in the core domain. In contrast, cell death was not observed after GGA treatment of wild-type *TP53* homozygote cells, such as mouse primary hepatocytes and human hepatoblastoma-derived HepG2 cells, in FBS-free medium [1].

During GGA-induced cell death, HuH-7 cells display dissipated inner membrane potential of mitochondria [3, 24]. This mitochondria-involved cell death showed characteristics of apoptosis, such as chromatin condensation as revealed by Hoechst staining. However, caspase inhibitors were unable to block GGA-induced cell death [3]. These results suggest that GGA-induced cell death is not a typical apoptotic process, but might be a caspase-independent and non-necrotic cell death. Recently, Okamoto et al found that GGA provides substantial accumulation of autophagosomes under serum starvation conditions in human hepatoma cells [24]. Autophagy-inducing stimuli should cause the depletion of cytoplasmic p53, which in turn is required for the induction of autophagy [68].

In chapter III, I speculated that the mutant p53 accumulated in the cytoplasm of HuH-7 cells might disturb GGA-induced accumulation of autophagosomes. In other words, GGA should act on

the accumulated p53 to remove it from the cytoplasmic compartment, translocating the cytoplasmic p53 into the nucleus and potentially reactivating the mutant p53 to induce cell death. In chapter III, it was found that a rapid nuclear translocation of p53 occurred after GGA treatment of HuH-7 cells. To evaluate the mechanism by which GGA translocates mutant cytoplasmic p53 to the nucleus, native forms of the cytoplasmic p53 were analyzed by applying GGA to post-mitochondrial fractions in a cell-free system.

III-3. Materials and Methods

III-3-1. Cell culture and drug treatment

Human hepatoma-derived HuH-7 (p53 Y220C), PLC/PRF/5 (p53 R249S), and HepG2 (p53 WT) cells were cultured in Dulbecco's modified Eagle's medium (D-MEM) (Wako, Osaka, Japan) supplemented with 5% fetal bovine serum (FBS). Hep3B cells (p53 null) were maintained in D-MEM containing 10% FBS and MEM non-essential amino acid solution (Sigma Aldrich, St. Louis, MO, USA). HuH-7, HepG2, and PLC/PRF/5 cells were obtained from the RIKEN cell bank (Tsukuba, Japan) and Hep3B cells were from DS Pharma Biomedical (Osaka, Japan). The cells were cultured with D-MEM containing 5% or 10% FBS for 2 days and the medium was replaced with FBS-free D-MEM 1 day before GGA treatment. GGA was a generous gift from Kuraray Company (Okayama, Japan).

To block nuclear translocation of p53, HuH-7 cells were treated with ivermectin (Sigma Aldrich) at a concentration of 2.5 μM for 1 h before the treatment of 20 μM GGA supplemented with 2.5 μM ivermectin.

III-3-2. Reverse-transcription real-time polymerase chain reaction (PCR)

HuH-7, PLC/PRF/5, HepG2, and Hep3B cells were treated with GGA (final concentrations of 2.5–50 μM in medium) or vehicle alone, and total RNA was isolated using the QuickGene RNA Cultured Cell Kit S (Wako) with QuickGene-810 (Kurabo, Osaka, Japan). Complementary DNA was generated using the Transcriptor® First Strand cDNA Synthesis Kit with random hexamer (Roche Diagnostics, Basel, Switzerland). Nucleotide sequences of the PCR primers, including those for the *p21*, *PUMA*, *TIGAR*, *SCO2*, *DRAM*, and *28S rRNA* cDNAs, are listed in **Table III-1**. Real-time PCR was performed with DyNAmo™ Capillary SYBR® Green qPCR Master mix (Finnzymes, Espoo, Finland), and cDNA on LightCycler1.5 (Roche Diagnostics) under conditions described in **Table III-2**.

Table III-1. The nucleotide sequences of each primers used for real time RT-PCR

Genes	Primer	Sequence (5' – 3')
p21	F	CTGGAGACTCTCAGGGTCGAAA
	R	GATTAGGGCTTCCTCTTGGAGA
PUMA	F	CCCAAGACTGTTGGGTCTG
	R	GCCGTAGTAATCCGTGAAGAG
TIGAR	F	CCAACGGTTCAGTGTATTTGTATG
	R	AGAACTAGCAGAGGAGAGAAGTAA
SCO2	F	CCCAAGACTGTTGGGTCTG
	R	GCCGTAGTAATCCGTGAAGAG
DRAM	F	CGCCTTCATTATCTCCTACG
	R	CGAAACATCCCACCAATCCA
28S rRNA	F	TTAGTGACGCGCATGAATGG
	R	TGTGGTTTCGCTGGATAGTAGGT

F: forward primer, R: reverse primer

Table III-2. The conditions of thermal cycler for real-time RT-PCR of *p21*, *PUMA*, *TIGAR*, *SCO2*, *DRAM* and *28s rRNA*.

	p21	
	Temperature	Slope
Denature	95ºC, 600 s	20ºC / s
PCR (45 cycles)	95ºC, 10 s 65ºC, 20 s 72ºC, 20 s	20ºC / s
Melting	95ºC, 0 s 57ºC, 15 s 98ºC, 0 s	20ºC / s 0.1ºC / s
Cooling	40ºC, 30 s	20ºC / s

	PUMA	
	Temperature	Slope
Denature	95ºC, 600 s	20ºC / s
PCR (40 cycles)	95ºC, 10 s 61ºC, 20 s 72ºC, 15 s	20ºC / s
Melting	95ºC, 0 s 61ºC, 15 s 98ºC, 0 s	20ºC / s 0.1ºC / s
Cooling	40ºC, 10 s	20ºC / s

	TIGAR	
	Temperature	Slope
Denature	95ºC, 600 s	20ºC / s
PCR (45 cycles)	95ºC, 10 s 56ºC, 20 s 72ºC, 15 s	20ºC / s
Melting	95ºC, 0 s 57ºC, 15 s 98ºC, 0 s	20ºC / s 0.1ºC / s
Cooling	40ºC, 10 s	20ºC / s

	SCO2	
	Temperature	Slope
Denature	95ºC, 600 s	20ºC / s
PCR (40 cycles)	95ºC, 10 s 56ºC, 20 s 72ºC, 20 s	20ºC / s
Melting	95ºC, 0 s 57ºC, 15 s 98ºC, 0 s	20ºC / s 0.1ºC / s
Cooling	40ºC, 30 s	20ºC / s

	DRAM	
	Temperature	Slope
Denature	95ºC, 600 s	20ºC / s
PCR (60 cycles)	95ºC, 10 s 55ºC, 10 s 72ºC, 20 s	20ºC / s
Melting	95ºC, 0 s 65ºC, 15 s 95ºC, 0 s	20ºC / s 0.1ºC / s
Cooling	40ºC, 30 s	20ºC / s

	28s rRNA	
	Temperature	Slope
Denature	95ºC, 600 s	20ºC / s
PCR (40 cycles)	95ºC, 15 s 60ºC, 30 s	20ºC / s
Melting	95ºC, 0 s 65ºC, 15 s 95ºC, 0 s	20ºC / s 0.1ºC / s
Cooling	40ºC, 30 s	20ºC / s

III-3-3. Immunoblotting

After GGA (20 μM) treatment, HuH-7, PLC/PRF/5, HepG2, and Hep3B cells were lysed with RIPA buffer and proteins were quantified using the Bradford assay (Bio-Rad, Hercules, CA, USA). Equal amounts (5–30 μg) of protein were separated by SDS-PAGE and transferred to semi-dry blotted PVDF membranes (Bio-Rad). Membranes were probed with a mouse monoclonal antibody against p53 (Clone BP53-12, Sigma Aldrich), rabbit polyclonal antibodies against PUMA (ab54288, Abcam, Cambridge, UK), phospho-p53 (phosphorylated at Ser^{15}) (Ab-3, Calbiochem, Darmstadt, Germany), acetyl-p53 (acetylated at Lys^{379}) (#2570, Cell Signaling Technology, Boston, MA, USA), β-actin (#4967, Cell Signaling Technology), porin (Ab-5, Calbiochem), and β-III-tubulin (T2200, Sigma Aldrich). HRP (horseradish peroxidase)-labeled secondary antibodies were detected with Immobilon Western Chemiluminescent HRP substrate (Merck Millipore, Billerica, MA, USA) on an ImageQuant LAS 4000 (GE Healthcare, Tokyo, Japan).

III-3-4. Immunofluorescence

After 20 μM GGA or ethanol treatment, HuH-7 and PLC/PRF/5 cells on a glass insert in a 24-well plate were rinsed with PBS(-) and fixed for 40 min with 4% paraformaldehyde containing 2% sucrose in PBS(-) and then rinsed with PBS(-). The cells were permeated with 0.5% TritonX-100 and blocked with 10% FBS. The cells were then incubated at 4ºC overnight with a monoclonal anti-p53 antibody (Cell Signaling Technology), followed by a 2.5 h incubation with an Alexa-488-labeled goat anti-mouse IgG antibody (Invitrogen, Molecular Probes, Tokyo, Japan). After rinsing with PBS(-), the cells were mounted in ParmaFluor (Beckman Coulter, Brea, CA, USA), covered on a slide glass, and observed under a confocal laser-scanning fluorescence microscope, an LSM700 2Ch URGB equipped with Axio Observer Z1 Bio (Carl Zeiss, Göttingen, Germany).

III-3-5. Subcellular fractionation and treatment with GGA

HuH-7 and HepG2 cells were washed on ice with ice-cold PBS(-), scraped off in PBS(-) and centrifuged at 500 × *g* for 5 min. The resultant cell pellets were gently suspended with PBS(-) and homogenized with a Dounce-type homogenizer on ice. The cell lysates were centrifuged at 600 × *g* for 14 min at 4°C to separate the nuclear fraction (pellet). The supernatant was centrifuged at 14,300 × *g* for 15 min at 4°C to obtain the post-mitochondrial fraction (supernatant), which contains other smaller organelles than mitochondria such as microsomes (fragmented endoplasmic reticulums), peroxisomes and lysosomes, and cytosol. The washed pellet was re-suspended with PBS(-) as the mitochondrial fraction. The post-mitochondrial fraction was centrifuged at 105,000 × *g* and 348,900 × *g* for 90 min at 4°C. The supernatants from the two centrifugations were designated as the cytosolic fraction and 348,900 × *g* supernatant fraction, respectively.

GGA (final concentration of 0–20 μM) was added to each above-described subcellular fraction (10 μg protein each), and samples were vortexed and incubated overnight at 4°C under dark conditions until electrophoresis.

III-3-6. BN-gradient PAGE followed by immunoblotting

After overnight incubation with GGA (0–20 μM), samples were prepared with 4 × Native PAGE™ Sample Buffer (Invitrogen) and subjected to electrophoresis at room temperature on 4–16% gradient Native PAGE Bis-Tris gels (Invitrogen) with a light-blue cathode buffer, according to the manufacturer's instructions. The separated proteins were blotted to a PVDF membrane under semi-dry conditions. The proteins on the membranes were fixed with 8% acetic acid for 15 min, rinsed with deionized water, and briefly air-dried. The membranes were washed in methanol to remove excess Coomassie blue dye, rinsed with deionized water, shaken in PBS-T (PBS(-) containing 0.1% polyoxyethylene sorbitan monolaurate) for 5 min, blocked in 5% skim milk in PBS-T for 1 h at room temperature, and incubated overnight with an anti-p53 monoclonal antibody (Sigma Aldrich).

III-3-7. Cross-linking SDS-PAGE

Prior to addition of a cross-linking agent, the pH of the solutions containing samples from GGA (0–20 μM) treatment in cell-free experiments was adjusted between 6.5 and 7.5 with 2 M HCl. The samples were then incubated with a 0.04 mM BMH (bis(maleimido) hexane; Pearce Biotechnology, Rockford, IL, USA) cross-linker for 2 h at 4°C. The non-reacted cross-linking agent was then quenched with 42 mM dithiothreitol, and the samples were subjected to SDS-PAGE followed by immunoblotting analysis.

III-3-8. Co-immunoprecipitation

After treatment with GGA (0–20 μM), the samples were incubated with normal rabbit IgG or the polyclonal anti-PARC antibody at 4°C for 1 h with gentle mixing. The immune complexes were precipitated with EZview Red Protein G Affinity Gel beads (Sigma Aldrich), which were pre-washed with PBS(-) twice for 1 h at 4°C with gentle mixing. The nonspecifically bound proteins were removed by washing the beads with PBS(-) three times at 4°C. The beads in PBS(-) were centrifuged for 30 s at 8,200 × *g*. The pellet was resuspended with 25 μL of PBS(-) and 2 × sample buffer, and the samples (10 μL) were subjected to SDS-PAGE and immunoblotting analysis.

III-3-9. Dual luciferase assay

HuH-7 cells were seeded in 96-well plates 1 day before transfection. Either the Cignal p53 reporter vector containing a p53-responsive consensus sequence (100 ng/well; Qiagen, Tokyo, Japan) or the PUMA Frag1-Luciferase vector containing the p53-responsive 5′-upstream regulatory region of the *PUMA* gene (120 ng/well; Addgene, Cambridge, MA, USA) and the pRL-SV40 control vector (3 ng/well; Promega, Tokyo, Japan) were co-transfected using Lipofectamine 2000 (Invitrogen) and cells were incubated overnight. The cells were treated with GGA (0–20 μM) after transfection, and firefly and renilla luciferase activities were analyzed by the Dual-Luciferase Reporter Assay System (Promega). The intensity of chemiluminescence was measured with CentroXS^3 (Berthold Technologies Japan, Tokyo, Japan).

III-3-10. Transfection with small interfering RNA (siRNA)

p53 siRNAs (sense: 5'-AGA-CCU-AUG-GAA-ACU-ACU-Utt-3') were purchased from FASMAC (Kanagawa, Japan). For transfection, HuH-7 cells were seeded on 3-cm dishes (Thermo Fisher Scientific, Nunc, Roskilde, Denmark) at a density of 3 or 5 × 10^4 cells/dish. Following incubation overnight, p53 siRNA or control siRNA-A (Santa Cruz Biotechnology, Santa Cruz, CA, USA) were transfected using Lipofectamine® 2000 (Thermo Fischer Scientific, Invitrogen, Tokyo, Japan) according to the manufacturer's instructions. Following incubation for 96 h, the cells were treated with GGA (0-20 μM). After GGA treatment, viable cell counting was performed using the Trypan Blue dye exclusion method (Sigma Aldrich).

III-4. Results

III-4-1. GGA treatment upregulates *PUMA* gene expression in HuH-7 cells

As repeatedly reported, GGA induces cell death in HuH-7 cells [2, 3]. In chapter 1, to clarify a molecular mechanism of GGA-induced cell death in the mutant *TP53* gene-harboring cells, I focused my attention on p53-target, energy metabolism-related genes, *SCO2* and *TIGAR*. As a result, a rapid increase in the cellular protein levels of SCO2 and TIGAR was found. Therefore, other p53 target genes expression was investigated. Especially PUMA is a critical mediator of p53-dependent and -independent cell death [59]. Treatment with 20 μM GGA clearly induced expression of *PUMA* mRNA levels as early as 2 h after treatment (**Fig. III-1A**). At 8 h, the levels reached almost 17.7-fold higher than control levels. In contrast, the mRNA levels of all other p53-target genes tested, including *TIGAR*, *DRAM*, *p21*, and *SCO2*, were not significantly induced after 24 h of GGA treatment, except that the cellular p21 mRNA levels were marginally up-regulated at this time point (**Fig. III-1A**). Furthermore the cellular level of PUMA protein relative to β-actin was slightly higher after 4 h of 20 μM GGA treatment, which occurred slightly after GGA induction of the *PUMA* mRNA level (**Fig. III-1B**).

III-4-2. Mutant p53 is involved in GGA-induced cell death of HuH-7 cells.

In order to know whether mutant p53 is involved in GGA-induced cell death, p53 knockdown experiment was conducted. Although the cellular levels of p53 in HuH-7 cells transfected with p53 siRNA were not completely knocked down, a significant down-regulation of cellular p53 levels was observed and GGA treatment did not change the cellular p53 levels (**Fig. III-2A**). However, GGA-induced cell death was significantly blocked in p53-siRNA-treated cells (**Fig. III-2B**), indicating that p53 knockdown indeed rescued cell death induced by GGA, confirming that GGA works through the mutant p53 in HuH-7 cells.

III-4-3. Mutant p53 relocates from the cytoplasm to the nucleus by GGA treatment

As it was proved that the mutant p53 might play a role in GGA-induced cell death in HuH-7 cells, it was speculated that GGA might translocate the mutant p53 into the nucleus to transactivate its target genes. As shown in **Fig. III-3A**, the cellular accumulation of the mutant p53 was observed in HuH-7 cells under basal conditions, compared with three other hepatoma cell lines. Changes in the subcellular localization of the accumulated p53 protein during GGA treatment were next investigated. At first, GGA-induced changes in the subcellular distribution of p53 were measured by subcellular fractionation followed by western blotting. Although I found that GGA treatment decreased the cytoplasmic p53, I failed to demonstrate GGA-induced nuclear accumulation of p53 (**Fig. III-3B**). However, as clearly shown in **Fig. III-3C**, an immunofluorescence technique revealed that the p53 protein in non-treated HuH-7 cells accumulated as reticular forms in the cytoplasm and was completely excluded from the nucleus, whereas GGA treatment for 3 h induced a dramatic subcellular shift of the p53 protein from the cytoplasm to the nucleus. At 6 h after addition of GGA, the cytoplasmic levels of p53 became undetectable. In other words, almost all of the cellular p53 concentrated in the nucleus and no p53 remained in the cytoplasm 6 h after GGA treatment. Furthermore, transient post-translational modifications of p53, such as Ser-15 phosphorylation [69] and Lys-379 acetylation [70], indicators for nuclear translocation, were induced by addition of GGA at 2 h (**Fig. III-3D**).

A possibility was next evaluated whether GGA-induced nuclear translocation was observed in PLC/PRF/5 cells, in which a lower cellular accumulation of mutant p53 was detected (**Fig. III-3A**). PLC/PRF/5 cells accumulated p53 in the cytoplasm in normal culture conditions, similar to HuH-7 cells (**Fig. III-3E**). PLC/PRF/5 cells also showed translocation of p53 from the cytoplasm to the nucleus by 3 h of GGA treatment, and a trivial amount of p53 remained in the cytoplasm 6 h after GGA treatment (**Fig. III-3E**).

III-4-4. GGA-induced changes in native forms of p53 in the cytoplasmic space

To elucidate the mechanism by which cytoplasmic p53 translocates to the nucleus upon GGA treatment, the post-mitochondrial fraction was used to examine a direct effect of GGA on native forms of p53 in the cytoplasm, as mutant p53 accumulates mostly in this fraction in HuH-7 cells, but less either in the cytosol or mitochondria fraction (**Fig. III-4A**).

Fig. III-4B clearly shows large native forms of p53 in the post-mitochondrial fractions using blue-native (BN)-gradient PAGE. Unfortunately, I failed to detect major p53-positive bands, but observed a faint, vague, and broad 670-kD band on the blot of the BN-gradient gel with control post-mitochondrial fractions, indicating that most of the cytoplasmic p53 could be too large in size to penetrate into the gradient gel. Relatively dense bands of a p53-containing complex were able to detected at a molecular size of around 670 kD with samples incubated with GGA (**Fig. III-4B**). More importantly, the total amount of p53 that penetrated into the BN-gradient gel increased in a GGA concentration-dependent manner (**Fig. III-4B**), whereas in ordinary SDS-PAGE, the total amount of p53 stayed constant in post-mitochondrial samples incubated with any concentrations of GGA (**Fig. III-4C**). Interestingly, a 210-kD complex of p53 (the molecular size equivalent to a p53 homotetramer) was evident in all GGA-treated samples (**Fig. III-4B**). Such changes were not observed with HepG2 cells (wild-type p53 control cell line).

Because of the relatively poor resolution of the BN-gradient PAGE, cross-linking SDS-PAGE was next used to examine GGA-induced changes in native forms of p53. In HuH-7 post-mitochondrial preparations incubated with increasing concentrations of GGA, a few major bands of p53-positive complexes larger than 250 kD were also detected by cross-linking SDS-PAGE (**Fig. III-4D**). Moreover, unlike the BN-gradient PAGE, a band of p53 monomer was detected in GGA-containing samples. These results were not observed with post-mitochondrial fractions of HepG2 cells and no GGA-induced changes were detected on the cross-linking SDS-PAGE membrane using HepG2 cells.

Both BN-gradient PAGE and cross-linking SDS-PAGE experiments strongly indicate that in HuH-7 cells prior to GGA treatment, most of the cytoplasmic p53 may exist as huge complexes larger than 670 kD, which do not enter the BN-gradient gel, and cell-free treatment with GGA reduced the molecular size of the cytoplasmic p53-containing complex down to 670 kD and less.

III-4-5. p53 is released from putative huge complexes with GGA treatment

The GGA-induced p53 complex of >250 kD disappeared from the gel when the same experiment was conducted with the cytosolic fraction instead of the post-mitochondrial fraction (**Fig. III-5A**), suggesting that the cytoplasmic p53 forms a huge multi-protein complex that sediments after 105,000 × *g* for 90 min or sticks to organelles, such as the endoplasmic reticulum.

Studies from the literature have reported one of the possible huge complexes of cytoplasmic p53 is the CUL9/PARC multi-protein complex, with a molecular size of approximately 1 MD [71]. In the post-mitochondrial fractions from HuH-7 cells, p53 was able to successfully co-immunoprecipitate with anti-PARC in the absence of GGA (**Fig. III-5B**), indicating that part of the cytoplasmic p53 might be complexed with PARC. Interestingly, the amount of p53 that co-immunoprecipitated with PARC was reduced after cell-free incubation of GGA in a concentration-dependent manner, indicating that p53 could be directly released from the PARC complex by addition of GGA in a cell-free system.

Another possibility for the large p53-containing complexes involving the interaction of p53 with microtubules was tested, based on the theory in which cytoplasmic p53 forms a tetramer when p53 moves into nuclei via microtubules [72]. As described above, cross-linking SDS-PAGE followed by western blotting with anti-p53 revealed that GGA induced the p53 complex of over 250 kD, as shown in **Fig. III-4D** and **Fig. III-5C**. When this membrane was re-probed with an anti-β-III-tubulin antibody, co-existence of tubulin with p53 in the >250 kD complex was detected, but most of β-III-tubulin was not detected in the control post-mitochondrial fraction probably because of cross-linking of α/β-subunit assembly by tubulin filaments (**Fig. III-5D**).

III-4-6. Nuclear translocation of mutant p53 upregulates *PUMA* mRNA levels in HuH-7 cells

It was next speculated whether GGA-induced nuclear translocation of p53 was involved in GGA-induced upregulation of *PUMA* mRNA levels in HuH-7 cells. Ivermectin, a newly established inhibitor specific against importin α/β-mediated nuclear import [73], was used to block GGA-induced nuclear translocation of p53. The drug suppressed GGA-induced nuclear translocation of p53 in HuH-7 cells and most of the cytoplasmic p53 remained around the perinuclear regions after 3 h of treatment with GGA (**Fig. III-6A**). Furthermore, it was found that ivermectin also significantly suppressed GGA-induced upregulation of *PUMA* mRNA, although *PUMA* mRNA levels were still up-regulated by 4.5-fold with GGA-induction in the presence of ivermectin (**Fig. III-6B**).

These findings led me to speculate whether GGA-induced nuclear-translocated mutant p53 is able to function in the transactivation and upregulation of *PUMA* gene expression. The impact of GGA on transcriptional activation of the *PUMA* gene was next evaluated by using p53 response elements. In a luciferase reporter assay using a standard p53-responsive consensus sequence, GGA treatment did not upregulate reporter gene expression, and even downregulated it in a dose-dependent manner (**Fig. III-6C**). In contrast, the reporter assay using the p53-responsive 5′-upstream regulatory region of the *PUMA* gene demonstrated GGA-induced upregulation of the reporter gene in a time-dependent manner (**Fig. III-6D**).

III-5. Discussion

GGA is a cancer-preventive diterpenoid that has been recently shown to induce mitochondria-mediated cell death with an incomplete autophagic response in HuH-7 cells [24]. In chapter 2, I have clearly demonstrated that mutant p53 that accumulates in the cytoplasm of human hepatoma cell lines, including HuH-7 and PLC/PRF/5, is translocated to the nuclear compartment immediately after treatment with GGA. Furthermore, p53 knockdown experiment clearly demonstrated that the mutant p53 might play an essential role in GGA-induced cell death. Therefore, prior to scrutiny at the molecular level as to the downstream signals of p53 occur in the GGA-treated hepatoma cell lines, it may be important to determine how GGA translocates cytoplasmic p53 to the nucleus.

In general, cytoplasmic accumulation of mutant p53 can be caused both by blocking proteasomal degradation of p53 as mediated by its binding with MDM2, a p53-specific E3 ubiquitin protein ligase, and by sequestration of p53 via formation of large p53-containing aggregates with other p53-binding cytoplasmic proteins, such as CUL9/PARC [74], heat-shock proteins (HSPs) [75, 76] , and other proteins. It is reasonable to speculate that GGA that penetrated in the cytoplasm of HuH-7 cells may be able to change native forms of cytoplasmic p53 from putative huge aggregates (sedimenting at 105,000 × *g* and 348,900 × *g* for 90 min; **Fig. III-5A** and **Fig. III-4A**, respectively) to a potent transportable form, which is likely composed of at least three components, such as tetrameric p53, motor proteins such as dynein, and subunits of microtubules [72]. Indeed, in cell-free experiments, I was able to demonstrate that GGA transforms native forms of cytoplasmic p53 from non-penetrating huge aggregates to penetrating approximate 670-kD complexes on both BN-gradient PAGE (**Fig. III-4B**) and crosslinking SDS-PAGE (**Fig. III-4D**) in a dose-dependent manner. Furthermore, β-III-tubulin was shown to be cross-linked to these complexes in the presence of GGA in a dose-dependent manner (**Fig. III-5D**). Co-precipitation of cytoplasmic p53 with CUL9/PARC was also shown using the post-mitochondrial fraction and GGA-dependent dissociation of p53 from CUL9/PARC. In this context, one can easily speculate that these cell-free

effects of GGA on native forms of cytoplasmic p53 may enable p53 to be transiently Ser-15 phosphorylated [77] and Lys-379 acetylated [78] (**Fig. 3D**).

In parallel with stimulating nuclear translocation of p53, GGA also induced a dramatic upregulation of the *PUMA* gene, a key regulator of p53-mediated cell death, at the mRNA and protein levels in HuH-7 cells. Furthermore, GGA-induced upregulation of *PUMA* mRNA levels is clearly dependent on nuclear translocation of p53, as ivermectin, a specific inhibitor of importin α/β, blocked GGA-induced nuclear translocation of p53 and also partially suppressed GGA-induced upregulation of *PUMA* mRNA levels. Together these findings strongly suggest that GGA may reactivate the mutant p53 (Y220C) as a transcription factor via its nuclear translocation. However, none of the mRNA levels of p53 target genes tested in chapters II and III, including *SCO2*, *TIGAR*, *DRAM*, and *p21*, were upregulated by GGA treatment, suggesting that GGA-induced transcriptional activation is specific for the *PUMA* gene in HuH-7 cells. In considering that the transactivation effect of GGA is specific for the *PUMA* gene, it is worth mentioning that p53-mediated transcription of the p53-responsive consensus sequence was inversely suppressed by GGA treatment in a dose-dependent manner (**Fig. III-6C**), indicating that the nuclear-translocated mutant p53 behaved as a dominant negative mutant against the consensus sequence in *TP53* heterozygotic HuH-7 cells (unpublished results). However, the nuclear-translocated p53 transactivated a reporter gene downstream of the p53-responsive 5′-upstream regulatory region of the *PUMA* gene after GGA treatment in a time-dependent manner in HuH-7 cells (**Fig. III-6D**), suggesting that the mutant p53 (Y220C) still retained its ability to play a role in transcription of the *PUMA* gene, which contains a low affinity BS1 p53 response element [80].

On the contrary, PLC/PRF/5 cells did not upregulate *PUMA* gene expression after GGA treatment (data not shown), although the cells showed translocation of cytoplasmic p53 to the nucleus after GGA treatment, similar to HuH-7 cells (**Fig. III-3E**). In this case, the nuclear-translocated p53 does not seem to transactivate the *PUMA* gene. While the Y220C mutation of p53 in HuH-7 cells resides at the beginning of the loop that connects β-strands S7 and S8 of the

β-sandwich in the core domain of p53, the R249S mutation in PLC/PRF/5 cells is located at a DNA-contact region of the α-helix of the DNA-binding domain [81]. The former mutant is categorized into class *iv*, with a determinant structural region of the β-sandwich, which shows less affinity to DNA (35–75% of wild type), but the latter mutant belongs to class *ii*, with a determinant structural region of the D-binding region, which completely loses binding affinity to DNA [82]. Therefore, I speculate that PLC/PRF/5 cells might be no longer able to transactivate the *PUMA* gene, even though GGA translocated cytoplasmic p53 to the nuclear compartment. Inasmuch as GGA induces cell death in PLC/PRF/5 cells without induction of the *PUMA* gene, I am speculating that PUMA may not be solely responsible for GGA-induced cell death, but may be rather supportive for the cell death in HuH-7 cells.

Finally, I should provide a perspective on a link between nuclear translocation of cytoplasmic p53 and the GGA-induced autophagic response in HuH-7 cells [24]. Given that PUMA is able to induce autophagy [60], GGA-mediated induction of *PUMA* gene expression through the nuclear-translocated p53 is not so much a question of cell-death inducing activity, but the GGA-induced disappearance of p53 from the cytoplasm may well be consistent with triggering autophagy. Kroemer's group noted that autophagy-inducing stimuli cause the depletion of cytoplasmic p53, which in turn is required for the induction of autophagy [83]. Whether the depletion of cytoplasmic p53 is necessary and sufficient for GGA-induced autophagy in HuH-7 cells has not yet been evaluated, though it is clear that both events occur within 3 h after GGA addition. Indeed, upon GGA treatment, PLC/PRF/5 cells continued to die even without induction of *PUMA*, suggesting that the up-regulation of *PUMA* expression is not essential for GGA-induced cell death. Unlike HepG2 cells, but similar to HuH-7 cells, PLC/PRF/5 cells showed a rapid nuclear translocation of the cytoplasmic p53 (data not shown) and a massive accumulation of autophagosomes (unpublished results) following GGA treatment, implying that a nuclear translocation of cytoplasmic p53 is important for GGA-induced autophagic cell death.

In conclusion, chapter III clearly illustrates that GGA, a cancer-preventive acyclic diterpenoid, induces rapid nuclear translocation of cytoplasmic p53 in human hepatoma-derived HuH-7 cells and results in selective and dramatic upregulation of *PUMA* gene expression, which might be linked to cell death with accumulation of autophagosomes [24].

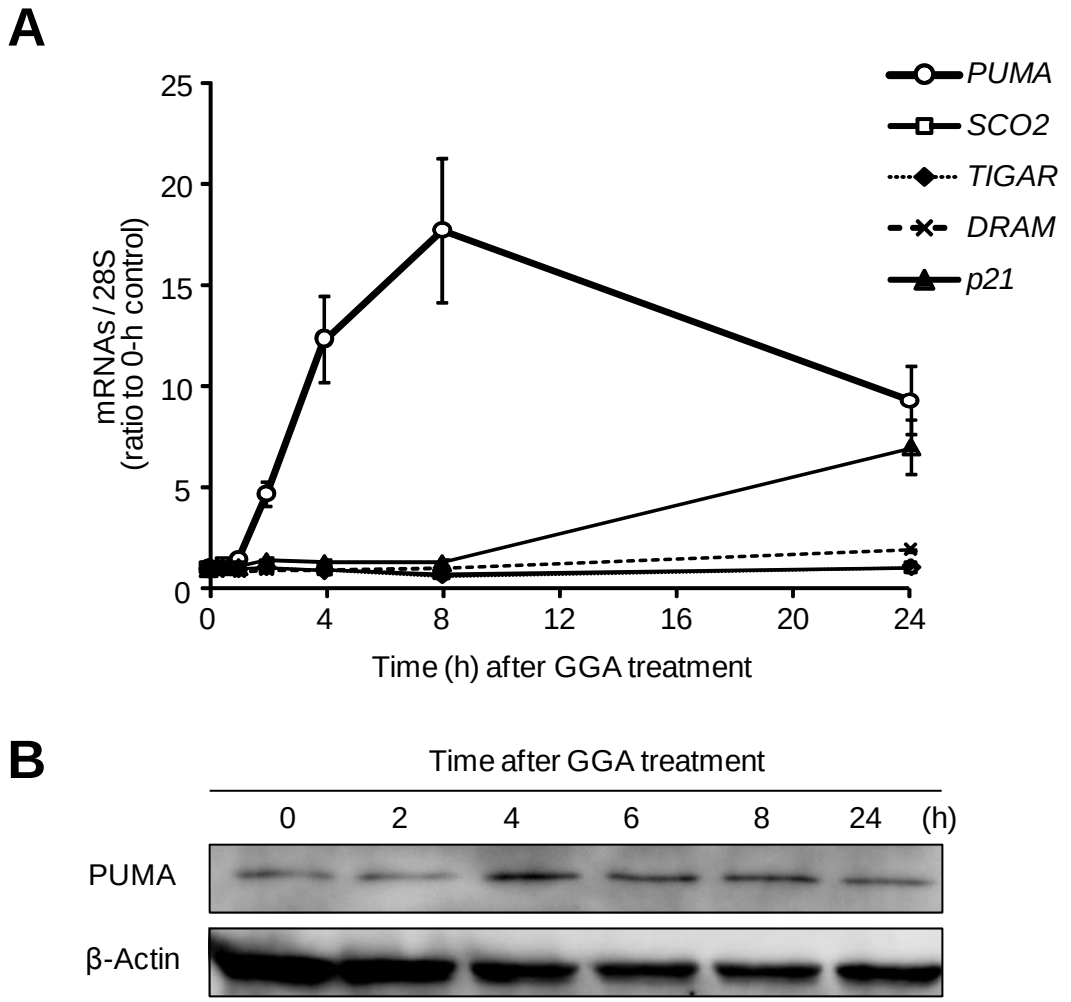

Fig. III-1. GGA treatment upregulates PUMA gene expression in HuH-7 cells.
(A) HuH-7 cells were treated with or without 20 μM of GGA for 0.5, 1, 2, 4, 8, and 24 h, and total mRNA was extracted to analyze *PUMA*, *SCO2*, *TIGAR*, *DRAM*, and *p21* mRNA expression by quantitative RT-PCR. For *PUMA*, each point represents the mean ± SE of six independent experiments, while data points for all other genes represent the mean ± SE of three independent experiments. (B) HuH-7 cells were treated with or without 20 μM of GGA for 2, 4, 6, 8, and 24 h. Whole cell lysates fractions were prepared and the PUMA level was analyzed by western blotting. Total β-actin was used as loading controls.

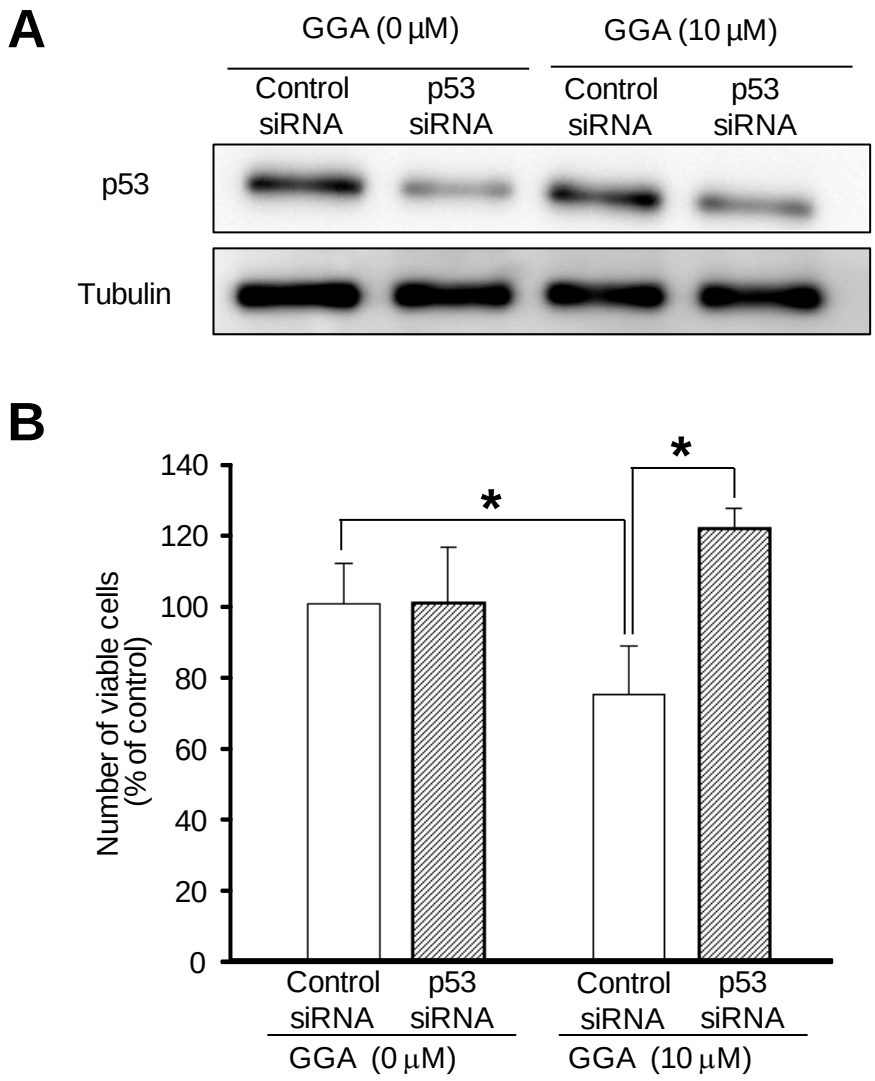

Fig. III-2. Mutant p53 is involved in GGA-induced cell death of HuH-7 cells.

(A) Cellular p53 protein level in HuH-7 cells, after treatment with control siRNA or p53 siRNA. Whole cell lysates were prepared and p53 level was analyzed by western blotting. Total tubulin was used as a loading control. (B) HuH-7cells were treated with 0, 10, 20 μM of GGA for 24 h after transfection with control siRNA or p53 siRNA. And living cells were counted by Trypan Blue dye-exclusion method. Values are means ± SE (n=4). The asterisks indicate statistically significant changes ($p < 0.05$) as determined by a t-test.

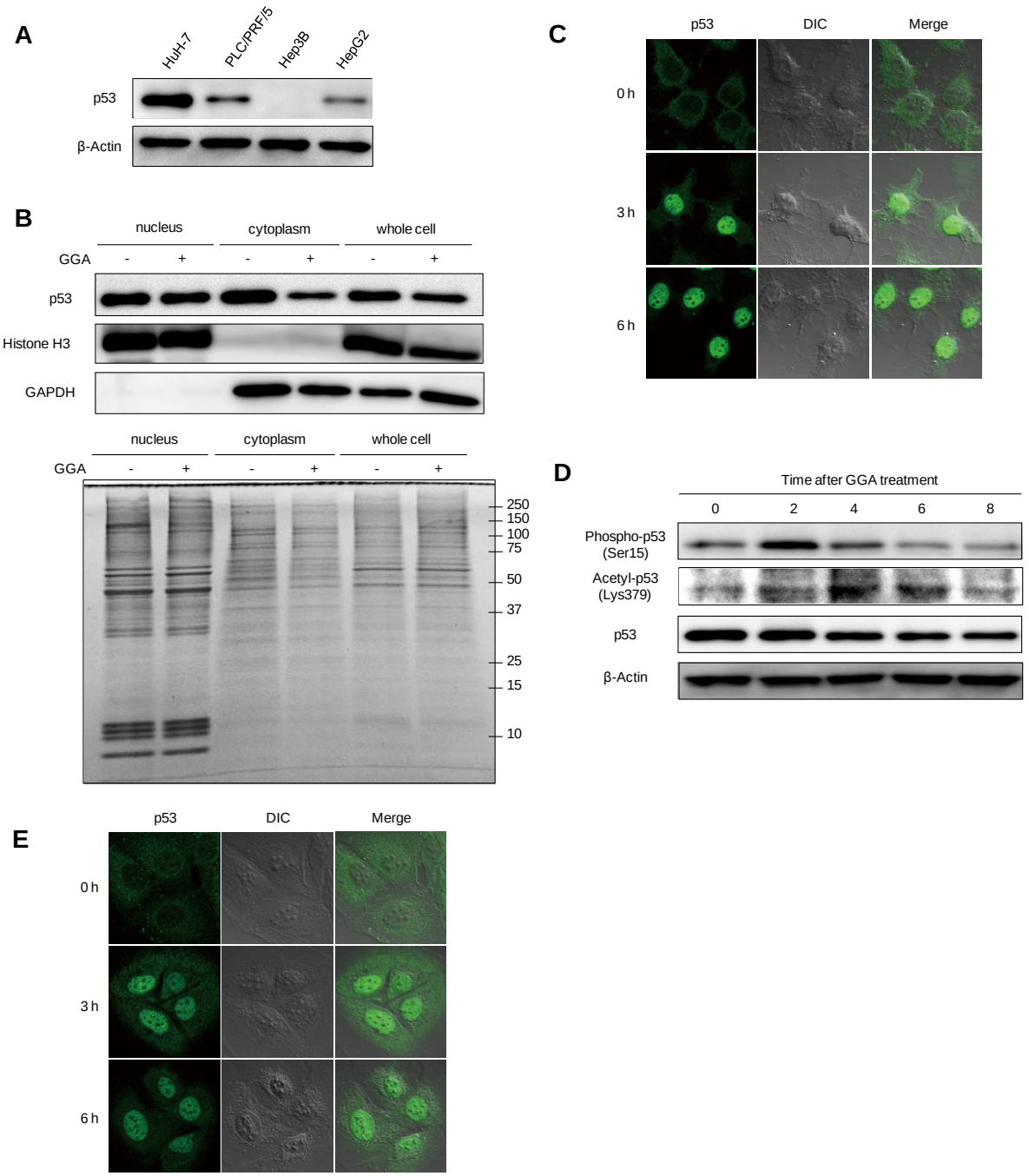

Fig. III-3. Mutant p53 is relocated from cytoplasm to the nucleus by GGA.

(A) Cellular p53 protein level in HuH-7, PLC/PRF/5, Hep3B and HepG2 cells. Whole-cell lysates were prepared and the p53 level was analyzed by western blotting. (B) Whole cell lysates of HuH-7 cells were separated into nucleus and cytoplasmic fractions. And protein concentration was determined using Bio-Rad Protein Assay reagent. Upper panel: aliquots (5 μg) of fractions were subjected to immunoblotting with anti-p53 primary antibody. Histone H3 and GAPDH were using as marker of nucleus and cytoplasm respectively. Lower panel: Coomassie Brilliant Blue stain. (C) HuH-7cells were treated with or without 20 μM of GGA for 3 and 6 h. Green

fluorescence-indicated the distribution of p53. (D) HuH-7cells were treated with or without 20 μM of GGA for 2, 4, 6 and 8 h. Whole-cell lysates were prepared and phospho-p53 (Ser15), acetyl-p53 (Lys379) and p53 levels were analyzed by western blotting. Total β-Actin was used as a loading control. (E) PLC/PRF/5 cells were treated with or without 20 μM of GGA for 3 and 6 h. Green fluorescence-indicated the distribution of p53.

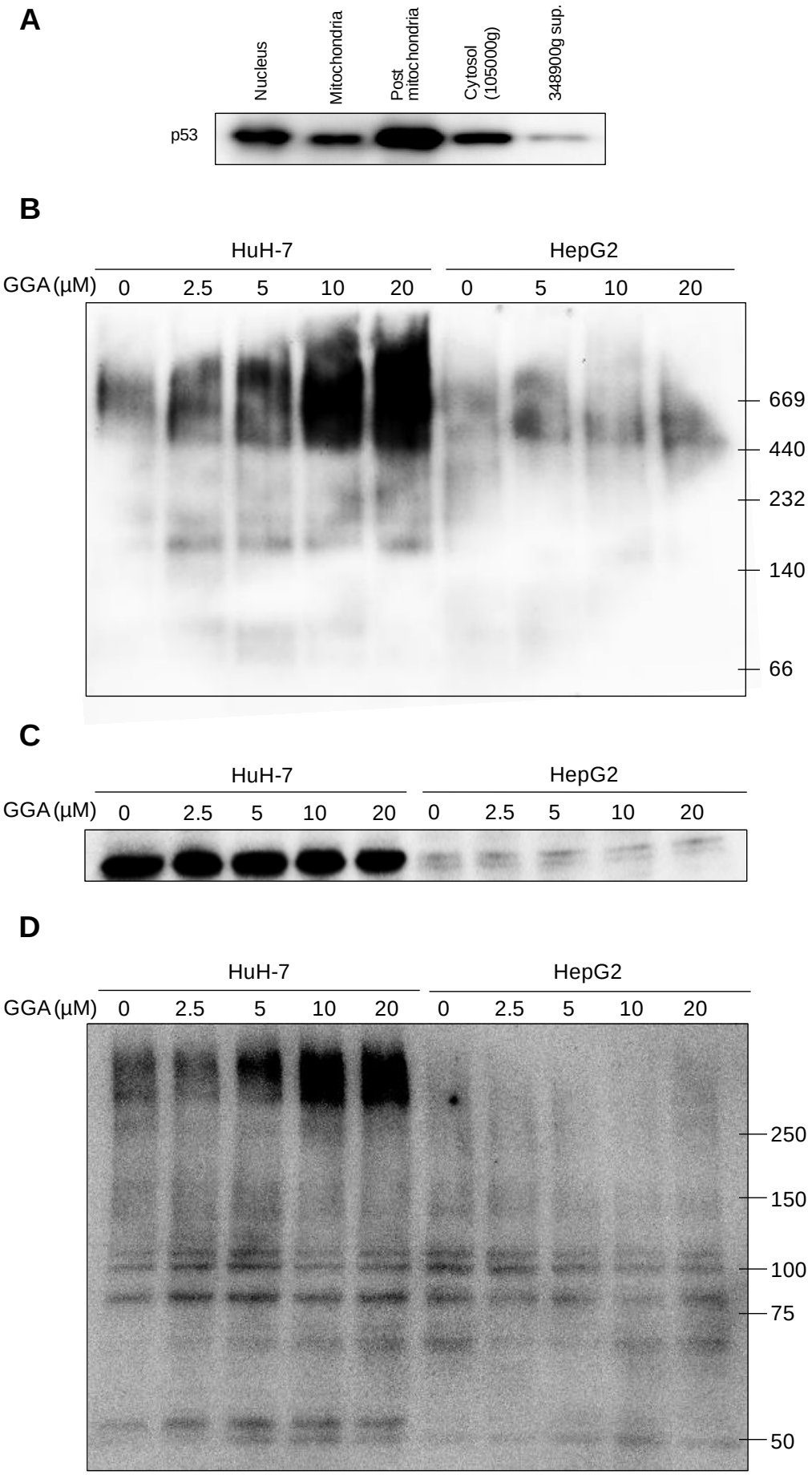
A
Nucleus
Mitochondria
Post mitochondria
Cytosol (105000g)
348900g sup.
p53
B
HuH-7
HepG2
GGA (μM)
0
2.5
5
10
20
0
5
10
20
669
440
232
140
66
C
HuH-7
HepG2
GGA (μM)
0
2.5
5
10
20
0
2.5
5
10
20
D
HuH-7
HepG2
GGA (μM)
0
2.5
5
10
20
0
2.5
5
10
20
250
150
100
75
50

Fig. III-4. GGA-induced changes in native forms of p53 in the post-mitochondrial fraction.
(A) Whole cell lysates of HuH-7 cells were separated into nucleus, mitochondrial, post-mitochondrial, cytosol and 348,900 × g supernatant-fractions. And protein concentration was determined using Bio-Rad Protein Assay reagent. Aliquots (5 μg) of fractions were subjected to immunoblotting with anti-p53 primary antibody.

The post-mitochondrial fractions from HuH-7 (p53 Y220C) and HepG2 (p53 WT) cells were incubated with GGA (0-20 μM) at 4˚C overnight. Samples (3.75 μg protein) were subjected to electrophoresis. (B) Analysis of p53 protein by BN-gradient PAGE. (C) Analysis of p53 protein by SDS-PAGE. (D) The post-mitochondrial fractions from HuH-7 and HepG2 cells were incubated with GGA (0-20 μM) at 4˚C overnight. Aliquots (5 μg protein) of samples were subjected to cross-linking SDS-PAGE followed by western blotting with anti-p53

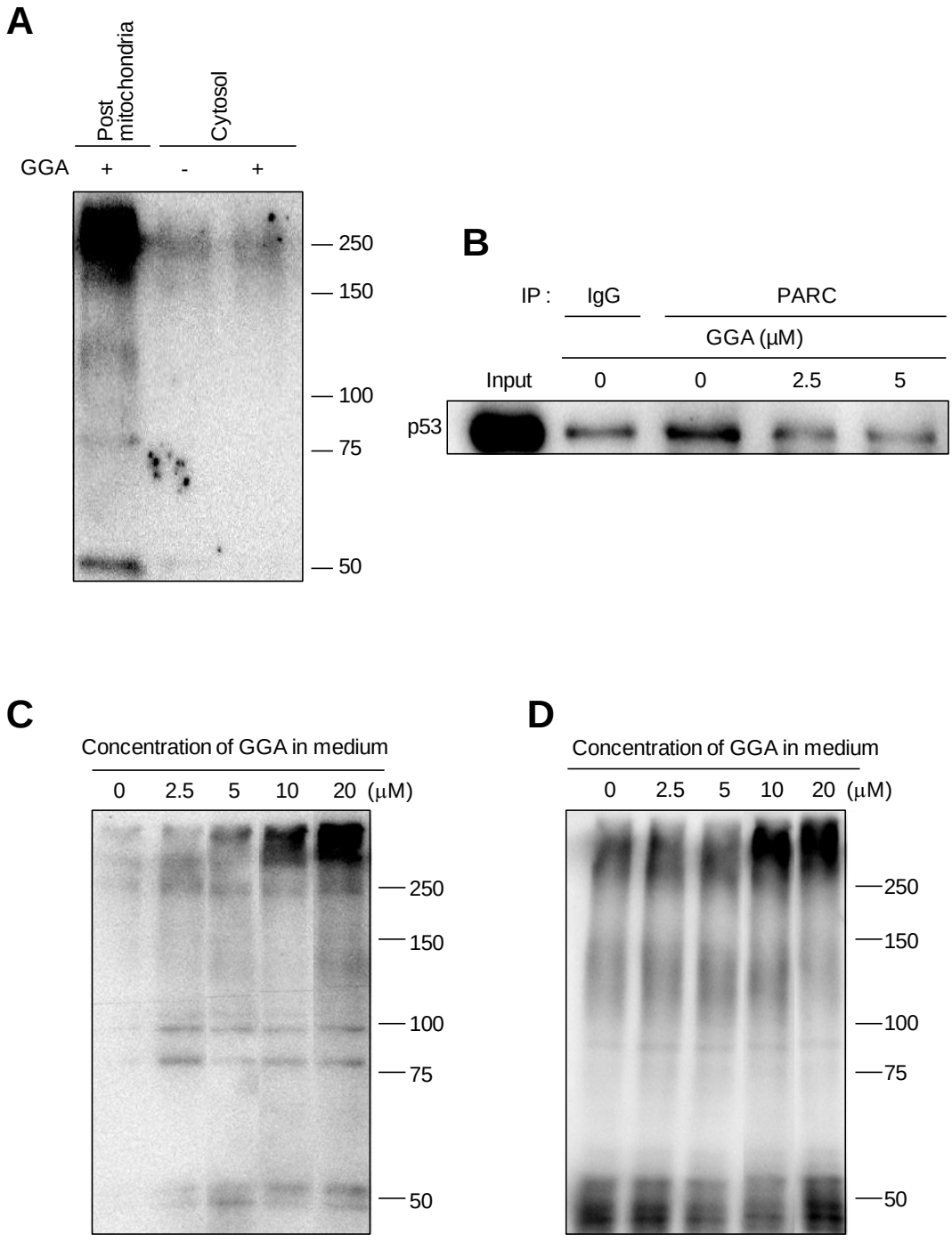

Fig. III-5. p53 is released from putative huge complexes after GGA treatment.

(A) The post-mitochondrial and the cytosolic fractions from HuH-7 cells were incubated with or without GGA (20 μM) at 4˚C overnight. Samples (5 μg protein) were subjected to cross-linking SDS-PAGE followed by western blotting with anti-p53. (B) The post-mitochondrial fraction from HuH-7 cells was incubated with GGA (0-5 μM) at 4˚C overnight, followed by immunoprecipitation with the anti-PARC antibody (PARC) or equi-amount of non-immune rabbit IgG (IgG). The immunoprecipitates were analyzed by immunoblotting with an anti-p53 antibody. 12.5 % of the

input was used (Input). The post-mitochondrial fraction from HuH-7 cells was incubated with GGA (0-20 μM) at 4˚C overnight. Aliquots (5 μg protein) of samples were subjected to cross-linking SDS-PAGE followed by western blotting with anti-p53 (C) and anti-β-III-tubulin (D).

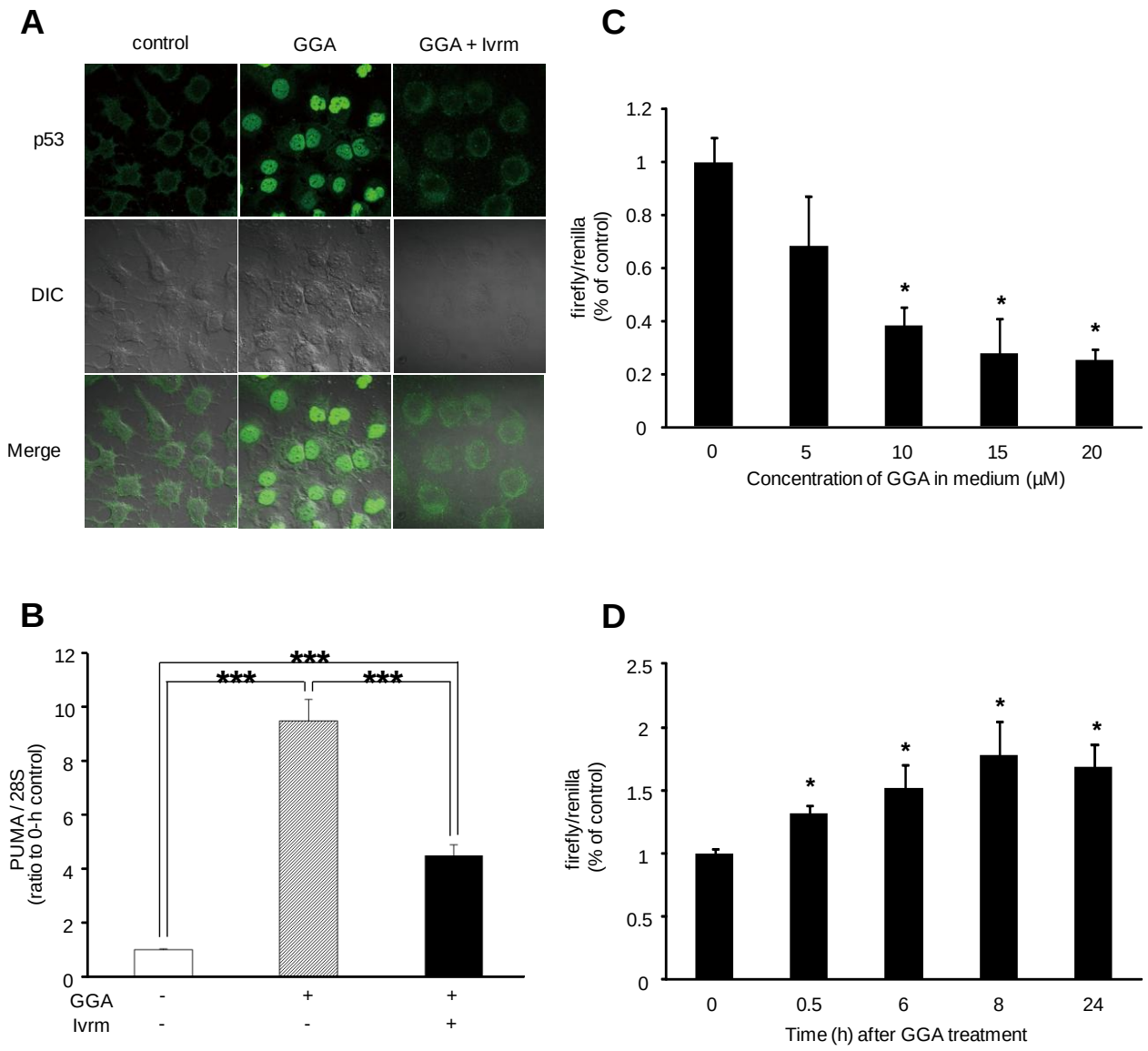

Fig. III-6. Nuclear translocation of mutant p53 upregulates *PUMA* gene expression.

(A) HuH-7 cells were cultured under the following conditions; no treatment (control), 20 μM GGA for 3h (GGA), or 20 μM GGA with ivermectin, a specific inhibitor of importin, for 3 h (GGA + Ivrm). Green fluorescence indicated the distribution of p53. (B) HuH-7 cells were cultured under the conditions as in (A), and total mRNA was extracted to analyze *PUMA* mRNA expression by quantitative RT-PCR. Values are means ± SE (n=4). (C) Dual luciferase reporter assay with the p53-responsive consensus sequence in HuH-7 cells after 24 h GGA (0-20 μM) treatment. The luciferase activity was normalized by renilla luciferase. (D) Dual luciferase reporter assay with p53-responsive 5'-upstream regulatory region of the PUMA gene in HuH-7 cells after GGA (20 μM) treatment. The luciferase activity was normalized by renilla luciferase. The asterisks (* and ***) indicate statistically significant changes ($p < 0.05$ and 0.001) respectively as determined by the Student's t-test.

Chapter IV

GGA induces unfolded protein response in HuH-7 cells

Chieko Iwao
Yoshihiro Shidoji

Polyunsaturated Branched-Chain Fatty Acid Geranylgeranoic Acid Induces Unfolded Protein Response in Human Hepatoma Cells.

PLOS ONE (2015) 10(7): e0132761. DOI: 10.1371 /journal. pone.

Molecular and Cellular Biology, Graduate School of Human Health Science,
University of Nagasaki, Nagasaki, Japan

IV-1. Abstract

The acyclic diterpenoid acid geranylgeranoic acid (GGA) has been reported to induce autophagic cell death in several human hepatoma-derived cell lines; however, the molecular mechanism for this remains unknown. In the present study, several diterpenoids were examined for ability to induce *XBP1* splicing and/or lipotoxicity for human hepatoma cell lines. Here it is shown that three groups of diterpenoids emerged: 1) GGA, 2,3-dihydro GGA and 9-*cis* retinoic acid induce cell death and *XBP1* splicing; 2) all-*trans* retinoic acid induces *XBP1* splicing but little cell death; and 3) phytanic acid, phytenic acid and geranylgeraniol induce neither cell death nor *XBP1* splicing. GGA-induced ER stress/ unfolded protein response (UPR) and its lipotoxicity were both blocked by co-treatment with oleic acid. The blocking activity of oleic acid for GGA-induced *XBP1* splicing was not attenuated by methylation of oleic acid. These findings strongly suggest that GGA at micromolar concentrations induces the so-called lipid-induced ER stress response/UPR, which is oleate-suppressive, and shows its lipotoxicity in human hepatoma cells.

IV-2. Introduction

GGA are able to induce cell death in HuH-7 cells [1], the mechanisms by which GGA induces cell death in human hepatoma cells have been investigated.

Over the past 15 years, Shidoji and his colleague have reported various cell-death related effects of GGA at micromolar concentrations in several cell culture systems: loss of mitochondrial membrane potential in HuH-7 cells [3], hyper-production of superoxide in transformed fibroblastic 104C1 cells [79], and rapid downregulation of cyclin D1 in three human hepatoma-derived cell lines [84]. Okamoto et al recently identified that HuH-7 cells undergo an incomplete autophagic response following GGA treatment [24], which may contribute to GGA-induced cell death. Here, while the initial phase of autophagy occurs, the maturation of autolysosomes or later stages of autophagy fail to proceed, leading to substantial accumulation of early/initial autophagic vacuoles, LC3β-II, and p62/SQSTM in HuH-7 cells [24].

In chapter III, I discussed that a nuclear translocation of cytoplasmic p53 is important for GGA-induced autophagic cell death. Then, in chapter IV, I investigated in detail what kind of cellular events GGA initially induces during incomplete autophagic response.

Possible mechanisms by which GGA could induce autophagy include impairing mTOR mediated suppression of autophagy through starvation stress such as amino acid depletion [85], activation of autophagy-initiating gene product, ATG4, which is induced by oxidative stress [86], and the ER stress-mediated UPR as an upstream signal from lipotoxicity with fatty acids [35]. Of these three potential triggering mechanisms, I focused on UPR-mediated induction of autophagy, as our previous data identified that GGA induced rapid translational downregulation of cyclin D1 [84]. This strongly suggests upregulation of the PERK pathway, which is one branch of the mammalian UPR and is associated with blocking of cyclin D1 translation [87]. Here, I describe the induction of an ER stress-triggered UPR involving XBP1 mRNA splicing and the upregulation of PERK-downstream gene expression by GGA treatment, resulting in the initiation of autophagy and

cell death. Furthermore, I demonstrate that several acyclic diterpenoid acids are capable of inducing cell death in human hepatoma cells.

IV-3. Materials and Methods

IV-3-1. Materials

GGA, phytenic acid, farnesoic acid and geranoic acid were generous gifts from Kuraray (Okayama, Japan). All-trans retinoic acid (ATRA) and 9-*cis* retinoic acid (9CRA) were obtained from Wako, Osaka, Japan. (*S*)-2,3-dihydroGGA, (*R*)-2,3-dihydroGGA and dolichoic acid were synthesized and provided by Dr. Sagami of Tohoku University, Sendai, Japan. Geranylgeraniol (GGOH), phytanic acid, arachidic acid, palmitic acid, oleic acid, fatty acid-free bovine serum albumin (BSA) and tunicamycin were purchased from Sigma Aldrich, St. Louis, MO, USA. IRE1 inhibitor III, 4μ8C (#412512), was from Calbiochem, Merck Millipore Japan, Tokyo, Japan.

IV-3-2. Cell culture

Human hepatoma-derived HuH-7, HepG2 and PLC/PRF/5 cells were obtained from RIKEN BioResource Center, Tsukuba, Japan, and cultured in high-glucose Dulbecco's modified Eagle's medium (D-MEM; Wako) supplemented with 5% fetal bovine serum (FBS; Hyclone Laboratories, Thermo Fisher Scientific, Waltham, MA, USA). The Hep3B cells were obtained from DS Pharma Biomedical, Osaka, Japan, and maintained in D-MEM containing 10% FBS and MEM nonessential amino acid solution (Sigma Aldrich). Cells were cultured with DMEM containing 5% or 10% FBS for 2 days followed by replacement with FBS-free D-MEM for a further 2 days before drug treatment. GGA, other diterpenoids or other lipids (in ethanol) were dispersed in FBS-free medium, except that palmitic acid was dissolved in FBS-free medium containing 1% BSA at a final concentration of 400 μM and preincubated at 37°C for 1 h prior to treatment.

IV-3-3. Reverse-transcription real-time polymerase chain reaction (RT-qPCR)

Cells were treated with GGA or other compounds, and total RNA was isolated using the Quick-Gene RNA cultured Cell kit S (Wako) with QuickGene-810 (Kurabo, Osaka, Japan). cDNA was generated using the Transcriptor® First Strand cDNA Synthesis kit with random hexamers

(Roche Diagnostics, Basel, Switzerland). Nucleotide sequences of the PCR primers for the DDIT3 (known as CHOP), PDIA4 (protein disulfide isomerase family A, member 4), ACSL3 (acyl-CoA synthetase long-chain family member 3) and 28S rRNA cDNAs are listed in **Table IV-1**. Real-time PCR was performed with DyNAmo Capillary SYBR Green qPCR Master mix (Finnzymes, Espoo, Finland), and cDNA on LightCycler1.5 (Roche Diagnostics) under conditions described in **Table IV-2**.

Table IV-1. The nucleotide sequences of each primers used for real time RT-PCR.

Genes	Primer	Sequence (5' – 3')
DDIT3	F	ATGGCAGCTGAGTCATTGCCTTTC
	R	AGAAGCAGGGTCAAGAGTGGTGAA
PDIA4	F	CGCGAGTTTGTCACTGCTTTC
	R	CGTCCTTCTTGGGGTCCATC
28S rRNA	F	TTAGTGACGCGCATGAATGG
	R	TGTGGTTTCGCTGGATAGTAGGT

IV-3-4. Immunoblotting

Following treatment with GGA or tunicamycin, HuH-7 cells were lysed with cell lysis buffer (Tris-based buffered saline containing 1% Nonidet P40, 0.5% sodium deoxycholate and 0.1% SDS) containing complete mini protease inhibitor cocktail (Roche Diagnostics) and proteins were quantified by Bradford assay (Bio-Rad, Hercules, CA, USA). Equal amounts (15 or 30 μg) of protein per sample were separated by SDS-PAGE. The semi-dry blotted polyvinylidene fluoride membranes (Bio-Rad) were probed with rabbit polyclonal antibody against XBP1s (#619502, BioLegend, San Diego, CA, USA), LC3 (PM036, Medical Biological Laboratories, Nagoya, Japan) and β-tubulin III (T2200, Sigma Aldrich). Horseradish peroxidase (HRP)-labeled secondary antibody (GE Healthcare, Tokyo, Japan) was detected with Immobilon Western Chemiluminescent HRP substrate (Merck Millipore Japan) using an ImageQuant LAS 4000 (GE Healthcare).

Table IV-2. The conditions of thermal cycler for real-time RT-PCR of *XBP1u, XBP1s, DDIT3, PDIA4* and *28s rRNA*.

	XBP1u	
	Temperature	Slope
Denature	95ºC, 600 s	20ºC / s
PCR (45 cycles)	95ºC, 10 s 65ºC, 20 s 72ºC, 20 s	20ºC / s
Melting	95ºC, 0 s 57ºC, 15 s 98ºC, 0 s	20ºC / s 0.1ºC / s
Cooling	40ºC, 30 s	20ºC / s

	XBP1s	
	Temperature	Slope
Denature	95ºC, 600 s	20ºC / s
PCR (45 cycles)	95ºC, 10 s 62ºC, 20 s 72ºC, 20 s	20ºC / s
Melting	95ºC, 0 s 57ºC, 15 s 98ºC, 0 s	20ºC / s 0.1ºC / s
Cooling	40ºC, 30 s	20ºC / s

	DDIT3	
	Temperature	Slope
Denature	95ºC, 600 s	20ºC / s
PCR (45 cycles)	95ºC, 10 s 54ºC, 20 s 72ºC, 20 s	20ºC / s
Melting	95ºC, 0 s 57ºC, 15 s 98ºC, 0 s	20ºC / s 0.1ºC / s
Cooling	40ºC, 30 s	20ºC / s

	PDIA4	
	Temperature	Slope
Denature	95ºC, 600 s	20ºC / s
PCR (40 cycles)	95ºC, 10 s 59ºC, 20 s 72ºC, 20 s	20ºC / s
Melting	95ºC, 0 s 57ºC, 15 s 98ºC, 0 s	20ºC / s 0.1ºC / s
Cooling	40ºC, 30 s	20ºC / s

	28s rRNA	
	Temperature	Slope
Denature	95ºC, 600 s	20ºC / s
PCR (40 cycles)	95ºC, 15 s 60ºC, 30 s	20ºC / s
Melting	95ºC, 0 s 65ºC, 15 s 95ºC, 0 s	20ºC / s 0.1ºC / s
Cooling	40ºC, 30 s	20ºC / s

IV-3-5. Immunofluorescence

Following treatment with GGA or other compounds, HuH-7 cells grown on glass inserts in a 24-well plate were rinsed with Ca-free PBS (PBS(-); Sigma Aldrich) and fixed for 40 min with 4% paraformaldehyde containing 2% sucrose in PBS(-), and then rinsed with PBS(-). Cells were then permeabilized with 0.5% Triton X-100 and nonspecific binding blocked with 10% FBS. Next, cells were incubated at 4°C overnight with polyclonal anti-XBP1s antibody, followed by 2.5 h incubation with Alexa-488-labeled goat anti-rabbit IgG antibody (Invitrogen, Molecular Probes, Tokyo, Japan). After rinsing with PBS(-), cells were mounted in PermaFluor (Beckman Coulter, Brea, CA, USA), covered on a glass slide, and observed under a confocal laserscanning fluorescence microscope, LSM700 2Ch URGB equipped with Axio Observer Z1 Bio (Carl Zeiss, Göttingen, Germany).

IV-3-6. Live-cell imaging

HuH7/GFP–LC3 cells [24] were cultured on glass-bottomed dishes (Matsunami) at a density of 3×10^4 cells/dish in a chamber unit (INUG2-ZIL; Tokai Hit, Hamamatsu, Shizuoka, Japan), equipped with a Carl Zeiss LSM 700 inverted laser-scanning confocal fluorescence microscope. Live-cell images were scanned after the addition of 10 μM GGA for 8 h in the absence or presence of 25 μM oleate.

IV-3-7. Cell viability assay

Cells (1000 cells/well) were seeded into a 96-well plate and cultured with D-MEM containing 5% FBS for 2 days before replacing the medium with FBS-free D-MEM for a further 2 days prior to 24 h treatments with GGA or other compounds. The CellTiter-Glo (Promega KK, Tokyo, Japan) was then used to measure cell viability by ATP levels as per manufacturer's instructions. The luminescence was recorded by using Centro XS3 LB960 (Berthold Technologies, Wildbad, Germany). Alternatively, HuH-7 cells were seeded into 3-cm dish at a density of 3×10^4 cells/dish and cultured with D-MEM containing 5% FBS for 2 days before replacing the medium with FBS-free D-MEM for a further 2 days prior to 24 h treatments with palmitic acid and oleic acid. A

number of viable cells were counted by trypan blue method after detachment with trypsin treatment.

IV-4. Results

IV-4-1. Rapid induction of *XBP1* mRNA splicing by GGA treatment in HuH-7 cells

First of all, 2 sets of primers for real-time RT-PCR were designed as shown in **Fig. IV-1A**, in order to quantitatively and separately measure the cellular contents of unspliced *XBP1* and spliced *XBP1* mRNAs. These primer sets enabled us to completely discriminate the spliced and unspliced forms of *XBP1* mRNA after 45 cycles of PCR (**Fig. IV-1B**), so that kinetics of GGA induced splicing of *XBP1* mRNA was studied to separately measure the cellular levels of *XBP1* mRNA each forms by quantitative RT-PCR with these primer sets.

Treatment with GGA rapidly induced *XBP1* mRNA splicing in HuH-7 cells (**Fig. IV-1C and 1D**). Following addition of 10 μM GGA to the culture medium, the level of unspliced *XBP1* (*XBP1u*) mRNA was immediately downregulated in a time dependent manner. Less than one-fifth the initial level of *XBP1u* mRNA was present 2 h after GGA treatment, and this fall was maintained until 4 h. However, by 8 h, the XBP1u level had recovered to that of control cells (bold line in **Fig. IV-1C**). Accordingly, the level of spliced *XBP1* (*XBP1s*) mRNA was increased 3.4-fold at 1 h and up to 5.4-fold at 4 h compared with the control level. From 8–24 h, the cellular levels of *XBP1s* mRNA gradually decreased from 3.5- to 1.5-fold (bold line in **Fig. IV-1D**), suggesting that the *XBP1* splicing induced by treatment with 10 μM GGA was a transient response.

Conversely, the effect of treatment with 20 μM GGA on *XBP1* splicing appeared sustainable during the experiment. Here, a more potent decrease in *XBP1u* mRNA was observed, with less than one-twentieth of the initial amount remaining 2 h following treatment, and one-fiftieth at 4 h. This decrease was sustained at 24 h (dotted line in **Fig. IV-1C**). Treatment with 20 μM GGA upregulated the level of *XBP1s* mRNA at 4 h in a similar manner to 10 μM GGA treatment; however, this upregulation continued and by 24 h the *XBP1s* mRNA level had increased 9.2-fold over that of control (dotted line in **Fig. IV-1D**). Two-way ANOVA revealed that kinetics of the cellular levels of either *XBP1u* or *XBP1s* mRNA was significantly different between 10 and 20 μM GGA-treated

cells.

It was next examined whether GGA-induced *XBP1* splicing was concentration-dependent by measuring *XBP1u* levels at 1 h following treatment with 0–20 μM GGA. No change in *XBP1u* level was observed following administration of 5 μM GGA (**Fig. IV-1E**), although a slight but significant increase in the level of *XBP1s* mRNA was detected (**Fig. IV-1F**). Treatment with 10 μM GGA significantly decreased the *XBP1u* mRNA level while 20 μM GGA almost completely depleted all *XBP1u* mRNA, giving an apparent EC_{50} of 10 μM (**Fig. IV-1E**). Furthermore, GGA increased *XBP1s* mRNA levels in a dose-dependent manner from a 1.4-fold increase over control at 5 μM to a 5.1-fold increase at 20 μM (**Fig. IV-1F**).

A time-dependent induction of *XBP1* mRNA splicing also followed treatment with 20 μM GGA in three other human hepatoma cell lines: PLC/PRF/5 (**Fig. IV-1G**), HepG-2 (**Fig. IV-1H**) and Hep3B (**Fig. IV-1I**).

IV-4-2. Structure specificity of diterpenoid-induced splicing of *XBP1* mRNA in HuH-7 cells

To determine whether GGA- analogous compounds could also induce *XBP1* mRNA splicing, HuH-7 cells were treated with (*S*)-2,3-dihydroGGA, (*R*)-2,3-dihydroGGA, ATRA, 9CRA, phytanic acid, phytenic acid, farnesoic acid, GGOH, dolichoic acid, geranoic acid, palmitic acid, and arachidic acid (chemical structures depicted in **Fig. IV-2**). **Fig. IV-3A** shows the dose-dependent effects of these compounds on *XBP1u* mRNA levels in HuH-7 cells after 1 h treatment. ATRA decreased *XBP1u* mRNA level in a concentration-dependent manner essentially identical to GGA. 9CRA, a stereoisomer of ATRA, and (*S*)-2,3-dihydroGGA also both induced splicing of *XBP1u* mRNA, but to a lesser degree than GGA. (*R*)-2,3-dihydroGGA, an enantiomer of (*S*)-2,3-dihydroGGA, triggered a decrease in *XBP1u* mRNA only at 20 μM. Other compounds listed in **Fig. IV-2** exhibited no detectable effect on *XBP1u* mRNA levels (see **Fig. IV-3C**).

Fig. IV-3B depicts the concentration- dependent appearance of *XBP1s* mRNA 1 h following treatment with the aforementioned compounds. ATRA induced an upregulation of *XBP1s* mRNA,

with saturation at 10 μM. In accordance with the changes of *XBP1u* mRNA, 9CRA was a weaker inducer of *XBP1s* mRNA than ATRA and GGA, as were both (*S*)- and (*R*)-2,3-dihydroGGA. From most to least potent, the *XBP1*-splicing inducing activity of these diterpenoid acids was: ATRA > GGA > 9CRA > (*S*)-2,3-dihydroGGA > (*R*)-2,3-dihydroGGA. The other compounds used failed to induce any change to the *XBP1s* mRNA level (**Fig. IV-3D**).

IV-4-3. Nuclear accumulation of XBP1s after GGA treatment

Treatment with 20 μM GGA led to detection of XBP1s protein at as early as 2 h and the protein became evident at 8 h and was still found until 24 h following treatment (**Fig. IV-4A**). Tunicamycin induced a transient increase of the cellular XBP1s protein level at 8 h and the protein level was decreased at 24 h after the treatment (**Fig. IV-4B**).

The subcellular distribution of GGA-induced XBP1s protein in HuH-7 cells were then examined, because XBP1s acts as a transcription factor that migrates to the nucleus. **Fig. IV-4C** depicts the distribution of XBP1s protein in both the cytoplasmic and nuclear space of HuH-7 cells under ethanol-control condition. At 8 h after addition of GGA, however, the XBP1s protein signal was increased and mainly localized in the nuclear space. Treatment with tunicamycin produced similar changes in subcellular distribution of XBP1s (**Fig. IV-4C**).

Fig. IV-4D shows that 2 isoprenoids with no activity to induce UPR such as GGOH and geranoic acid failed to translocate XBP1s to nuclei, whereas other UPR-inducing isoprenoids of GGA and ATRA were both effective to induce nuclear translocation of XBP1s.

IV-4-4. Specificity of diterpenoid-induced cell death in HuH-7 cells

To examine whether GGA-induced *XBP1* splicing is connected to GGA-induced cell death, cell viability assays were conducted following similar treatments of HuH-7 cells to those described above. The degree of cell viability at 24 h following treatment with 0–50 μM of the various compounds was assessed using the CellTiter-Glo assay. The three acyclic diterpenoid acids GGA, (*S*)-2,3-dihydroGGA, and (*R*)-2,3-dihydroGGA, which all triggered *XBP1* mRNA splicing, induced

cell death in a dose-dependent manner (**Fig. IV-4A**). The potency of this cell death inducing activity was: GGA > (*S*)-2,3-dihydroGGA > (*R*)-2,3-dihydro GGA, as judged by calculating the IC50 values shown in **Fig. IV-2**. Although both ATRA and 9CRA were capable of inducing *XBP1* mRNA splicing, 50 μM ATRA treatment still resulted in 64% cell viability, so an IC_{50} could not be determined. In contrast, 9CRA demonstrated an IC50 of 26 μM, which is slightly greater than the IC50 of (*R*)-2,3-dihydroGGA. All other compounds failed to induce cell death, as shown in **Fig. IV-5B** and **Fig. IV-2**.

IV-4-5. GGA-induced *XBP1* splicing shared a similarity with lipid-induced UPR

Fig. IV-6 demonstrates that tunicamycin treatment results in activation of the three canonical branches of UPR signaling such as *XBP1s* (mRNA processed by IRE1), *DDIT3* (PERK-downstream gene) and *PDIA4* (ATF6-target gene) in HuH-7 cells. However, GGA treatment induces only two of these, with no upregulation of *PDIA4* mRNA (**Fig. IV-6C**). Lipid-induced UPR such as that triggered by palmitate is known to be suppressed by co-treatment with the mono-unsaturated fatty acid oleate [88]. Therefore, by using oleate GGA-induced UPR was compared with palmitate- induced UPR or tunicamycin-induced UPR in HuH-7 cells. As shown in top panels of **Fig. IV-7A and 7B**, I was able to confirm that palmitate induced upregulation of *XBP1s* and *DDIT3* mRNAs was dose-dependently suppressed by co-treatment with oleate in hepatoma cell lines [89]. Here it was shown that GGA-induced *XBP1* mRNA splicing and upregulation of *DDIT3* mRNA were both efficiently and dose-dependently suppressed by co-treatment with oleate (middle panels of **Fig. IV-7A and 7B**), linear regression analysis giving IC50 value of 15–20 μM (**Fig. IV-7C and 7D**). In contrast, tunicamycin-induced upregulation of *XBP1s* and *DDIT3* mRNAs were both unaffected by co-treatment with oleate even at its 400 μM (bottom panels of **Fig. IV-7A and 7B**). As expected, oleate treatment alone upregulated neither *XBP1s* nor *DDIT3* mRNAs (data not shown).

In chapter IV, it has been repeatedly reported that palmitate-induced UPR is mediated by ER

membrane phospholipid saturation and palmitate-induced UPR can be overcome either by membrane phospholipid unsaturation [17, 90] or channeling of toxic palmitate to oleate-induced lipid droplets [91, 92] with oleate overloading. In either case, overloaded oleate should be incorporated into ER membrane phospholipids or triacylglycerols in lipid droplets through oleoyl-CoA intermediate, respectively. Therefore, in place of oleate as a suppressor of GGA-induced UPR, used was oleic acid methylester or methyl oleate, which is not a direct substrate for long chain fatty acyl-CoA synthase (ACSL). Methyl oleate efficiently blocked both palmitate-induced and GGA- induced *XBP1* splicing (**Fig. IV-8A and 8B**, respectively). Consistently, cellular expression of the *ACSL3* gene was not significantly induced by co-treatment with oleate (**Fig. IV-8C**).

IV-4-6. Rescue from GGA-induced cell death by oleate co-treatment

Palmitate (400 μM)- induced cell death was suppressed by 25-μM oleate co-treatment and increasing concentrations (100 and 400 μM) of oleate apparently enhanced the cell growth in the presence of 400 μM palmitate in 96-well plates measured by CellTiter Glo assay (**Fig. IV-9A**). GGA at 50 μM induced complete cell death in HuH-7 cells and co-treatment with oleate even at 25 μM perfectly rescued the cells from GGA-induced cell death (**Fig. IV-9B**). These preventive effects of oleate on lipid-induced cell death were mostly reproduced by methyl oleate co-treatment (**Fig. IV-9C and 9D**). Suppressive effect of oleate on palmitate- induced cell death was essentially observed in 3-cm dishes also by trypan blue dye exclusion method, but the growth enhancement with higher oleate was not detected (**Fig. IV-9E**). Oleate-mediated suppression of GGA- induced cell death did not occur when the cells were pretreated with oleate 1–24 h before GGA treatment (**Fig. IV-9F**).

IV-4-7. Inhibition of GGA-induced UPR attenuates GGA-induced accumulation of LC3-II

Simultaneous treatment with 4μ8C suppressed GGA-induced *XBP1* mRNA splicing in a dose-dependent manner. The presence of 5 μM 4μ8C, an inhibitor specific for IRE1 endonuclease

activity, prevented GGA-induced splicing of *XBP1u* mRNA, and at higher concentrations *XBP1u* mRNA levels even increased 2-fold over the control level (**Fig. IV-10A**). Consistently, 4μ8C caused a dose-dependent impairment of GGA-induced upregulation of *XBP1s* mRNA (**Fig. IV-10B**). In contrast, co- treatment of HuH-7 cells with 32 μM 4μ8C did not attenuate GGA-induced accumulation of LC3-II, a hallmark of autophagosomes, at all (**Fig. IV-10C**). However, co- treatment with 25 μM oleate effectively prevented GGA-induced accumulation of LC3-II (**Fig. IV-10D**). In accordance with this biochemical finding, GGA-induced accumulation of GFP-LC3 puncta (autophagosomes) was attenuated by co-treatment with 25 μM oleate (**Fig. IV-10E**).

IV-5. Discussion

I have addressed how GGA initiates signaling linked to GGA-induced cell death in HuH-7 cells. Both GGA and 2,3-dihydroGGA immediately induce an ER stress response/UPR. Furthermore, GGA-induced *XBP1* mRNA splicing was blocked by co-treatment with oleate, indicating that GGA induces a typical lipid-induced ER stress response/UPR. GGA-induced accumulation of the autophagosome marker LC3-II and GGA- induced cell death were also both prevented by co-treatment with oleate. Together, these data strongly demonstrate that polyunsaturated branched-chain fatty acid GGA induces ER stress response/UPR, which may be associated with GGA-induced cell death in human hepatoma cells.

GGA has been repeatedly reported to induce programmed cell death in human hepatoma cell lines [1-3, 24, 93]; however, the precise molecular mechanism by which this occur remains elusive. So far, Shidoji and his colleague have reported that hyperproduction of superoxide in mitochondria, increase in the cellular level of LC3-II, dissipation of mitochondrial inner-membrane potential, and finally a massive accumulation of autophagosomes all occur following GGA treatment. Therefore, it was speculated that a massive accumulation of autophagosomes or incomplete autophagic response might be directly linked to GGA-induced cell death [24]. To begin investigating this, it was needed to determine exactly how GGA initiates an autophagic response. In chapter 3, at least three cellular conditions are known to trigger the autophagic response: starvation stress, oxidative stress, and ER stress [94]. Okamoto et al have previously reported that Tiron, a superoxide scavenger, slightly delayed GGA-induced conversion of LC3-I to LC3-II [24]. This indicates that mitochondrial oxidative stress is partially involved in triggering autophagy, but only to a small degree.

Here, I have demonstrated for the first time that GGA causes a lipid-induced ER stress-mediated UPR, as evidenced by the rapid upregulation of *XBP1* mRNA splicing and the cellular level of *DDIT3* mRNA, which may be associated with GGA-induced cell death. Of the three canonical signaling arms of the UPR, a typical lipid-induced UPR consists of IRE1 and PERK pathways [46].

XBP1 mRNA splicing is brought about by activation of IRE1 ribonuclease activity. *XBP1s* mRNA encodes the functionally active transcription factor, whereas *XBP1u* encodes an isoform that is constitutively expressed and thought to function as a negative feedback regulator of XBP1s. Indeed, GGA induced an upregulation of cellular XBP1s levels and its nuclear accumulation by 8 h. Meanwhile, GGOH, an inactive GGA derivative that does not induce *XBP1* splicing, did not affect the subcellular distribution of XBP1s. Another branch of the lipid-induced UPR is a PERK pathway, which phosphorylates eIF2α and attenuates protein translation. Phosphorylation of eIF2α also allows for preferential translation of the activating transcription factor 4, which targets the *DDIT3* (formerly named as *CHOP*) gene. The rapid upregulation of PERK pathway can very well explain our previous finding of GGA-induced rapid translational attenuation of *cyclin D1* gene expression through phosphorylation of eIF2α [84].

Multiple lines of evidence have shown that lipid-induced ER stress/UPR is a possible molecular mechanism for the effects of lipotoxicity [35]. In particular, the long-chain fatty acid palmitate is well documented as an inducer of ER stress via direct sensing of the acyl-chain saturated lipid composition of the ER membrane lipid [90]. Interestingly, unlike the canonical UPR, lipid-induced ER stress does not activate the ATF6 branch of UPR [46, 95]. Hence, here the cellular expression levels have been measured of the ATF6-target chaperone gene, *PDIA4* [46, 96], and as a result, GGA failed to increase the cellular level of *PDIA4* mRNA (**Fig. IV-6C**). Furthermore, it was found that GGA-induced UPR was suppressed by oleate co-treatment, as was palmitate-induced UPR. This leads us to categorize GGA-induced UPR as a form of lipid-induced ER stress or saturated fatty acid-induced ER stress, because tunicamycin-induced UPR was not attenuated by co-treatment with oleate. However, at least two points remain unclear: GGA is not a saturated fatty acid and is even a poly-unsaturated branched-chain fatty acid or 3,7,11,15-tetramethyl-2,6,10,14-hexadecatetraenoic acid, and the EC_{50} of GGA for *XBP1* splicing is under 10 μM, whereas 400–1000 μM palmitate is typically required to induce ER stress in cellular systems [89]. In any case, the present study clearly shows conclusive evidence that GGA is one of the

natural lipids that induce a lipid-induced ER stress response/UPR at sub-ten μM, which is potentially responsible for lipotoxicity or lipid-induced cell death, while canonical lipid-induced ER stress response occurs with some hundreds μM saturated fatty acids such as palmitate.

Among the diterpenoids tested herein, the lipid were categorized as three groups: 1) GGA, 2,3-dihydroGGA and 9CRA induce cell death and *XBP1* splicing; 2) ATRA induces *XBP1* splicing but little cell death; and 3) phytanic acid, phytenic acid and GGOH induce neither cell death nor *XBP1* splicing. In the near future experiment, one should clarify why ATRA-induced UPR is not linked to cell death, whereas GGA-induced UPR is apparently linked to cell death in HuH-7 cells.

Scant evidence for a molecular role of ER stress response/UPR in triggering autophagy is currently available. A single report of XBP1s directly binding the beclin 1 (*BECN1*) gene promoter exists [97]. These authors concluded that XBP*1* splicing triggers an autophagic signal pathway through XBP1s-mediated transcriptional regulation of the *BECN1* gene, which product consists a triggering complex of autophagy with PI3-kinase [97]. Therefore, the effect of a specific IRE1 endonuclease inhibitor, 4μ8C, on GGA-induced autophagy was assessed. This inhibitor completely blocked GGA-induced *XBP1* splicing but did not attenuated GGA-induced cellular accumulation of LC3β-II, suggesting that *XBP1* splicing may not be an upstream signal for the GGA-induced incomplete autophagic response.

Rather than co-treatment with 4μ8C, co-treatment with oleate more broadly prevents GGA-induced UPR including IRE1 and PERK pathways. The mono-unsaturated fatty acid attenuated GGA-induced accumulation of autophagosomes to the greater extent (**Fig. IV-10E**), suggesting that except *XBP1* splicing, some other GGA-inducible UPRs such as IRE1 kinase cascade and PERK pathway may cause a shift in cellular autophagic response [98]. On the other hand, one cannot exclude the possibility that incomplete autophagic response induced by GGA may be the signal upstream of the UPR [99-101].

In conclusion, I describe here in chapter IV that GGA induces ER stress/UPR, which may be associated with GGA-induced cell death. I have further demonstrated that GGA-induced UPR could be an upstream signal for the GGA-induced incomplete autophagic response.

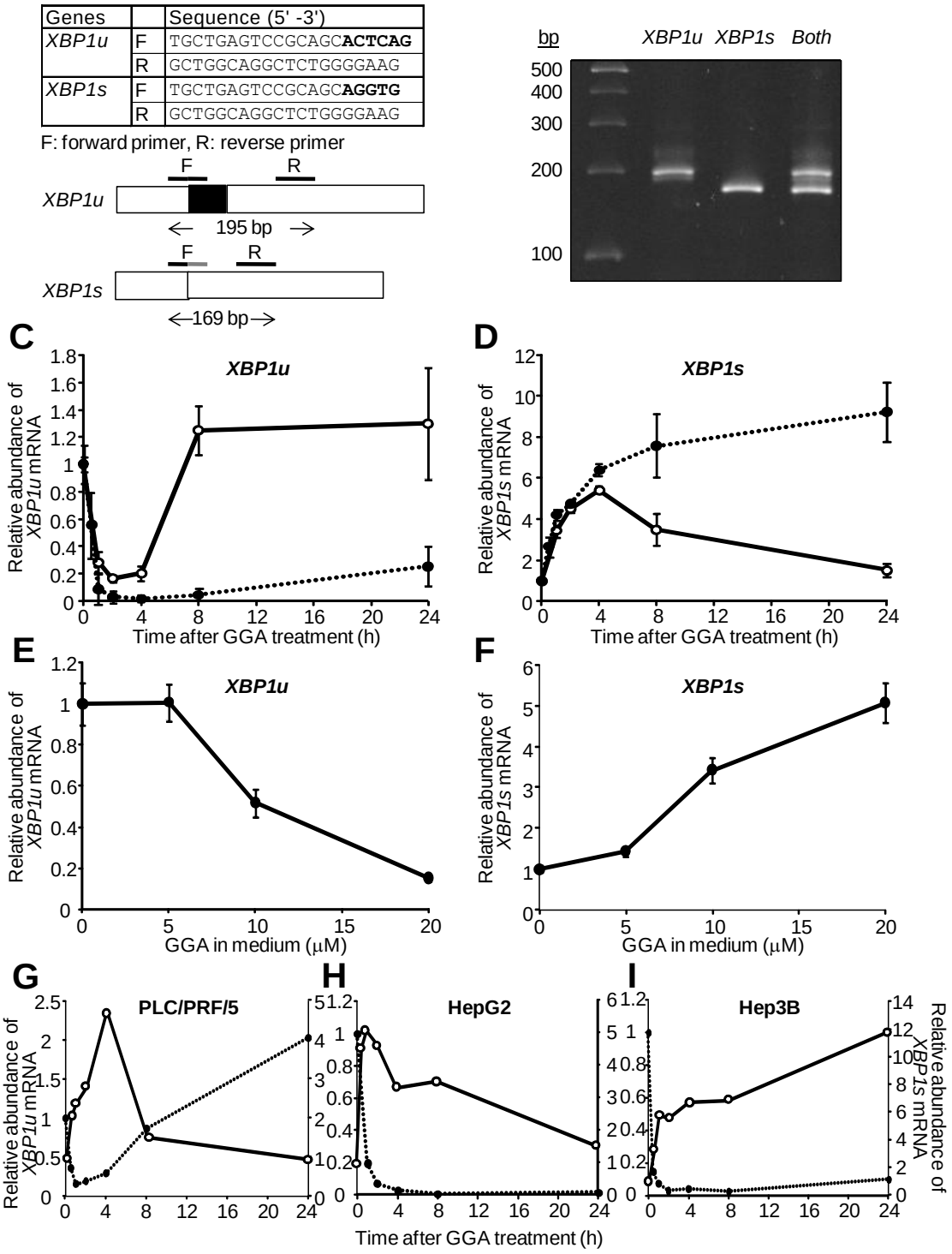

Fig. IV-1. Rapid induction of *XBP1* mRNA splicing by GGA treatment in HuH-7 cells.
Quantitative RT-PCR primers discriminating the spliced and unspliced forms of *XBP1* mRNA were designed and their nucleotide sequences are shown in (A). Total mRNA was extracted from HuH-7 cells and RT-qPCR was performed using either these *XBP1u* or *XBP1s* primers. Following qPCR (45 cycles), products of *XBP1u* or *XBP1s* amplification were diluted by 10 or 50 fold, respectively,

prior to electrophoresis by E-Gel 48 (4% agarose) to validate the discriminating primers (B). HuH-7 cells were treated with 10 (open circle) or 20 μM GGA (closed circle) for 0, 1, 2, 4, 8, and 24 h. Total mRNA was extracted to measure the cellular levels of *XBP1u* (C) and *XBP1s* (D) mRNA by quantitative reverse-transcription (RT)-PCR in duplicate. Each point represents the mean ± SD (n = 3). HuH-7 cells were treated with GGA (0–20 μM) for 1 h, and total mRNA was extracted to estimate the cellular levels of *XBP1u* (E) and *XBP1s* (F) mRNA by RT-qPCR. Each point represents the mean ± SE of seven independent experiments. Asterisks (*, **, ***) indicate statistically significant difference from a control sample at 0 h with p value of < 0.05, 0.01, 0.001, respectively, as determined by ANOVA followed by post hoc multiple comparison test. PLC/PRF/5 (G), HepG2 (H) or Hep3B (I) cells were treated with 20 μM GGA for 0, 0.5, 1, 2, 4, 8, and 24 h, and total mRNA was extracted to analyze *XBP1u* and *XBP1s* mRNA expression by RT-qPCR. Closed and open circles indicate the relative abundance of XBP1u and XBP1s mRNA, respectively.

Name	Chemical Structure	IC_{50} (μM, M ± SE)	R square*
GGA	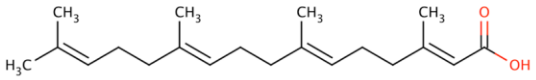	8.87 ± 1.03	0.9679
(*S*)-2,3-dihydroGGA	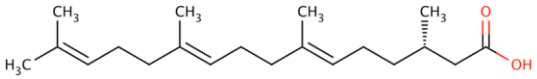	20.03 ± 0.56	0.9359
(*R*)-2,3-dihydroGGA	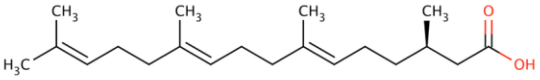	25.05 ± 1.89	0.8878
9CRA	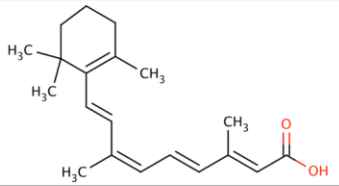	25.79 ± 2.21	0.8535
ATRA	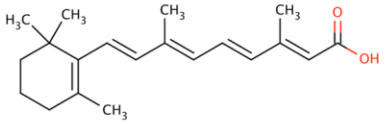	>50	
Phytanic acid	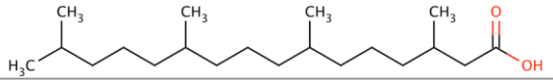	-	
Phytenic acid	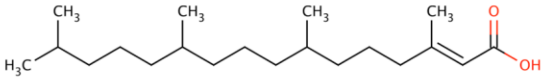	-	
Farnesoic acid	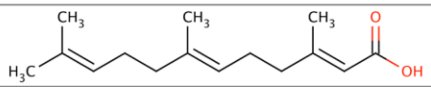	-	
Geranoic acid	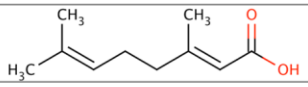	-	
Geranylgeraniol	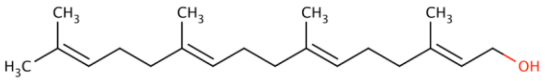	-	
Dolichoic acid	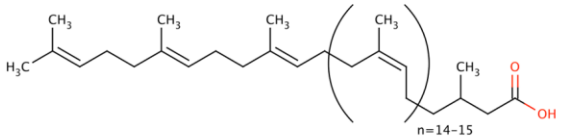	-	
Palmitic acid	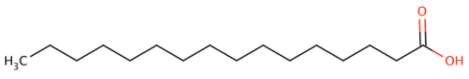	-	
Arachidic acid	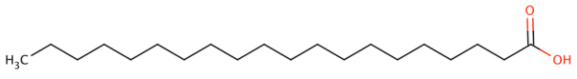	-	

*: The value R^2 quantifies goodness of fit to an equation of dose-response curve.

Fig. IV-2. List of compounds tested and their IC_{50} values determined by CellTiter Glo assay and GraphPad Prism.

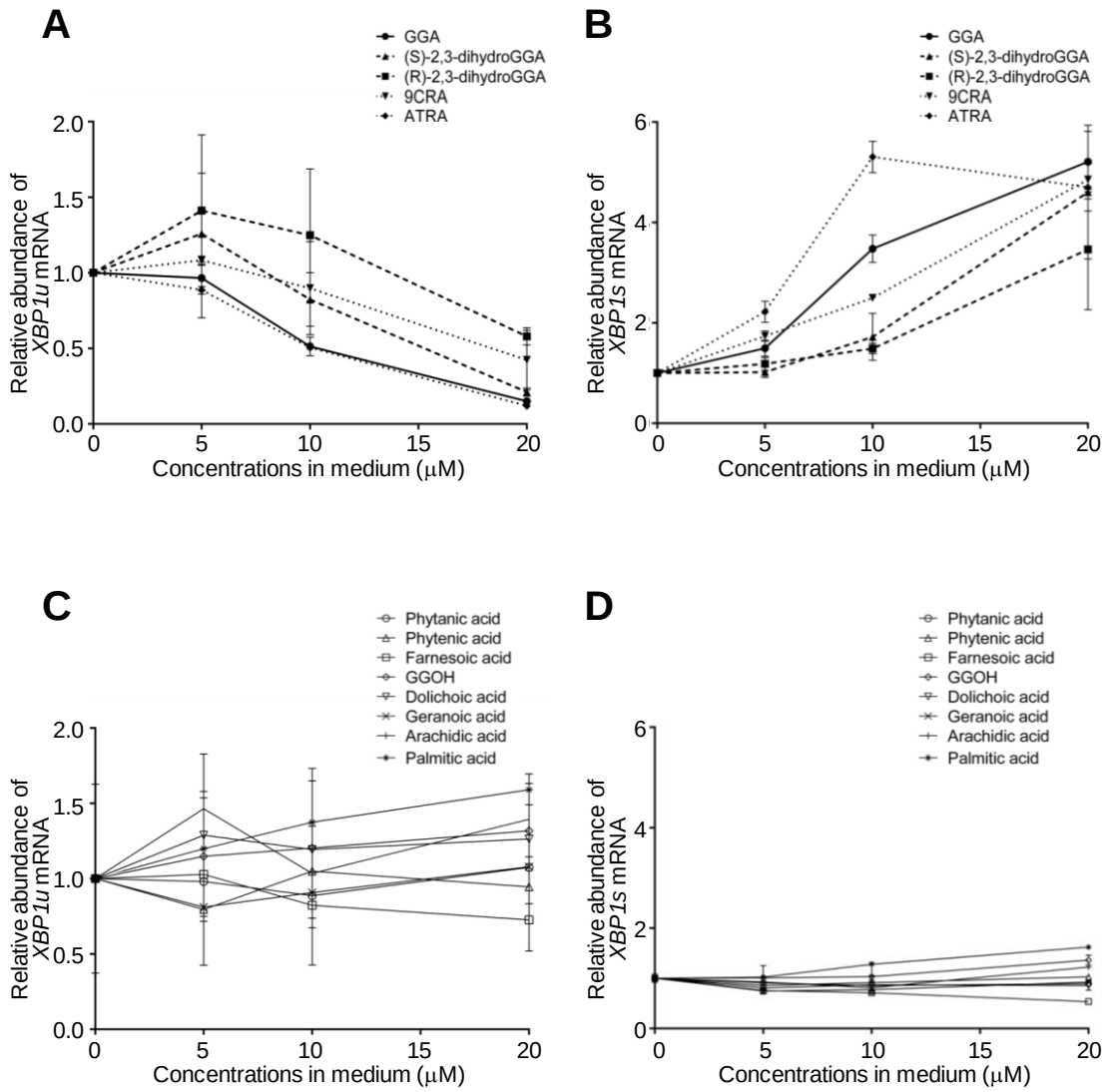

Fig. IV-3. Specificity of diterpenoid-induced splicing of *XBP1* mRNA in HuH-7 cells. HuH-7 cells were treated with GGA, (*S*)-2,3-dihydroGGA, (*R*)-2,3-dihydroGGA, ATRA, 9CRA, phytanic acid, phytenic acid, farnesoic acid, GGOH, dolichoic acid, geranoic acid, palmitic acid, or arachidic acid (0–20 μM) for 1 h. Total mRNA was extracted to analyze the cellular levels of *XBP1u* (A, C) and *XBP1s* (B, D) mRNA by RT-qPCR. Panels (A), (B) GGA, (*S*)-2,3-dihydroGGA, (*R*)-2,3-dihydroGGA, ATRA, or 9CRA are shown. These acids significantly changed both mRNA levels as revealed by ANOVA ($p < 0.05$). Panels (C), (D) phytanic acid, phytenic acid, farnesoic acid, GGOH, dolichoic acid, geranoic acid, palmitic acid and arachidic acid (0–20 μM) are plotted. Effects of each compound in this group on both mRNA levels are not statistically significant. Each point represents the mean ± SE (n = 1–7).

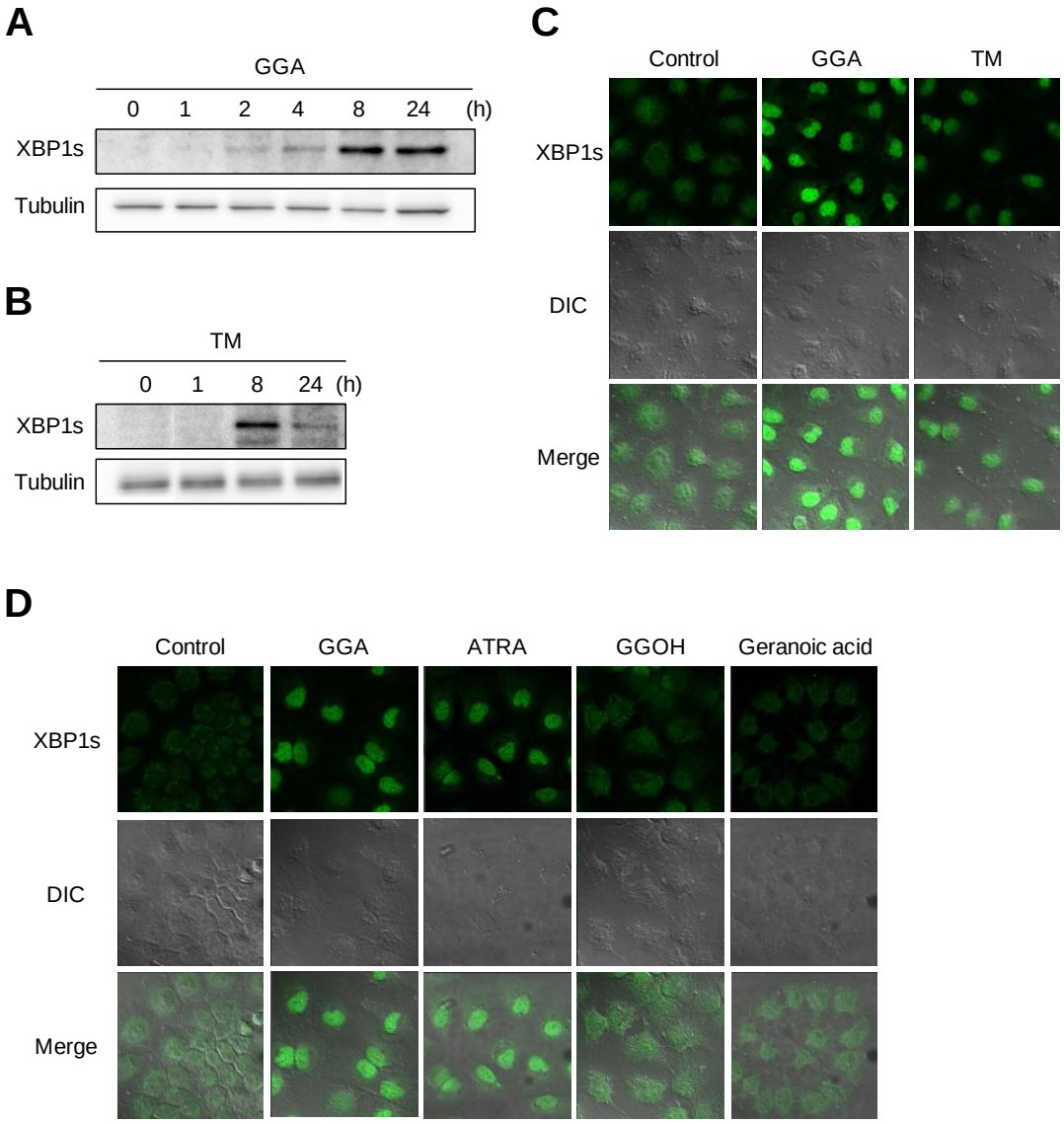

Fig. IV-4. Nuclear accumulation of XBP1s after GGA treatment.

(A), (B) HuH-7 cells were treated with 20 μM GGA (GGA) for 0, 1, 2, 4, 8, and 24 h or 0.25 μg/mL tunicamycin (TM) for 0, 1, 8, and 24 h. Whole-cell lysates were prepared, 30 μg of total protein per lane were used for GGA-treated cell lysates, 15 μg were used for TM-treated cell lysates and XBP1s levels were analyzed by western blotting. Total tubulin-βIII was used as a loading control. (C) HuH-7 cells were cultured under the following conditions: vehicle control (Control), 20 μM GGA for 8 h (GGA) or 0.25 μg/mL tunicamycin for 8 h (TM). Green fluorescence indicates the distribution of XBP1s. DIC: differential interference contrast. (D) HuH-7 cells were cultured with vehicle alone (Control), 10 μM GGA (GGA), 10 μM ATRA (ATRA), 10 μM GGOH (GGOH) or 10 μM geranoic acid (Geranoic acid) for 8 h. Green fluorescence indicates the distribution of XBP1s protein in cells.

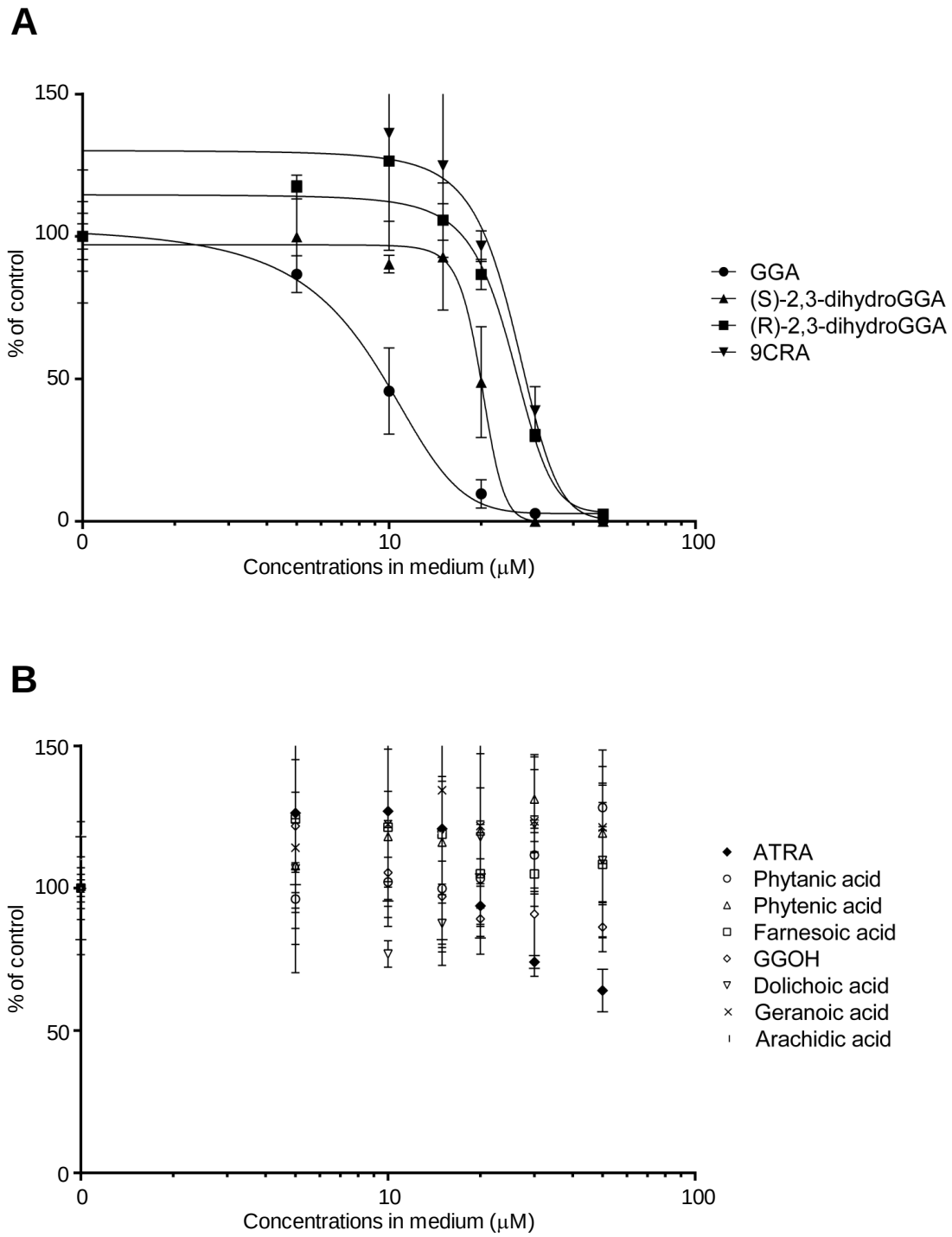

Fig. IV-5. Specificity of diterpenoid-induced cell death in HuH-7 cells.

Viable cells were measured using the CellTiter-Glo assay at 24 h after treatment with 0–50 μM of GGA, (*S*)-2,3-dihydroGGA, (*R*)-2,3-dihydroGGA, or 9CRA (A), and ATRA, phytanic acid, phytenic acid, farnesoic acid, GGOH, dolichoic acid, geranoic acid, or arachidic acid (B). Experiments were performed in triplicate. Values are the means ± SE (n = 3). Inhibition curves for each compound in panel (A) were created to find IC_{50} (shown in **Fig. 2**) using GraphPad Prism 6, whereas the software failed to fit a dose-response curve to find IC_{50} for each compound in panel (B).

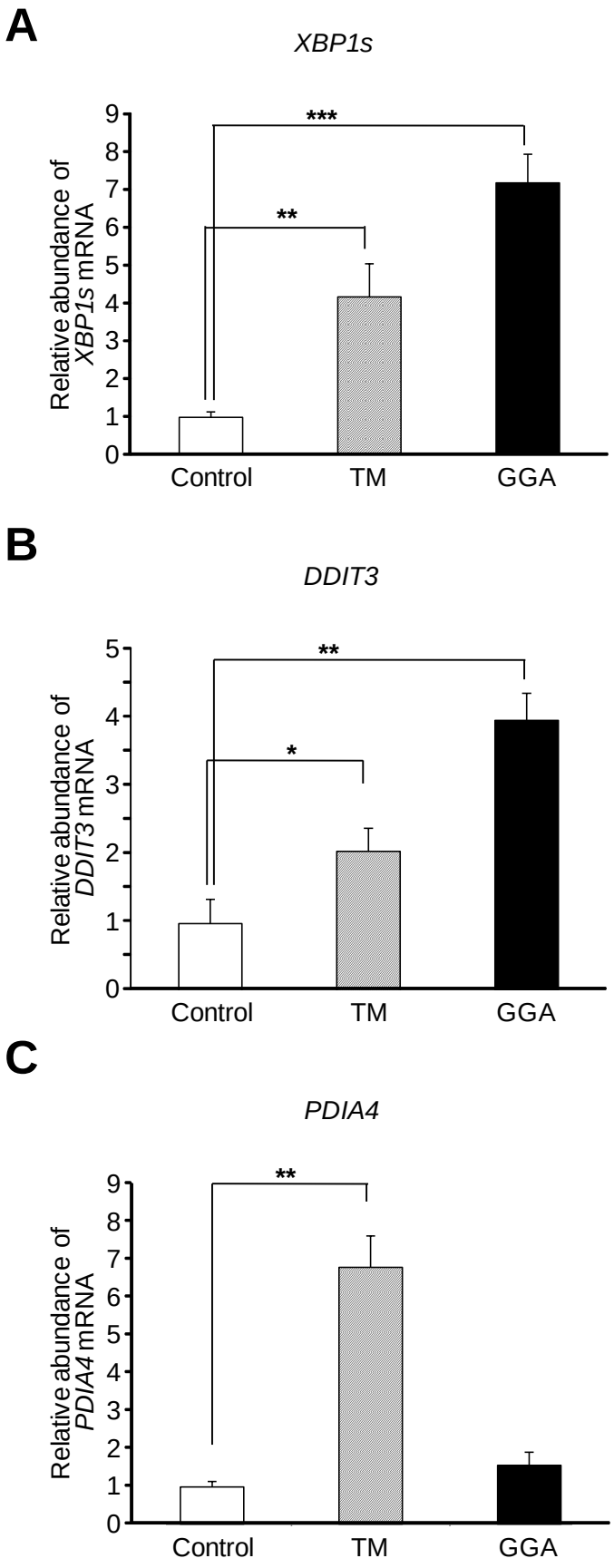

Fig. IV-6. Similarity of GGA-induced UPR with palmitate-induced UPR.

HuH-7 cells were treated with 20 μM GGA (GGA), 0.25 μg/mL tunicamycin (TM) or ethanol vehicle alone (Control) for 8 h. Then total mRNA was extracted to analyze the cellular levels of *XBP1s* (A) and *DDIT3* (B) mRNAs by RT-qPCR. HuH-7 cells were treated with 20 μM GGA (GGA), 0.25 μg/mL tunicamycin (TM) or ethanol vehicle alone (Control) for 24 h, and total mRNA was extracted to analyze *PDIA4* mRNA (C). Each point represents the mean ± SD (n = 3). All the P values were evaluated by t-test. *, $P<0.05$, **, $P<0.01$, ***, $P<0.005$.

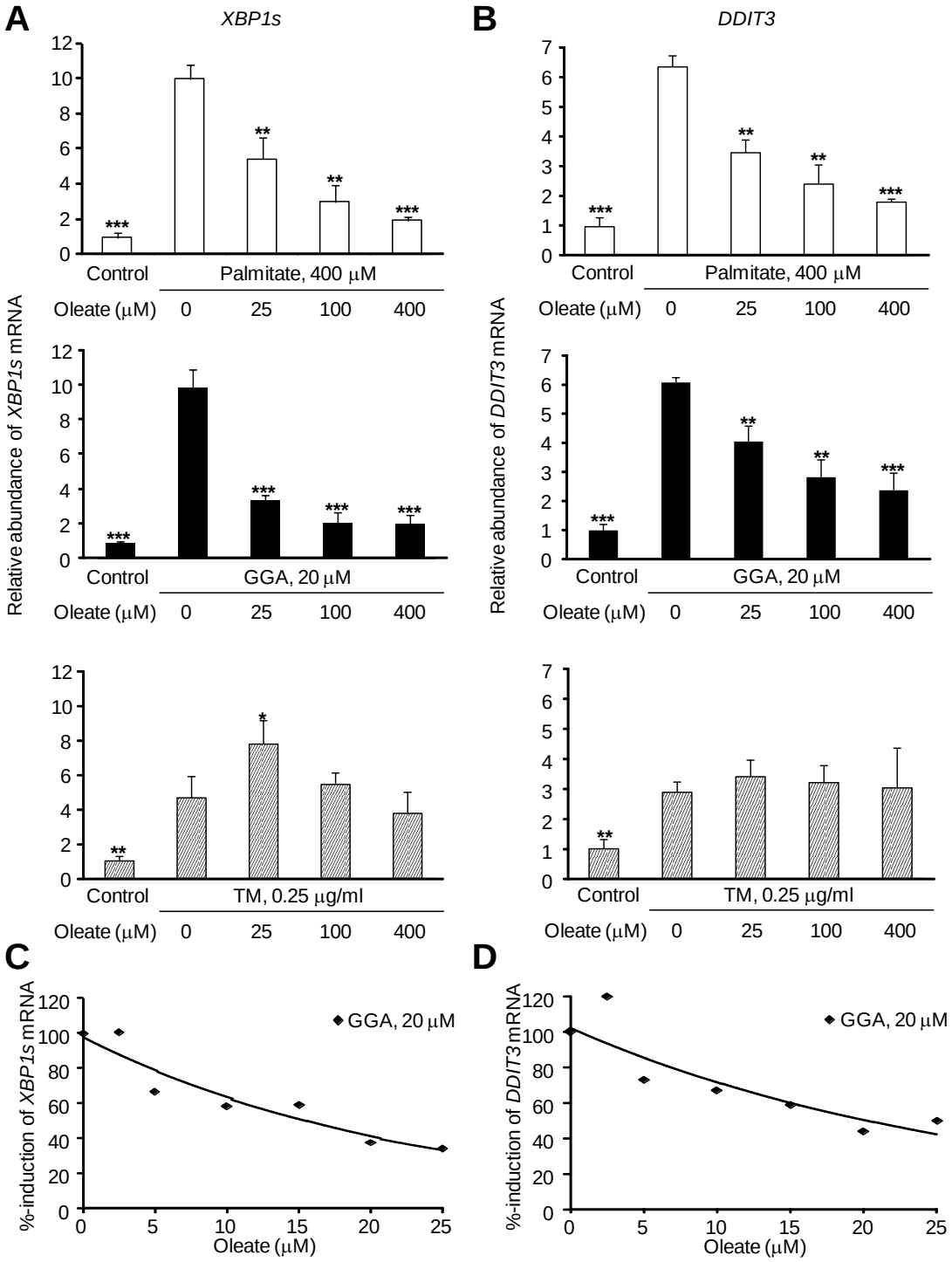

Fig. IV-7. Suppression of GGA-induced UPR with oleate.

HuH-7 cells were treated with 400 μM palmitate (Palmitate), 20 μM GGA (GGA) or 0.25 μg/mL of tunicamycin (TM) for 8 h in the presence of oleate (0, 25, 100 or 400 μM). Total mRNA was extracted to analyze the cellular levels of *XBP1s* (A) and *DDIT3* (B) mRNA by RT-qPCR. Each point represents the mean ± SD (n = 3). The asterisks (*, **, ***) indicate statistical significance ($p < 0.05$, 0.01, 0.001, respectively), compared with each relevant control induced by palmitate (400 μM), GGA (20 μM) or TM (0.25 μg/mL) alone as determined by Student's t-test. (C), (D) HuH-7 cells were treated with 20 μM GGA in the absence or presence of oleate (2.5, 5, 10, 15, 20 or 25

μM) for 8 h. Total mRNA was extracted to measure the cellular levels of *XBP1s* (C) and *DDIT3* (D) mRNA by quantitative reverse-transcription (RT)-PCR in triplicate.

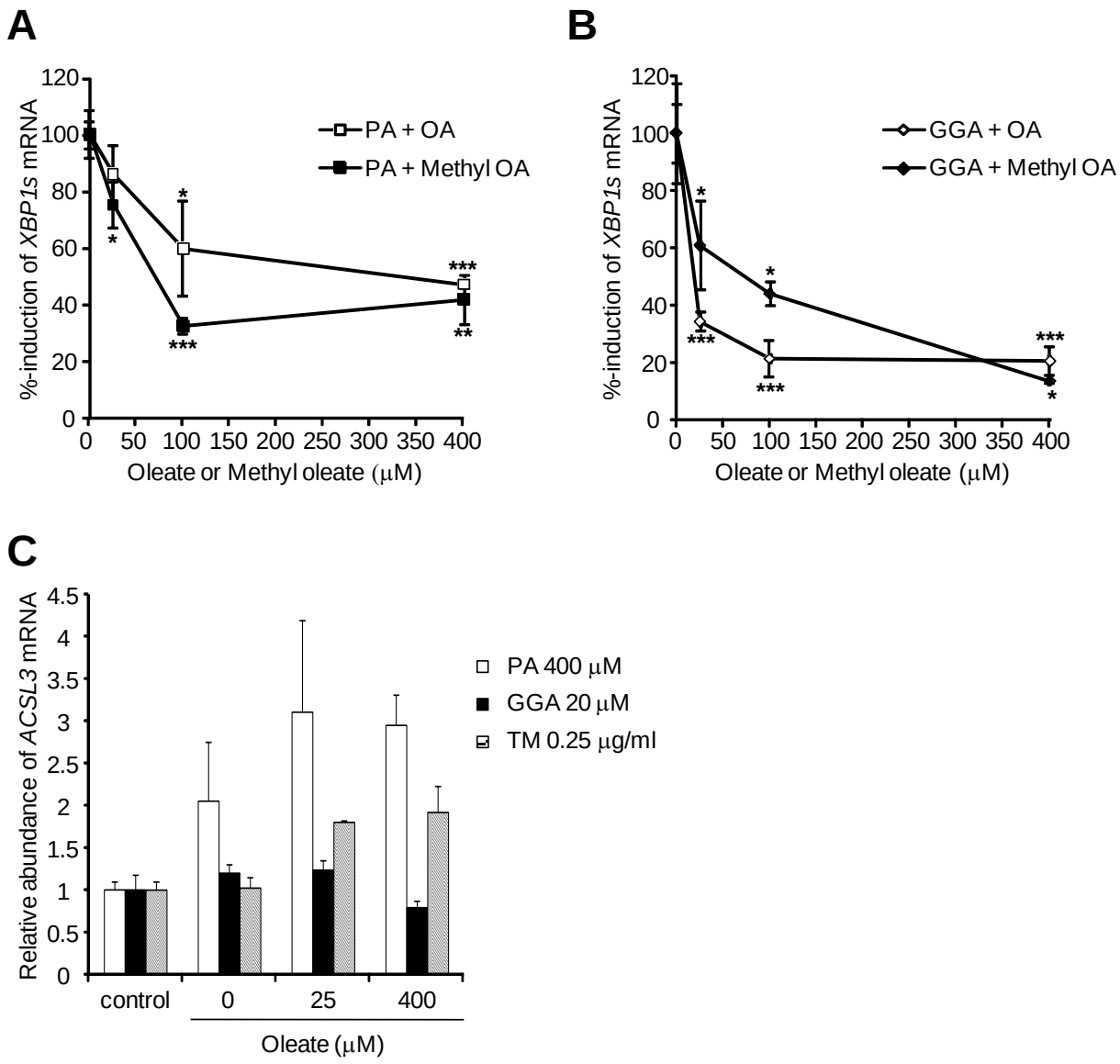

Fig. IV-8. Methyl oleate-mediated suppression of GGA-induced UPR.

(A) HuH-7 cells were treated with 400 μM palmitate (PA) for 8 h in the absence or presence of 25, 100 or 400 μM oleate (open square) or methyl oleate (closed square). Total mRNA was extracted to measure the cellular level of *XBP1s* mRNA by RT-qPCR. Each point represents the mean ± SD (n = 3). (B) HuH-7 cells were treated with 20 μM GGA for 8 h in the absence or presence of 25, 100 or 400 μM oleate (open diamond) or methyl oleate (closed diamond). Total mRNA was extracted to measure the cellular level of *XBP1s* mRNA by RT-qPCR. Each point in panel (A) and (B) represents the mean ± SD (n = 3) of % induction to palmitate (A) and GGA (B) control, respectively. The asterisks (*, **, ***) indicate statistical significance ($p < 0.05$, 0.01, 0.001, respectively), compared with each relevant control induced by palmitate (400 μM) or GGA (20 μM) alone as determined by Student's t-test. (C) HuH-7 cells were treated with vehicle alone (control), 400 μM palmitate (PA), 20 μM GGA or 0.25 μg/ml of tunicamycin (TM) for 8 h in the presence of oleate (OA) (0, 25 or 400 μM). Total mRNA was extracted to analyze the cellular levels of *ACSL3* mRNA by RTqPCR. Each point represents the mean ± SD (n = 3).

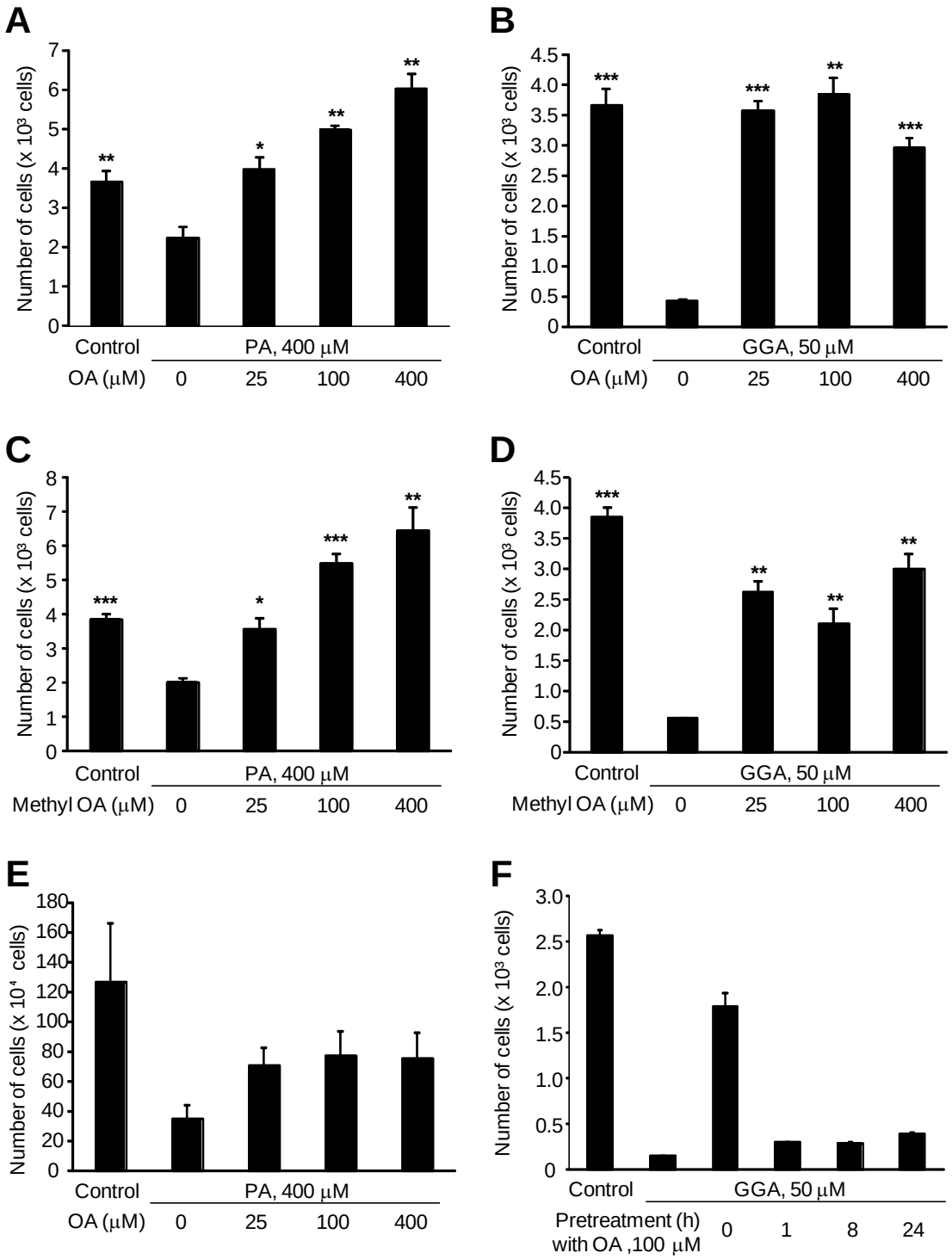

Fig. IV-9. Oleate-mediated suppression of GGA-induced cell death.

HuH-7 cells were treated with 400 μM palmitate (PA, A) or 50 μM GGA (B) in the absence or presence of oleate (25, 100 or 400 μM) for 24 h. The cells were treated with 400 μM palmitate (PA, C) or 50 μM GGA (D) in the absence or presence of methyl oleate (25, 100 or 400 μM) for 24 h. Viable cells were measured using the CellTiter-Glo assay kit. Values are the means ± SE (n = 3, 6 or 15). The asterisks (*, **, ***) indicate statistical significance ($p < 0.05$, 0.01, 0.001, respectively), compared with each relevant control induced by palmitate (400 μM) or GGA (50 μM) alone as determined by Student's t-test. (E) HuH-7 cells were treated with 400 μM palmitate (PA)

in the absence or presence of oleate (25, 100 or 400 μM) for 24 h. Viable cells were measured using the Trypan blue method. Values are the means ± SD (n = 7). (F) HuH-7 cells were treated with vehicle alone (control), 50 μM GGA in the absence or presence of 100 μM oleate or with pretreatment of 100 μM OA 0–24 h before 50 μM GGA treatment. 0-h pretreatment means that the cells were treated simultaneously with 50 μM GGA and 100 μM OA. Viable cells were measured using the CellTiter-Glo assay kit. Each point represents the mean± SD (n = 3, 6 or 18).

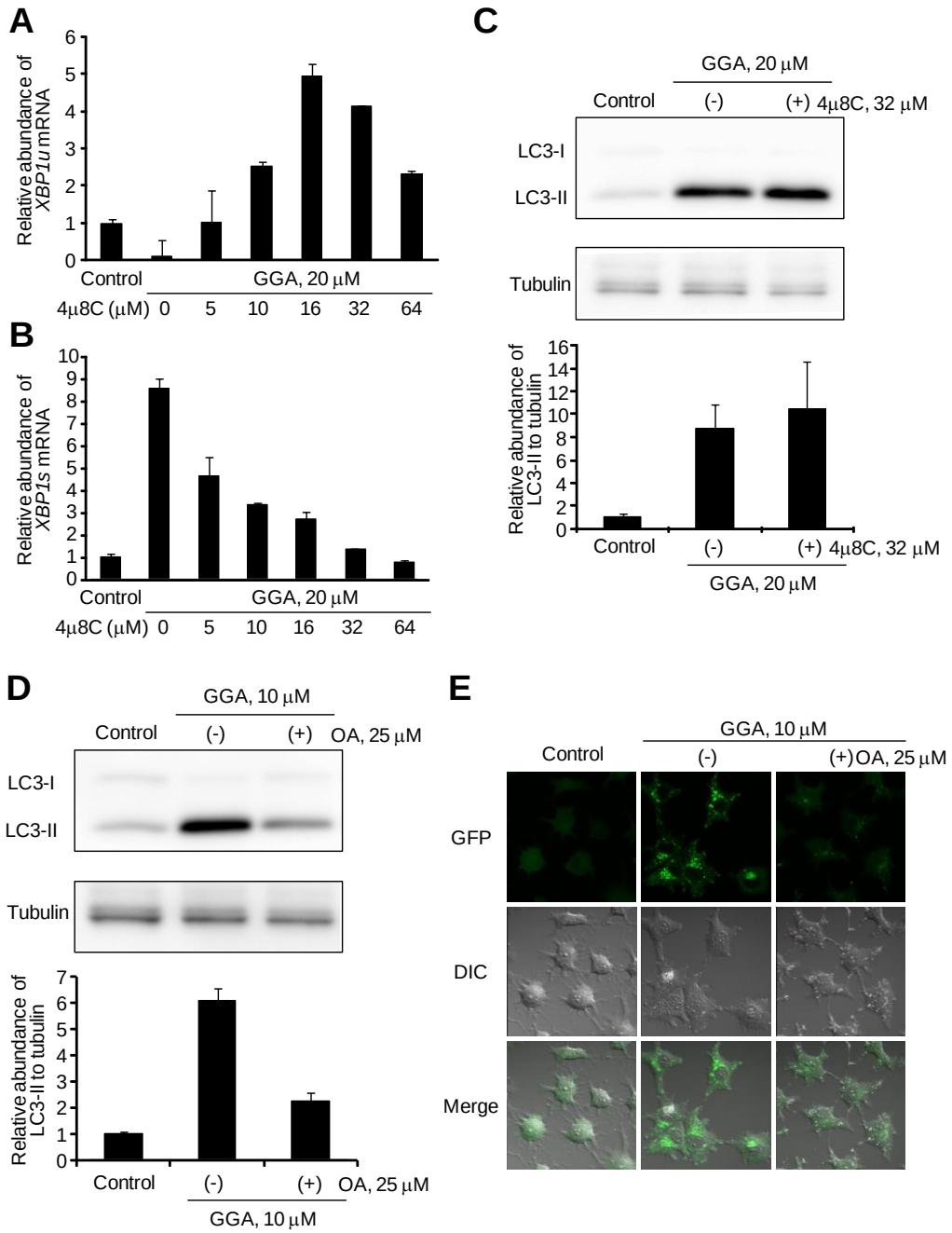

Fig. IV-10. Attenuation of GGA-induced LC3β-II accumulation by oleate co-treatment.

HuH-7 cells were treated with 0–64 μM 4μ8C for 8 h in the absence or presence of 20 μM GGA. Total mRNA was extracted to analyze *XBP1u* (A) and *XBP1s* (B) mRNA expression by RT-qPCR. (C) HuH-7 cells were treated with 20 μM GGA in the absence or presence of 32 μM 4μ8C for 8 h. (D) HuH-7 cells were treated with 10 μM GGA in the absence or presence of 25 μM oleate for 8 h. Whole-cell lysates (15 μg/lane) were prepared and LC3 levels were analyzed by western blotting. Tubulin-βIII was used as a loading control. Levels of LC3-II expression were quantified with ImageJ densitometric analysis (mean ± SE, n = 3). Representative blots and corresponding quantification of LC3-II / Tubulin-βIII are shown. (E) A stable clone of HuH-7/GFP-LC3 was treated with 10 μM GGA in the absence or presence of 25 μM oleate for 8 h. Live-cell imaging was performed with the green fluorescence for GFP on an LSM700 confocal laser-scanning fluorescence microscope.

Chapter V

General Discussion

Chieko Iwao

Molecular and Cellular Biology, Graduate School of Human Health Science, University of Nagasaki, Nagasaki, Japan

GGA has been repeatedly reported to induce cell death in HuH-7 cells [2, 3]. And Shidoji and his colleague have reported various cell-death related effects of GGA at micro-molar concentrations in HuH-7 cells: chromatin condensation, large-scale DNA fragmentations, nucleosomal-scale ladder formation and dramatic loss of $\Delta\Psi m$ and incomplete autophagic response [3, 8, 9, 24]. Recently I keep my eyes on GGA-induced incomplete autophagic response. GGA induces initial phase of autophagy, but fails the maturation of autolysosomes, and leads to substantial accumulation of early/initial autophagic vacuoles, LC3-II, and p62/SQSTM in HuH-7 cells.

Hence in the present thesis study, I have tried to investigate the mechanisms by which GGA induces incomplete autophagy-related cell death in HuH-7 cells by focusing on the tumor suppressor gene *TP53*.

V-1. How GGA affects p53 in HuH-7 cells?

V-1-1. Upregulation of p53-target SCO2, TIGAR and PUMA

In chapters II and III, I investigated changes in cellular expression of 3 *TP53*-targeted genes, *SCO2*, *TIGAR* and *PUMA*, after GGA treatment. The *SCO2*, *TIGAR* and *PUMA* genes are related to respiration, inhibition of glycolysis and cell death, respectively [16]. As a result, it has been found GGA induces upregulation of the *SCO2*, *TIGAR* and *PUMA* genes at their protein levels in HuH-7 cells, which possess the mutant *TP53* gene [50].

Interestingly GGA-induced upregulation of the *SCO2* and *TIGAR* genes was found only at their protein level and not at their mRNA levels, although the *PUMA* gene is upregulated at its transcript level by GGA treatment. Insofar as the *PUMA* gene, I am now speculating p53 might be reactivated after GGA treatment and the resultant reactivated p53 may play a role as transcription factor in the *PUMA* gene expression. But the upregulatory effects of GGA on SCO2 and TIGAR protein levels should be post-transcriptional, because their transcript levels were not changed by GGA treatment.

Recently one novel mechanism for cellular functions of p53 has been suggested that p53 might play a role as a translational regulator [102, 103]. In detail, p53 in the cytoplasm can suppress

translation of several proteins by its binding to polyribosomes. In chapter III, it was found that the mutant p53 accumulated in the cytoplasm in HuH-7 cells, and GGA almost completely removed the mutant p53 from cytoplasm and conveyed it to nuclei. So, prior to GGA treatment, the accumulated p53 in cytoplasm may be able to suppress translation of SCO2 and TIGAR proteins and then, after GGA treatment, the suppression must be cancelled, resulting in upregulation of the cellular level of these proteins (see Fig. V-1).

V-1-2. GGA-induced changes in metabolomics profiles.

Furthermore, metabolic alterations were globally surveyed associated with GGA-induced upregulation of TIGAR and SCO2 protein. It was found GGA-induced time-dependent increase of the cellular F6-P level, the inverse decrease of the cellular F1,6-DP level, and upregulation of the cellular NADH level, all of which are consistent with GGA-induced upregulation of TIGAR and SCO2 proteins. In other words, as described in chapter I, TIGAR is an enzyme of F2,6-DPase, which accumulates F6-P in cells and then blocks glycolysis by directing the pathway into the pentose phosphate shunt. And SCO2 is a mitochondrial chaperone, which is required for the proper assembly of COX (or complex IV) that is directly responsible for the reduction of oxygen during aerobic respiration. Hence, I speculated GGA might be able to ameliorate the Warburg effect by shifting cellular energetic status from glycolysis essential for cancer cells to aerobic respiration through upregulation of TIGAR and SCO2 proteins. However, taking account of GGA induced-upregulation of NADH, loss of $\Delta\Psi m$ and hyperproduction of mitochondrial superoxide [3], I have rather considered mitochondrial electron transport chain may not work well after GGA treatment, so that GGA probably induces impairment of oxidative phosphorylation that efficiently reforms ATP from ADP.

V-1-3. GGA-induced nuclear translocation of the mutant p53.

From these results that GGA may shift an energetic state from glycolysis to respiration dependency by reactivating the mutant p53 and the reactivated p53 can transactivate the *PUMA*

gene, I decided to examine more in detail how GGA affects the mutant p53 in HuH-7 cells. It was found that mutant p53 that accumulates in the cytoplasm of HuH-7 cells is translocated to the nuclear compartment immediately after treatment with GGA. In cell-free experiments, I was able to demonstrate that GGA transforms native forms of cytoplasmic p53 from non-penetrating huge aggregates (complex with CUL9/PARC and organelles which are excluded by sedimenting at 105,000 × *g* for 90 min, for example ER) to penetrating approximate 670-kD complexes on both BN-gradient PAGE and crosslinking SDS-PAGE in a dose-dependent manner. And it is also important for autophagy to mention that autophagy-inducing stimuli cause the depletion of cytoplasmic p53 [83]. Therefore, it is strongly suggested that a nuclear translocation of cytoplasmic p53 may be important for GGA-induced autophagic cell death.

V-2. GGA-induced UPR is an upstream signal of GGA-induced autophagy.

In chapter IV, I focused on ER, where the p53-containing huge complexes are harbored in HuH-7 cells and UPR occurs as an initiating signal linked to autophagic cell death. GGA activates IRE1α and PERK pathways, but does not activate ATF6α pathway and the activation of the IRE1α and PERK pathways is blocked by co-treatment with oleate. These are typical characteristics of lipid-induced UPR, for example palmitic acid-induced UPR [46]. So GGA induces so-called "lipid-induced UPR" but not canonical UPR. Further, GGA-induced UPR is somewhat different from palmitate-induced UPR in at least 2 points, palmitate is saturated fatty acid but GGA is polyunsaturated fatty acid, and palmitate usually induces UPR at > 400 μM but GGA induces it at sub-ten μM.

Furthermore, oleate co-treated with GGA perfectly rescued the cells from GGA-induced cell death and inhibited GGA-induced accumulation of LC3-II. And used was methyl oleate, which is not a direct substrate for long chain fatty ACSL (acyl-CoA synthetase long-chain), instead of oleate. Methyl oleate also suppressed GGA-induced UPR as well as GGA-induced cell death, suggesting

that oleate itself or unesterified oleate prevents GGA-induced UPR and cell death. So it could be described that GGA induces ER stress/UPR, which might be associated with GGA-induced autophagic cell death. But a specific IRE1 endonuclease inhibitor, 4μ8C does not attenuate GGA-induced cellular accumulation of LC3-II. So it is suggested a possibility that GGA-induced *XBP1* splicing itself may not be essential for GGA-induced incomplete autophagic response and cell death, but GGA-induced other signals of IRE1 and PERK pathways of UPR may be important for GGA-induced autophagic cell death.

V-3. Conclusions.

Taken together all with the previous findings on GGA, here it is demonstrated how GGA induces cell death in human hepatoma HuH-7 cells through incomplete autophagic response. First, GGA at micromolar concentrations causes the lipid-induced UPR, which may trigger an initial phase of autophagic response. Second, GGA-induced UPR may cause a release of the cytoplasmic p53 stored in the ER into the nuclei, then the resultant functional p53 might be involved in GGA-induced upregulation of the *PUMA* gene and removal of the cytoplasmic p53 may release the p53-mediated translational suppression of TIGAR and SCO2. Two of TIGAR and SCO2 proteins cause a metabolic shift from glycolysis to aerobic respiration together. In this respect, a recent paper is interesting that XBP1s directly binds to and activates the promoter of PPAR α, which stimulates mitochondrial β-oxidation, providing a large amount of NADH and acetyl-CoA [104]. So, one cannot exclude a possibility that GGA-induced UPR and GGA-induced upregulation of p53-target TIGAR and SCO2 may coordinately play their role in GGA-induced energetic changes or amelioration of the Warburg effect of malignant cells. But, these metabolic changes may be lethal for malignant cells, because their mitochondria become to produce a large excess of superoxide [24].

Finally, it is worthwhile to mention that a precise molecular mechanism of GGA-induced cell death, particularly at the most last part of cell death, is beyond the scope of the present study. To put

it another way, in this work, it was not addressed how GGA-induced incomplete autophagic response causes cell death. It is intuitively speculated that incompleteness of autophagic response should be linked to cell death, because autophagy is an effective mechanism originally for cell survival, not for cell death.

Therefore, as prospects for the future, more detailed studies on a molecular mechanism how GGA induces cell death in human hepatoma cells are definitely required. Furthermore, one should be even aware that any signals from GGA-induced UPR have not yet been illustrated linked to GGA-induced incomplete autophagic response.

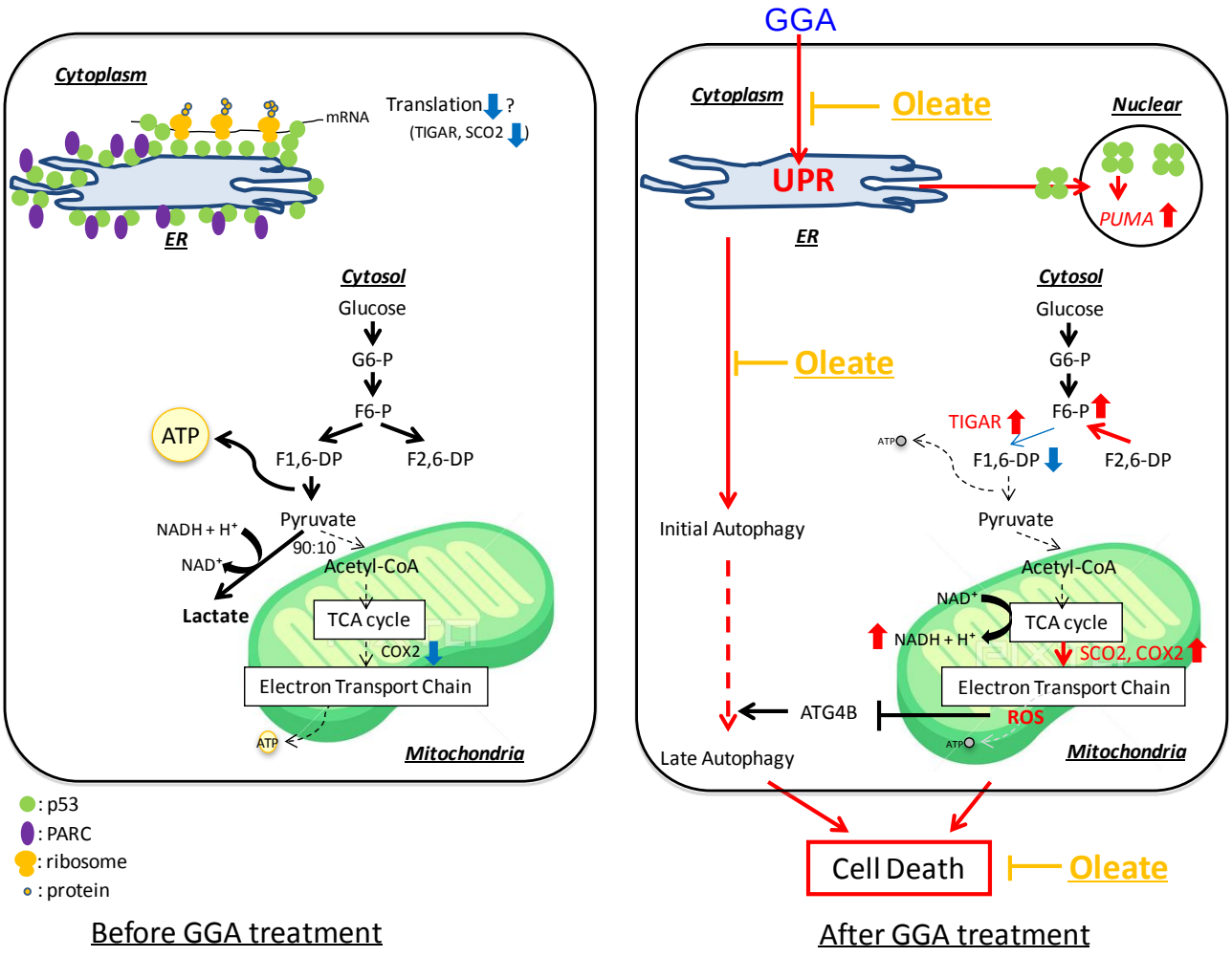

Fig.V-1. Hypothetical mechanisms underlying GGA-induced cell death in HuH-7 cells.

Acknowledgments

This work was carried out in the Laboratory of Molecular and Cellular Biology, Graduate School of Human Health Science, University of Nagasaki in Nagayo, Nagasaki during the years 2012 – 2015.

I would like to show my greatest appreciation to my supervisor, Professor Yoshihiro Shidoji, whose encouragement, guidance and support from the initial to the final level enabled me to develop an understanding of the subject

I would like to special thank to Chiharu Sakane, a former graduate student of the Shidoji research group, who give me many experimental technique.

Finally, I owe my deepest gratitude to my parents and family for their generous support and warm encouragement.

March 2016

Chieko Iwao

References

1. Shidoji, Y. and Ogawa, H. Natural occurrence of cancer-preventive geranylgeranoic acid in medicinal herbs. *J Lipid Res.* **45**: 1092-1103 (2004).
2. Nakamura, N., Shidoji, Y., Yamada, Y., Hatakeyama, H., Moriwaki, H. and Muto, Y. Induction of apoptosis by acyclic retinoid in the human hepatoma-derived cell line, HuH-7. *Biochem Biophys Res Commun.***207**: 382-388 (1995).
3. Shidoji, Y., Nakamura, N., Moriwaki, H. and Muto, Y. Rapid loss in the mitochondrial membrane potential during geranylgeranoic acid-induced apoptosis. *Biochem Biophys Res Commun.* **230**: 58-63 (1997).
4. Muto, Y., Moriwaki, H., Ninomiya, M., Adachi, S., Saito, A., Takasaki, K.T., Tanaka, K., Tsurumi, K., Okuno, M., Tomita, E., Nakamura, T. and Kojima, T. Prevention of second primary tumors by an acyclic retinoid, polyprenoic acid, in patients with hepatocellular carcinoma. Hepatoma prevention group. *N Engl J Med.* **334**: 1561-1567 (1996).
5. Muto, Y., Moriwaki, H. and Saito, A. Prevention of second primary tumors by an acyclic retinoid in patients with hepatocellular carcinoma. *N Engl J Med.* **340**: 1046-1047 (1999).
6. Honda, M., Yamashita, T., Arai, K., Sakai, Y., Sakai, A., Nakamura, M., Mizukoshi, E. and Kaneko, S. Peretinoin, acyclic retinoid, improves the hepatic gene signature of chronic hepatitis c following curative therapy of hepatocellular carcimona. *BMC Cancer*. **13**: 191 (2013).
7. Muto, Y., Moriwaki, H. and Omori, M. In vitro binding affinity of novel synthetic polyprenoids (polyprenoic acids) to cellular retinoid-binding proteins. *Gann.* **72**: 974-977 (1981).
8. Yamada, Y., Shidoji, Y., Fukutomi, Y., Ishikawa, M., Kaneko, T., Nakagama, H., Imawari, M., Moriwaki, H. and Muto, Y. Positive and negative regulations of albumin gene expression by retinoids in human hepatoma cell lines. *Mol Carcinog.* **10**: 151-158 (1994).
9. Nakabayashi, H., Taketa, K., Yamane, T., Miyasaki, M., Miyano, K. and Sato, J. Phenotypical stability of a human hepatoma cell line, HuH-7, in long-term culture with chemically defined medium. *Gann.* **75**: 151-158 (1984).
10. Kumagai, S., Narasaki, R. and Hasumi, K. Glucose-dependent active ATP depletion by koningic acid kills high-glycolytic cells. *Biochem Biophys Res Commun.* **365**: 362-368 (2008).
11. Lowe, S.W. and Lin, A.W. Apoptosis in cancer. *Carcinogenesis.* **21**: 485-495 (2000).
12. Ashkenazi, A. and Dixit, V.M. Death receptors: signaling and modulation. *Science*. **281**: 1305-1308 (1998).
13. Bates, S. and Vousden, K.H. Mechanisms of p53-mediated apoptosis. *Cell Mol Kife Sci.* **55**: 28-37 (1999).
14. Vousden, K.H. p53: death star. *Cell.* **103**: 691-694 (2000).
15. Toledo, F. and Wahl, G.M. Regulation the p53 pathway: in vitro hypotheses, in vivo veritas. *Nat Rev Cancer*. **6**: 909-923 (2006).
16. Bensaad, K. and Vousden, K.H. p53: new roles in metabolism. *Trends Cell Biol.* **17**: 286-291 (2007).

17. Green, D.R. and Chipuk, J.E. p53 and metabolism: Inside the TIGAR. *Cell.* **126**: 31-32 (2006).
18. Yu, J., Zhang, L., Hwang, P.M., Kinzler, K.M. and Vogeulstein, B. PUMA induces the rapid apoptosis of colorectal cancer cells. *Mol Cell.* **7**: 673-682 (2001).
19. Bensaad, K., Tsuruta, A., Selak, M.A., Vidal, M.N., Nakano, K., Bartrond, R., Gottlieb, E. and Vousden, K.H. TIGAR, a p53-inducible regulator of glycolysis and apoptosis. *Cell.* **126**: 107-120.
20. Matoba, S., Kang, J.G., Patino, W.D., Wragg, A., Boehm, M., Gavrilova, O., Hurley, P.J., Bunz, F. and Hwang, P.M. p53 regulates mitochondrial respiration. *Science.* **312**: 1650-1653 (2006).
21. Kim, J.W. and Dang, C.V. Cancer's molecular sweet tooth and the Warburg effect. *Cancer Res.* **66**: 1650-1653 (2006).
22. Bui, T. and Thompson, C.B. Cancer's sweet tooth. *Cancer Cell.* **9**: 419-420 (2006).
23. Corcoran, C.A., Huang, Y. and Sheikh, M.S. The regulation of energy generating metabolic pathway by p53. *Cancer Biol Ther.* **5**: 1610-1613 (2006).
24. Okamoto, K., Sakimoto, Y., Imai, K., Senoo, H. and Shidoji, Y. Induction of an incomplete autophagic response by cancer-preventive geanylgeranoic acid (GGA) in a human hepatoma-derived cell line. *Biochem J.* **440**: 63-71 (2011).
25. Hochstrasser, M. Ubiquitin-dependent protein degradation. *Annu Rev Genet.* **30**: 405-439 (1996).
26. Mortimore, G.E. and Poso, A.R. Intracellular protein catabolism and its control during nutrient depeivation and supply. *Annu Rev Nutr.* **7:** 539-564 (1987).
27. Seglen, P.O. and Bohley, P. Autophagy and other vacuolar protein degradation mechanisms. *Experientia.* **48**: 158-172 (1992).
28. Mizushima, N., Ohsumi, Y. and Yoshimori, T. Autophagosome formation in mammalian cells. *Cell Struct Funct.* **27**: 421-429 (2002).
29. Kabeya, Y., Mizushima, N., Ueno, T., Yamamoto, A., Kirisako, T., Noda, T., Kominami, E., Ohsumi, Y. and Yoshimori, T. LC3, a mammalian homologue of yeast Apg8p, is localized in autophagosome membranes after processing. *Embo J.* **19**: 5720-5728 (2000).
30. Levine, B. and Klionsky, D.J. Development by self-digestion: molecular mechanisms and biological functions of autophagy. *Dev Cell.* **6**: 463-477 (2004).
31. Hara, T., Nakamura, K., Matsui, M., Yamamoto, A., Nakahara, Y., Suzuki-Migishima, R., Yokoyama, M., Mishima, K., Saito, I., Okano, H. and Mizushima, N. Suppression of basal autophagy in neural cells causes neurodrgenerative disease in mice. *Nature.* **441**: 885-889 (2006).
32. Komatsu, M., Waguri, S., Chiba, T., Murata, S., Iwata, J., Tanida, I., Ueno, T., Koike, M., Uchiyama, Y., Kominami, E. and Tanaka, K. Loss of autophagy in the central nervous ayatem causes neuurodegeneration in mice. *Nature.* **441**: 880-884 (2006).
33. Komatsu, M., Ueno, T., Waguri, S., Uchiyama, Y., Kominami, E. and Tanaka, K. Constitutive autophagy: vital role in clearance of unfavorable proteins in neurons. *Cell Death Differ.* **14**: 887-894 (2007).

34. Komatsu, M., Waguri, S., Ueno, T., Iwata, J., Murata, S., Tanida, I., Ezaki, J., Mizushima, N., Ohsumi, Y., Uchiyama, Y., Kominami, E., Tanaka, K. and Chiba, T. Impairment of starvation-induced and constitutive autophagy in Atg7-deficient mice. *J Cell Biol.* **169**: 425-434 (2005).
35. Biden, T.J., Boslem, E., Chu, K.Y. and Sue, N. Lipotoxic endoplasmic reticulum stress, b cell failure, and type 2 diabetes mellitus. *Trends Endocrinol Metab*. **25**: 389-398 (2014).
36. Walter, P. and Ron, D. The unfolded protein response: from stress to homeostatic regulation. *Science*. **25**: 1081-1086 (2011).
37. Urra, H. and Hetz, C. The ER in 4D: a novel stress pathway controlling endoplasmic reticulum membrane remodeling. *Cell Death Differ.* **19**: 1893-1895 (2012).
38. Malhi, H. and Kaufman, R.J. Endoplasmic reticulum stress in liver disease. *J Hep.* **54**: 795-809 (2011).
39. Feng, B., Yao, P.M., Li, Y., Devlin, C.M., Zhang, D., Harding, H.P., Sweeney, M., Rong, J.X., Kuriakose, G., Fisher, E.A., Marks, A.R., Ron, D. and Tabas, I. The endoplasmic reticulum in the site of cholesterol-induced cytotoxicity in macrophages. *Nat Cell Biol.* **5**: 781-792 (2003).
40. Kharroubi, I., Ladriere, L., Cardozo, A.K., Dogusan, Z., Cnop, M. and Eizirik, D.L. Free fatty acids and cytokines induce pancreatic beta-cell apoptosis by different mechanisms: role of nuclear factor-kappaB and endoplasmic reticulum stress. *Endocrinology.* **45**: 5087-5096 (2004).
41. Borradaile, N.M., Buhman, K.K., Listenberger, L.L., Magee, C.J., Morimoto, E.T., Ory, D.S. and Schafer, J.E. A critical role for eukaryotic elongation factor 1A-1 in lipotoxic cell death. *Mol Biol Cell.* **17**: 770-778 (2005).
42. Ariyama, H., Kono, N., Matsuda, S., Inoue, T. and Arai, H. Decrease in membrane phospholipid unsaturation induces unfolded protein response. *J Biol Chem*. **285**: 22027-22035 (2010).
43. Ozcan, U., Cao, Q., Yilmaz, E., Lee, A.H., Iwakoshi, N.N., Ozdelen, E., Tuncman, G., Gorgun, C., Glimcher, L.H. and Hotamisligil, G.S. Endoplasmic reticulum stress links obesity, insulin action, and type 2 diabetes. *Science*. 306: 457-461 (2004).
44. Fu, S., Yang, L., Li, P., Hofmann, O., Dicker, L., Hide, W., Lin, X., Watkins, S.M., Ivanov, A.R. and Hotamisligil, G.S. Aberrant lipid metabolism disrupts calcium homeostasis causing liver endoplasmic reticulum stress in obesity. *Nature*. **473**: 528-531 (2011).
45. Glegor, M.F., Yang, L., Fabbrini, E., Mohammed, B.S., Eagon, J.C., Hotamisligil, G.S. and Klein, S. Endoplasmic reticulum stress is reduced in tissues of obese subjects after weight loss. *Diabetes.* **58**: 693-700 (2009).
46. Kitai, Y., Ariyama, H., Kono, N., Oikawa, D., Iwawaki, T. and Arai, H. Membrane lipid saturation activates IRE1a without inducing clustering. *Genes Cells.* **18**: 798-809 (2013).
47. Ariyama, H., Kono, N., Matsuda, S., Inoue, T. and Arai, H. Decrease in membrane phospholipid unsaturation induces unfolded protein response. *J Biol Chem.* **285**: 22027-22035 (2010).
48. Sali, A., Glaeser, R., Earnest, T. and Baumeister, W. From words to literature in structural proteomics. *Nature*. **422**: 216-225 (2003).
49. Fiala, G.J., Schamel, W.W. and Blumenthal, B. Blue native polyacrylamide gel electrophoresis

(BN-PAGE) for analysis of multiprotein complexes from cellular lysates. *J Vis Exp*. **24**: 2164 (2011).

50. Hsu, I.C., Tokiwa, T., Bennett, W., Metcalf, R.A., Welsh, J.A., Sun, T. and Harris, C.C. P53 gene mutation and integrated hepatitis b viral DNA sequences in human liver cancer cell lines. *Carcinogenesis.* **14**: 987-992 (1993).
51. Mollereau, B. and Ma, D. The p53 control of apoptosis and proliferation: Lessons from drosophila. *Apoptosis.* **19**: 1421-1429 (2014).
52. Meek, D.W. Regulation of the p53 response and its relationship to cancer. *Biochem J.* **469**: 325-346 (2015).
53. Leary, S.C., Sasarman, F., Nishimura, T. and Shoubridge, E.A. Human sco2 is required for the synthesis of co ii and as a thiol-disulphide oxidoreductase for sco 1. *Hum Mol Genet.* **18**: 2230-2240 (2009).
54. Miller-Fleming, L., Olin-Sandoval, V., Campbell, K. and Ralser, M. Remaining mysteries of molecular biology: The role of polyamines in the cell. *J Mol Biol.* **10**: 1016 (2015).
55. Pegg, A.E. The function of spermine. *IUBMB Life.* **66**: 8-18 (2014).
56. Smirnova, O.A., Isaguliants, M.G., Hyvonen, M.T., Keinanen, T.A., Tunitskaya, V.L., Vepsalainen, J., Alhonen, L., Kochetkov, S.N. and Ivanov, A.V. Chemically induced oxidative stress increases polyamine levels by activating the transcription of ornithine decarboxylase and spermidine/spermine-nl-acethyltransferase in human hepatoma huh7 cells. *Biochimie*. 94: 1876-1883 (2012).
57. Muller, P.A., Vousden, K.H. and Norman, J.C. p53 and its mutations in tumor cell migration and invasion. *J Cell Biol.* **192**: 209-218 (2011).
58. Cheok, C.F., Verma, C.S., Baselga, J. and Lane, D.P. Translating p53 into the clinic. *Nat Rev Clin Oncol.* **8**: 25-37 (2011).
59. Yu, J. and Zhang, L. PUMA, a potent killer with or without p53. *Oncogene.* **27**: 71-83 (2008).
60. Yee, K.S., Wilkinson, S., James, J., Ryan, K.M. and Vousden, K.H. PUMA- and Bax-induced autophagy contributes to apoptosis. *Cell Death Differ.* **16**: 1135–1145 (2009).
61. Brown, C.J., Cheok, C.F., Verma, C.S. and Lane, D.P. Reactivation of p53: from peptides to small molecules. *Trends Pharmacol Sci.* **32**: 53–62 (2011).
62. Li, D., Marchenko, N.D., Schulz, R., Fischer, V., Velasco-Hernandez, T., Talos, F. and Moll, U.M. Functional inactivation of endogenous MDM2 and CHIP by HSP90 causes aberrant stabilization of mutant p53 in human cancer cells. *Mol Cancer Res.* **9**: 577–588 (2011).
63. Kaustov, L. Lukin, J., Lemak, A., Duan, S., Ho, M., Doherty, R., Penn, L.Z. and Arrowsmith, C.H. The conserved CPH domains of Cul7 and PARC are protein-protein interaction modules that bind the tetramerization domain of p53. *J Biol Chem.* **282**: 11300–11307 (2007).
64. Pei, X.H., Bai, F., Li, Z., Smith, M.D., Whitewolf, G., Jin, R. and Xiong, Y. Cytoplasmic CUL9/PARC ubiquitin ligase is a tumor suppressor and promotes p53-dependent apoptosis. *Cancer Res.* **71**: 2969–2977 (2011).
65. Vousden, K.H. and Ryan, K.M. p53 and metabolism. *Nat Rev Cancer.* **9**: 691–700 (2009).

66. Crighton, D., Wilkinson, S., Oprey, J., Syed, N., Smith, P., Harrison, P.R., Gasco, M., Garrone, O., Crook, T. and Ryan, K.M. DRAM, a p53-induced modulator of autophagy, is critical for apoptosis. *Cell*. **126**: 121–134 (2006).
67. Mah, L.Y., O'Prey, J., Baudot, A.D., Hoekstra, A. and Ryan, K.M. DRAM-1 encodes multiple isoforms that regulate autophagy. *Autophagy.* **8**: 18–28 (2012).
68. Maiuri, M.C., Gallizzi, L., Morselli, E., Kepp, O., Malik, S.A. and Kroemer, G. Autophagy regulation by p53. *Curr Opin Cell Biol.* **22**: 181–185 (2010).
69. Beghin, A., Matera, E. L., Brunet-Manquat, S. and Dumontet, C. Expression of Arl2 is associated with p53 localization and chemosensitivity in a breast cancer cell line. *Cell Cycle*. **7**: 3074–3082 (2008).
70. Azmi, A. S., Philip, P.A., Wang, A., Banerjee, S., Zafar, S.F., Goustin, A.S., Almhanna, K., Yang, D., Wang, S., Sarkar, F.H. and Mohammad, R.M. Reactivation of p53 by novel MDM2 inhibitors: implications for pancreatic cancer therapy. *Curr Cancer Drug Targets*. **10**: 319–331 (2010).
71. Nikolaev, A.Y., Li, M., Puskas, N., Qin, J. and Gu, W. Parc: a cytoplasmic anchor for p53. *Cell*. **112**: 29–40 (2003).
72. Trostel, S.Y., Sackett, D.L. and Fojo, T. Oligomerization of p53 precedes its association with dynein and nuclear accumulation. *Cell Cycle*. **5**: 2253–2259 (2006).
73. Wagstaff, K.M., Sivakumaran, H., Heaton, S.M., Harrich, D. and Jans, D.A. Ivermectin is a specific inhibitor of importin alpha/beta-mediated nuclear import able to inhibit replication of HIV-1 and dengue virus. *Biochem J*. **443**: 851–856 (2012).
74. Woo, M.G., Xue, K., Liu, J., McBride, H. and Tsang, B.K. Calpain-mediated processing of p53-associated parkin-like cytoplasmic protein (PARC) affects chemosensitivity of human ovarian cancer cells by promoting p53 subcellular trafficking. *J Biol Chem.* **287**: 3963–3975 (2012).
75. Giustiniani, J., Daire, V., Cantaloube, I., Durand, G., Pous, C., Perdiz, D. and Baillet, A. Tubulin acetylation favors Hsp90 recruitment to microtubules and stimulates the signaling function of the Hsp90 clients Akt/PKB and p53. *Cell Signal.* **21**: 529–539 (2009).
76. Wiech, M., Olszewski, M.B., Tracz-Gaszewska, Z., Wawezynow, B., Zylicz, M. and Zylicz, A. Molecular mechanism of mutant p53 stabilization: the role of HSP70 and MDM2. *PLoS One*. **7**: e51426 (2012).
77. Jin, S., Mazzacurati, L., Zhu, X., Tong, T., Song, Y., Shujuan, S., Petrik, K.L., Rajasekaran, B., Wu, M. and Zhan, Q. Gadd45a contributes to p53 stabilization in response to DNA damage. *Oncogene*. **22**: 8536–8540 (2003).
78. Bhattacharya, S., Chaum, E., Johnson, D.A. and Johnson, L.R. Age-related susceptibility to apoptosis in human retinal pigment epithelial cells is triggered by disruption of p53-Mdm2 association. *Invest Ophthalmol Vis Sci.* **53**: 8350–8366 (2012).
79. Shidoji, Y., Okamoto, K., Muto, Y., Komura, S., Ohishi, N. and Yagi, K. Prevention of geranylgeranoic acid-induced apoptosis by phospholipid hydroperoxide glutathione peroxidase

gene. *J Cell Biochem.* **97**: 178–187 (2006).

80. Fen, C.X., Coomber, D.W., Lane, D.P. and Ghadessy, F.J. Directed evolution of p53 variants with altered DNA-binding specificities by in vitro compartmentalization. *J Mol Biol.* **371**: 1238–1248 (2007).
81. Joerger, A.C. and Fersht, A.R. Structure-function-rescue: the diverse nature of common p53 cancer mutants. *Oncogene*. **26**: 2226–2242 (2007).
82. Bullock, A.N., Henckel, J. and Fersht, A.R. Quantitative analysis of residual folding and DNA binding in mutant p53 core domain: definition of mutant states for rescue in cancer therapy. *Oncogene*. **19**: 1245–1256 (2000).
83. Morselli, E., Tasdemir, E., Maiuri, M.C., Galluzzi, L., Kepp, O., Criollo, A., Vicencio, J.M., Soussi, T. and Kroemer, G. Mutant p53 protein localized in the cytoplasm inhibits autophagy. *Cell Cycle*. **7**: 3056–3061 (2008).
84. Shimonishi, S., Muraguchi, T., Mitake, M., Sakane, C., Okamoto, K. and Shidoji, Y. Rapid downregulation of cyclin D1 induced by geranylgeranoic acid in human hepatoma cells. *Nutr cancer.* **64**: 473-480 (2012).
85. Hosokawa, N., Hara, T., Kaizuka, T., Kishi, C., Takamura, A., Iemura, S., Natsume, T., Takehana, K., Yamada, N., Guan, J.L., Oshiro, N. and Mizushima, N. Nutrient-dependent mTORC 1 association with the ULK1-Atg13-FIP200 complex required for autophagy. *Mol Biol Cell.* **20**: 1981-1991 (2009).
86. Malaciya, R., Laskin, J.D. and Laskin, D.L. Oxidative stress-induced autophagy: Role in pulmonary toxicity. *Toxicol Appl Pharmacol.* 275: 145-151 (2014).
87. Brewer, J.W. and Diehl, J.A. Perk mediates cell-cycle exit during the mammalian unfolded protein response. *Proc Natl Acad U S A.* **97**: 12625-12630 (2000).
88. Dhayal, S. and Morgan, N.G. Structure-activity relationships influencing lipid-induced changes in eIF2α phosphorylation and cell viability in BRIN-BD11 cells. *FEBS Lett.* **585**: 2243-2248 (2011).
89. Somemeriweiss, D., Gorski, T., Richter, S., Garten, A. and Kiess, W. Oleate rescues INS-1E β-cells from palmitate-induced apoptosis by preventing activation of the unfolded protein response. *Bio chem. Biophys Res Commun.* **441**: 770-776 (2013).
90. Volmer, R., van der Ploeg, K. and Ron, D. Membrane lipid saturation activates endoplasmic reticulum unfolded protein response transducers through their transmembrane domains. *Genes Cell.* **18**: 798-809 (2013).
91. Bosma, M., Dapito, D.H., Drosatos-Tampakaki, Z., Huiping-Son, N., Huang, L.S., Kersten, S., Drosatos, K. and Goldberg, I.J. Sequestration of fatty acids in triglycerides prevents endoplasmic reticulum stress in an in vitro model of cardiomyocyte lipotoxicity. *Biochim Biophys Acta.* 1841: 1648-1655 (2014).
92. Listenberger, L.L., Han, X., Lewis, S.E., Cases, S., Farese, R.V. Jr., Ory, D.S. and Schaffer, J.E. Triglyceride accumulation protects against fatty acid-induced lipotoxicity. *Proc Natl Acad Sci U S A.* **100**: 3077-3082 (2003).

93. Nakamura, N., Shidoji, Y., Moriwaki, H. and Muto, Y. Apoptosis in human hepatoma cell line induced by 4,5-didehydrogeranylgeranoic acid (acyclic retinoid) via down-regulation of transforming growth factor alpha. *Biochem Biophys Res Commun.* **219**: 100-104 (1996).
94. Coto-montes, A., Boga, J.A., Rosales-Corral, S., Fuentes-Broto, L., Tan, D.X. and Reiter, R.J. Role of melatonin in the regulation of autophagy and mitophagy: A review. *Mol Cell Endocrinol.* **361**: 12-23 (2012).
95. Karaskov, E., Scott, C., Zhang, L., Teodoro, T., Ravazzola, M. and Volchuk, A. Chronic palmitate but not oleate exposure induces endoplasmic reticulum stress, which may contribute to INS-1 pancreatic β cell apoptosis. *Endocrinology.* **147**: 3398-3407 (2006).
96. Shoulders, M.D., Ryno, L.M., Genereux, J.C., Moresco, J.J., Tu, P.G., Wu, C., Yates, J.R. 3rd., Su, A.I., Kelly, J.W. and Wiseman, R.L. Stress-independent activation of XBP1s and/or ATF6 reveals three functionally diverse ER proteostasis environments. *Cell Rep.* **3**: 1279-1292 (2013).
97. Margariti, A., Li, H., Chen, T., Martin, D., Vizcay-Barrena, G., Alma, S., Karamariti, E., Xiao, Q., Zampetaki, A., Zhang, Z., Wang, W., Jiang, Z., Gao, C., Ma, B., Chen, Y.G., Cockerill, G., Hu, Y., Xu, Q. and Zeng, L. XBP1 mRNA splicing triggers an autophagic response in endothelial cells through BECLIN-1 transcriptional activation. *J Biol Chem.* **288**: 859-872 (2013).
98. Ding, W.X. and Yin, X.M. Sorting, recognition and activation of the misfolded protein degradation pathways through macroautophagy and the proteasome. *Autophagy.* **4**: 141-150 (2008).
99. Yang, L., Li, P., Fu, S., Calay, E.S. and Hotamisligil, G.S. Defective hepatic autophagy in obesity promotes ER stress and causes insulin resistance. *Cell Metab.* **11**: 467-478 (2010).
100. Jia, W., Pua, H.H., Li, Q.J. and He, Y.W. Autophagy regulates endoplasmic reticulum homeostasis and calcium mobilization in T lymphocytes. *J Immunol.* **186**: 1564-1574 (2011).
101. Sheng, R., Liu, X.Q., Zhang, L.S., Gao, B., Han, R., Wu, Y.Q., Zhang, X.Y. and Qin, Z.H. Autophagy regulates endoplasmic reticulum stress in ischemic preconditioning. *Autophagy.* **8**: 310-325 (2012).
102. Kroemer, G., Bravo-San Pedro, J.M. and Galluzzi, L. Novel function of cytoplasmic p53 at the interface between mitochondria and the endoplasmic reticulum. *Cell Death Dis.* **6**: e1698 (2015).
103. Marcel, V., Catez, F. and Diaz, J.J. p53, a translational regulator: contribution to its tumor tumor-suppressor activity. *Oncogene.* **34**: 5513-5523 (2015).
104. Shao, M., Shan, Bo., Liu, Y., Deng, Y., Yan, C., Wu, Y., Mao, T., Qiu, Y., Zhou, Y., Jiang, S., Jia, W., Li, J., Li, J., Rui, L., Yang, L. and Liu, Y. Hepatic IRE1α regulates fasting-induced metabolic adaptive programs through the XBP1s-PPARα axis signaling. *Nat Commun.* **5**: 3528 (2014).